Fall 1-31-2012

Target localization in passive and active systems : performance bonds

Vlad Mihai Chiriac
New Jersey Institute of Technology

Copyright Warning & Restrictions

The copyright law of the United States (Title 17, United States Code) governs the making of photocopies or other reproductions of copyrighted material.

Under certain conditions specified in the law, libraries and archives are authorized to furnish a photocopy or other reproduction. One of these specified conditions is that the photocopy or reproduction is not to be "used for any purpose other than private study, scholarship, or research." If a, user makes a request for, or later uses, a photocopy or reproduction for purposes in excess of "fair use" that user may be liable for copyright infringement,

This institution reserves the right to refuse to accept a copying order if, in its judgment, fulfillment of the order would involve violation of copyright law.

Please Note: The author retains the copyright while the New Jersey Institute of Technology reserves the right to distribute this thesis or dissertation

Printing note: If you do not wish to print this page, then select "Pages from: first page # to: last page #" on the print dialog screen

ABSTRACT

TARGET LOCALIZATION IN PASSIVE AND ACTIVE SYSTEMS: PERFORMANCE BOUNDS

by
Vlad Mihai Chiriac

The main goal of this dissertation is to improve the understanding and to develop ways to predict the performance of localization techniques as a function of signal-to-noise ratio (SNR) and of system parameters. To this end, lower bounds on the maximum likelihood estimator (MLE) performance are studied. The Cramer-Rao lower bound (CRLB) for coherent passive localization of a near-field source is derived. It is shown through the Cramer-Rao bound that, the coherent localization systems can provide high accuracies in localization, to the order of carrier frequency of the observed signal. High accuracies come to a price of having a highly multimodal estimation metric which can lead to sidelobes competing with the mainlobe and engendering ambiguity in the selection of the correct peak. The effect of the sidelobes over the estimator performance at different SNR levels is analyzed and predicted with the use of Ziv-Zakai lower bound (ZZB). Through simulations it is shown that ZZB is tight to the MLEs performance over the whole SNR range. Moreover, the ZZB is a convenient tool to assess the coherent localization performance as a function of various system parameters.

The ZZB was also used to derive a lower bound on the MSE of estimating the range and the range rate of a target in active systems. From the expression of the derived lower bound it was noted that, the ZZB is determined by SNR and by the ambiguity function (AF). Thus, the ZZB can serve as an alternative to the ambiguity function (AF) as a tool for radar design. Furthermore, the derivation is extended to the problem of estimating target's location and velocity in a distributed multiple input multiple output (MIMO) radar system. The derived bound is determined by

SNR, by the product between the number of transmitting antennas and the number of receiving antennas from the radar system, and by all the ambiguity functions and the cross-ambiguity functions corresponding to all pairs transmitter-target-receiver. Similar to the coherent localization, the ZZB can be applied to study the performance of the estimator as a function of different system parameters. Comparison between the ZZB and the MSE of the MLE obtained through simulations demonstrate that the bound is tight in all SNR regions.

TARGET LOCALIZATION IN PASSIVE AND ACTIVE SYSTEMS: PERFORMANCE BOUNDS

by
Vlad Mihai Chiriac

A Dissertation
Submitted to the Faculty of
New Jersey Institute of Technology
in Partial Fulfillment of the Requirements for the Degree of
Doctor of Philosophy in Electrical Engineering

Department of Electrical and Computer Engineering, NJIT

January 2012

APPROVAL PAGE

TARGET LOCALIZATION IN PASSIVE AND ACTIVE SYSTEMS: PERFORMANCE BOUNDS

Vlad Mihai Chiriac

Dr. Alexander M. Haimovich, Dissertation Advisor — Date
Professor, Department of Electrical and Computer Engineering, NJIT

Dr. Yeheskel Bar-Ness, Committee Member — Date
Distinguished Professor, Department of Electrical and Computer Engineering, NJIT

Dr. Ali Abdi , Committee Member — Date
Associate Professor, Department of Electrical and Computer Engineering, NJIT

Dr. Osvaldo Simeone, Committee Member — Date
Assistant Professor, Department of Electrical and Computer Engineering, NJIT

Dr. Hana Godrich , Committee Member — Date
Postdoctoral Research Associate, Department of Electrical Engineering, Princeton University

BIOGRAPHICAL SKETCH

Author: Vlad Mihai Chiriac

Degree: Doctor of Philosophy

Date: January 2012

Undergraduate and Graduate Education:

- Doctor of Philosophy in Electrical Engineering,
  New Jersey Institute of Technology, Newark, NJ, 2012
- Master of Science in Electrical Engineering,
  Gheorghe Asachi University, Iasi, Romania, 2004
- Bachelor of Science in Electrical Engineering,
  Gheorghe Asachi University, Iasi, Romania, 2003

Major: Electrical Engineering

Presentations and Publications:

V.M. Chiriac, A.M. Haimovich, "Ziv - Zakai lower bound on target localization estimation in MIMO radar systems," *IEEE Radar Conf.* May, 2010.

H. Godrich, V.M. Chiriac, A.M. Haimovich, and R.S. Blum "Target tracking in MIMO radar systems: Techniques and performance analysis," *IEEE Radar Conf.* May, 2010.

V.M. Chiriac, A.M. Haimovich, S.C. Schwartz, and J.A. Dabin, "Performance bound for localization of a near field source," *Proc. of 43th Asilomar Conf. Signals, Syst. Comput.*, November, 2009.

V.M. Chiriac, A.M. Haimovich, "Ziv - Zakai Lower Bound for Localization and Velocity Estimation in MIMO Radar Systems," to be submitted to *IEEE Transactions on Signal Processing.*

Sotiei mele, Roxana, pentru dragostea, rabdarea, sprijinul si incurajarile oferite.
To my wife, Roxana, for her love, endless patience, support, and encouragement.

Parintilor mei, Aurica si Mihai, pentru dragostea, incredearea si sustinerea acordata.
To my parents, Aurica and Mihai, for their love, faith, and support throughout my whole life.

Bunicilor mei, Maria si Pavel, pentru dragostea, suportul moral si rabdarea lor.
To my grandparents, Maria and Pavel for their love, moral support and patience. They have been waiting so long for this.

Surorii mele, Andreea, pentru dragostea, increderea si suportul acordat.
To my sister, Andreea, for her love, trust, and support.

ACKNOWLEDGMENT

First and foremost, I would like to express my deepest appreciation to my advisor Dr. Alexander M. Haimovich, who supplied wisdom, guidance, inspiration, advice and help. His trusting support and constructive criticism were crucial to clarify my ideas. He made this work a great learning experience.

Special thanks to Dr. Stuart C. Schwartz, (in memoriam) for partnering with Dr. Alexander M. Haimovich and me in this research collaboration, for his valuable suggestions and encouragement towards the realization of this project.

I would like to express my sincere gratitude to Dr. Yeheskel Bar-Ness, Dr. Ali Abdi, Dr. Osvaldo Simeone, and Dr. Hana Godrich for serving as committee members. I appreciate their time as well as their comments and guides on the dissertation.

Ms. Marlene Toeroek deserves a very special acknowledgment from all of us from CWCSPR. She keeps the ship afloat, always being ready to help us, making everything easy.

Further thanks go to Dr. Ronald Kane, Ms. Clarisa Gonzalez-Lenahan, and Dr. Marino Xanthos, the staff of the Graduate Studies office of NJIT, Mr. Jeffrey Grundy, and the staff of the Office for International Students and faculty for their advice, help and support with administrative matters during my PhD studies.

Special thanks go to Ross Memorial Fellowship fund and for the financial support during my doctoral studies.

I also would like to thank all my colleagues at CWCSPR for all the great moments we shared. Especially, I would like to thank Ciprian Romeo Comsa for sharing experience, knowledge, and friendship during the time of study.

Finally, this research would not have been possible without the support of my family. My wife, Roxana, gave me the strength to face difficult time, the happiness

to enjoy what I was doing, and the wisdom on which to build my dreams. To my parents and my grandparents who installed in me a sense of curiosity which has fueled my scientific interest. Thanks for their continuous love and support. To my sister, Andreea, I have to express thanks for her love, encouragement and support. My gratitude and my love to them are beyond words.

TABLE OF CONTENTS

TABLE OF CONTENTS
(Continued)

Chapter **Page**

LIST OF FIGURES

LIST OF FIGURES
(Continued)

Figure **Page**

CHAPTER 1

INTRODUCTION

Localization is, and will be, an active area full of new applications, each characterized by its own set of requirements. The quest for new localization applications arise in many fields of interest, and is driven by the aspiration of obtaining higher localization accuracies. Thus, it is important to evaluate and to analyze the performance of developed systems. To evaluate the performance of estimating systems one can resort to lower bounds on the minimum mean square error (MSE). Lower bounds not only can serve as a benchmark for the system performance, but can also be used to assess performance as a function of various system parameters. This thesis focuses on deriving lower bounds on target localization in passive and active systems.

To position an emitting target, passive localization systems process the noisy observations collected by sensors. The noisy observations are attenuated and delayed versions of the emitted signal. In the literature, based on the information used (attenuation or delay), several classes of localization techniques were defined: received signal strength indicator (RSSI) [1–4], time of arrival (TOA) [5–7], time difference of arrival (TDOA) [8–10], angle of arrival (AOA) [11–14].

RSSI technology is based on the property that, the strength of an electromagnetic wave decays at a rate that is inversely proportional to the range from the source to the sensor, when the propagation takes place in a free space channel [15]. Because in most of the practical applications the propagation doesn't take place in free space channel and the mathematical model for other channels has imperfect characterization, the RSSI technology provides raw location estimates [16].

One of the most accurate techniques for passive localization is the TOA, as noted in [16]. In principle, the TOA technique locates the target by measuring the

time-of-flight (TOF) (i.e., the time between transmission and reception) at three or more sensors, and performing trilateration. The reception time is estimated by filtering the noisy observations with a filter matched to the transmitted signal, or by correlating the noisy observations with the transmitting signal. Thus, the system needs to know the transmission time and the transmitted signal in order to perform localization. Moreover, accurate results are obtained if the sensors are synchronized in time with the target.

The TDOA technique overcomes some of the requirements of TOA by measuring the difference of TOF between pairs of sensors. TDOAs are estimated by performing cross-correlations between signals received at two different sensors. TDOA based localization can be accomplished either by formulating a joint statistic that incorporates all TDOA observations or by performing ranging between pairs of sensors and subsequently, solving a set of nonlinear equations to estimate the source location.

The principle of AOA is based on measuring the direction from which was transmitted the signal at two or more sensors and performing the intersection of the measured directions. In order to estimate the direction, localization systems based on AOA require directional antennas, such as an adaptive phased array of two or more antenna elements, at each sensor. The direction is obtained from the phase difference between the signals collected by the antenna elements. AOA provide accurate locations if the sensors are synchronized in time, and for each directional antenna, the antenna elements are synchronized in phase.

The TOA, and TDOA are non-coherent processing techniques in the sense that they exploit the envelope, but not the phase, of signals observed at the sensors. On the other hand, the AOA exploits the phases only between the signals observed at one sensor. The coherency is lost when processing the signals from all the sensors. In a recent work by Lehmann et al. [17], on localization employing active sensors (i.e.,

sensor that transmit probing signals, such as in radar), a technique which exploits the phase information among pairs of sensors was proposed. Because the technique exploits the coherency between all the received signals, it was referred as coherent localization. Coherent techniques have been shown to offer great improvements in accuracy, particularly at high signal to noise ratio (SNR) [17]. This is due to the fact that the accuracy in coherent localization, as expressed through the Cramer-Rao bound, is proportional to the carrier frequency of the observed signal, whereas for non-coherent localization, the accuracy is proportional to the bandwidth of the observed signal.

In spite of providing high accuracies, the coherent localization is a nonlinear problem, for which the estimation metric is often multimodal. For a noisy-free environment, the estimation metric has a mainlobe corresponding to the true value of the estimate and sidelobes corresponding to highly probable, erroneous estimates. The synergy between sidelobes and noise in causing estimation errors leads to distinct regions of operation of the nonlinear estimator, that correspond to distinct ranges of signal-to-noise ratio (SNR). For high SNR, the estimated parameter is affected by small noise errors that cannot cast the estimate outside the main lobe of the estimation metric. This region is the asymptotic region, and it is characterized by small estimation errors. As the SNR decreases, the errors become global and spread beyond the local vicinity of the true value of the estimated parameter. Below a certain value of SNR, the global errors dominate the estimation performance leading to a drastic increase in the mean square error (MSE). In this region, sidelobes compete with the mainlobe, engendering ambiguity in the selection of the correct peak. This region is the ambiguity region. At low SNR, the behavior of the estimator is completely dominated by noise effects. In this regime, no useful information can be obtained about the estimated parameter, and estimation errors are bound only by the *a priori* information about the limits on the parameter values. This behavior of

the MSE is known in the literature as *threshold phenomena*, and it is exhibited by other estimation problems like, delay estimation [18–24], bearing estimation [25–28].

To evaluate such the complex behavior of estimators, one can resort to lower bounds on the minimum MSE. In the literature, one of the most popular lower bounds is the Cramer-Rao lower bound (CRLB) [29]. The use of the CRLB is justified by the fact that in many estimation problems, the maximum likelihood estimator (MLE) approaches the CRLB arbitrarily close in the asymptotically high SNR region. If the estimator operates below the threshold SNR[1], the errors become global and the estimator's performance departs from CRLB. Thus, CRLB cannot predict the estimator's performance below the threshold SNR.

The Barankin bound (BB) has been developed to evaluate the estimation performance and to predict the threshold SNR [30]. The BB have been applied to a variety of estimation problems in [31–35], and it proves that it can take into consideration the global errors because below some SNR, the BB departs from the CRLB. In spite of predicting the estimation performance for range of SNRs, the BB as well as the CRLB do not take into consideration any *a priori* information about the estimated parameters. Moreover, both bounds apply only to unbiased estimates, whereas the MLE becomes biased below the threshold SNR, [36, 37].

A prediction of the system performance free from the bias assumption can be obtained using the Ziv-Zakai lower bound (ZZB) [38]. The ZZB is a Bayesian bound that assumes a random parameter model with known *a priori* distribution. A brief review of the Bayesian lower bounds is presented in Chapter 2. Bell et al. extended the ZZB from scalar to vector parameter estimation [39], and used it to develop a lower bound on the MSE in estimating the 2-D bearing of a narrowband plane wave [25]. The principle of ZZB for scalar parameter estimation and for vector parameter

[1]Threshold SNR represents the SNR where the estimator's performance starts to be affected by global errors.

estimation is introduced in Chapter 2. In the literature, the ZZB was used as a lower bound for different estimations problems [18–20, 22, 23, 25, 40–45].

The ZZB for coherent location estimation in passive and active systems are derived in Chapter 3 and 4, respectively. The derived ZZB relate the estimation mean square error (MSE) to systems parameters like number of sensors and their location, carrier frequency, bandwidth. From numerical calculations of the bounds, all three operation regions of a nonlinear estimator can be distinguished: the noise-dominated region, the ambiguity region, and the ambiguity free region. Moreover, numerical examples demonstrate that the ZZB closely predict the performance of the MLE across the full range of SNR values.

A problem related to the estimation of the location is the estimation of target's range and range rate. In Chapter 5 this problem is analyzed with the use of ZZB in the context of radar systems. An important tool in radar analysis is the ambiguity function (AF) [46], which for a noisy free environment, displays the inherent tradeoff between the ability to estimate the range and range rate of a moving target. It is shown in Chapter 5 that, the ZZB is determined by both the SNR and the AF, and thus, ZZB provides a more complete analysis than AF. Further on this analysis is extended to the problem of estimating target's location and velocity.

CHAPTER 2

LOWER BOUNDS ON THE MINIMUM MEAN SQUARE ERROR

The aim of this chapter is to review briefly the Bayesian lower bounds and to introduce the principle of Ziv-Zakai lower bound (ZZB).

In order to review lower bounds on the minimum mean square error, consider the following general model for a random parameter estimation problem [29] (see Figure 2.1):

- Parameter space - represents all the possible values taken by the vector estimated parameter $\boldsymbol{\theta}$
- Observation space - represents all the possible values taken by the vector observations $\mathbf{r}$
- Probabilistic mapping from parameter space to observation space - represents the probability law that governs the effect of $\boldsymbol{\theta}$ on observations
- Estimation rule - represents the mapping of the observations into an estimate of the parameter $\boldsymbol{\theta}$, $\hat{\boldsymbol{\theta}}(\mathbf{r})$

The evaluation of an estimation rule can be done using the following three performance measures:

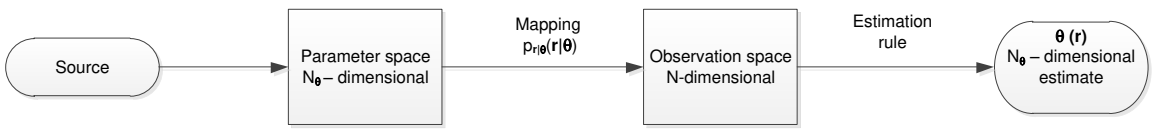

Figure 2.1 General parameter estimation model (from [29])

- Bias $E_{\mathbf{r},\theta}\left[\hat{\boldsymbol{\theta}}(\mathbf{r}) - \boldsymbol{\theta}\right]$,
- Mean square error $E_{\mathbf{r},\theta}\left[\left(\hat{\boldsymbol{\theta}}(\mathbf{r}) - \boldsymbol{\theta}\right)^2\right]$,
- Variance $\text{var}\left(\hat{\boldsymbol{\theta}}(\mathbf{r})\right) = E_{\mathbf{r},\theta}\left[\left(\hat{\boldsymbol{\theta}}(\mathbf{r}) - \boldsymbol{\theta}\right)^2\right] - E_{\mathbf{r},\theta}\left[\hat{\boldsymbol{\theta}}(\mathbf{r}) - \boldsymbol{\theta}\right]$

where $E_{\mathbf{r},\theta}[]$ represents the expectation with respect to observations $\mathbf{r}$ and to estimated parameter $\boldsymbol{\theta}$. However, calculations of the performance measures for different estimators is frequently difficult, if not impossible. To circumvent this disadvantage, researchers have developed lower bounds on the MSE.

The estimators can be affected by two types of errors: local errors (the estimator's output is in the vicinity of the $\boldsymbol{\theta}$'s true value), and global errors (the estimator's output can be any value from the parameter space). In order that the lower bounds to be able to capture the effect of both errors, the set of possible values of the parameters to be estimated must be known beforehand. This leads to Bayesian type bounds. The characteristic of these bounds is that, they assume a random parameter model with known *a priori* distribution. In [40], the Bayesian bounds are classified in two categories: "Weiss-Weinstein family" bounds, and "Ziv-Zakai family" bounds.

2.1 Weiss-Weinstein Bounds

The most known lower bound from the "Weiss-Weinstein family" bounds is the Bayesian Cramer-Rao lower bound (BCRLB) [29, pp 72-73]. The BCRLB, as all the other lower bounds from "Weiss-Weinstein family", can be derived from a "covariance inequality" which was derived by Weiss and Weinstein in [47]. Weiss and Weinstein showed that for any function $\Psi(\mathbf{r}, \theta)$ such that the expectation of $\Psi(\mathbf{r}, \theta)$ conditioned on $\mathbf{r}$ equal to zero (i.e., $E[\Psi(\mathbf{r}, \theta)|\mathbf{r}] = 0$), the MSE is lower bounded by:

$$\boldsymbol{\Phi} = E_{\theta,\mathbf{r}}[\epsilon\epsilon^T] = E_{\mathbf{r},\theta}[(\hat{\theta}(\mathbf{r}) - \theta)(\hat{\theta}(\mathbf{r}) - \theta)^T] \geq \mathbf{V}\mathbf{P}^{-1}\mathbf{V}^T \tag{2.1}$$

where

$$V_{ij} = E_{\mathbf{r},\theta}\left[\theta_i \Psi_j\left(\mathbf{r},\theta\right)\right], \quad i,j = 1,\ldots,N_\theta \tag{2.2}$$

$$P_{ij} = E_{\mathbf{r},\theta}\left[\Psi_i\left(\mathbf{r},\theta\right)\Psi_j\left(\mathbf{r},\theta\right)\right], \quad i,j = 1,\ldots,N_\theta \tag{2.3}$$

and the matrix inequality means that $\Phi - \mathbf{V}\mathbf{P}^{-1}\mathbf{V}^T$ is a nonnegative definite matrix. N_θ represents the dimension of θ. Starting from (2.1), which is referred as the covariance inequality, and choosing different functions $\Psi\left(\mathbf{r},\theta\right)$, one can obtain different lower bounds. The BCRB is obtained by choosing:

$$\Psi_j\left(\mathbf{r},\theta\right) = \frac{\partial \ln p\left(\mathbf{r},\theta\right)}{\partial \theta_j} \qquad j = 1,\ldots,N_\theta \tag{2.4}$$

where $p\left(\mathbf{r},\theta\right)$ represents the joint probability distribution function (pdf) of $\mathbf{r}$ and θ.

Replacing (2.4) into (2.1), the MSE is lower bounded by:

$$\mathbf{\Phi} \geq \mathbf{J}_B^{-1} \tag{2.5}$$

where

$$\begin{aligned}\mathbf{J}_B &\triangleq E_{\mathbf{r},\theta}\left[\frac{\partial}{\partial\theta}\log\, p\left(\mathbf{r},\theta\right)\left(\frac{\partial}{\partial\theta}\log\, p\left(\mathbf{r},\theta\right)\right)^T\right] \\ &= E_{\mathbf{r},\theta}\left[\frac{\partial}{\partial\theta}\log\, p\left(\mathbf{r}|\theta\right)\left(\frac{\partial}{\partial\theta}\log\, p\left(\mathbf{r}|\theta\right)\right)^T\right] + E_\theta\left[\frac{\partial}{\partial\theta}\log\, p\left(\theta\right)\left(\frac{\partial}{\partial\theta}\log\, p\left(\theta\right)\right)^T\right]\end{aligned} \tag{2.6}$$

is the Bayesian information matrix (BIM), and it is formed by two terms: the first term is the contribution of the data i.e., the expectation of the Fisher information

matrix (FIM) over θ, and the second term is the contribution of the *a priori* parameter information term. Inequality 2.5 represents the BCRB.

The BCRB can be evaluated if two regularity conditions are fulfilled [29]: - the joint pdf $p(\mathbf{r}, \boldsymbol{\theta})$ is twice differentiable with respect to the estimated parameter, and the derivatives are absolutely integrable. This conditions are not always fulfilled. For example, for random variables uniformly distributed over a finite interval, the joint pdf is not smooth at the endpoints of the parameter space, and the derivatives don't exist.

Choosing higher derivatives of the joint pdf $p(\mathbf{r}, \boldsymbol{\theta})$ leads to two other lower bounds the Bhattacharyya bound [29] and the Bobrovsky-Zakai bound [48], but these bounds are subject to more strict regularity conditions [49]. In [50], Weiss and Weinstein proposed a new lower bound free from regularity conditions, but in order to provide good predictions of the maximum likelihood estimator it needs to be optimized over some free variables [40].

2.2 Ziv-Zakai Bounds

In the Ziv-Zakai lower bound family are included the original Ziv-Zakai bound (ZZB), [38], improvements of the original bound made by Chazan, Zakai, and Ziv, [51], Bellini and Tartara, [52], and the extension of the ZZB to the vector parameters estimation made by Bell, [39]. In the following the principle of ZZB is introduced first for scalar parameter estimations and then for vector parameter estimations.

The scalar Ziv-Zakai lower bound (ZZB) is a Bayesian bound for an unknown parameter θ given the *a priori* probablity density $p_\theta(\theta)$. We seek to lower bound the MSE

$$\mathrm{E}\left[|\epsilon|^2\right] = \mathrm{E}\left[\left|\widehat{\theta}\,(r) - \theta\right|^2\right] \tag{2.7}$$

where θ is the true value and $\widehat{\theta}$ is the estimate. The MSE is computed as an average of probabilities of error of a sequence of binary tests between pairs of values of the estimated parameter, a notion stemming from the identity, [53],

$$\mathrm{E}\left[|\epsilon|^2\right] = \frac{1}{2}\int_0^\infty \Pr\left(|\epsilon| \geq \frac{h}{2}\right) h dh \tag{2.8}$$

and lower bounding $\Pr\left(|\epsilon| \geq \frac{h}{2}\right)$. The estimation probability of error $\Pr\left(|\epsilon| \geq \frac{h}{2}\right)$ can be viewed from a detection theory point of view by noting that $\Pr\left(|\epsilon| \geq \frac{h}{2}\right)$ is also the probability of a binary hypothesis problem in which θ equals either some value φ (H_0 hypothesis) or the value $\varphi + h$ (H_1 hypothesis). Therefore, $\Pr\left(|\epsilon| \geq \frac{h}{2}\right)$ can be lower bounded by the minimum probability of error obtained from the likelihood ratio test corresponding to the two hypotheses H_0 and H_1, $P_\epsilon\left(\varphi, \varphi + h\right)$

$$\Pr\left(|\epsilon| \geq \frac{h}{2}\right) \geq \int_{-\infty}^{\infty} \left(p_\theta(\varphi) + p_\theta(\varphi + h)\right) P_\epsilon\left(\varphi, \varphi + h\right) \mathrm{d}\varphi \tag{2.9}$$

Substituting (2.9) in (2.8) yields the ZZB for the scalar case

$$\mathrm{E}\left[|\epsilon|^2\right] \geq \frac{1}{2}\int_0^\infty V\left\{\int_{-\infty}^{\infty} \left(p_\theta(\varphi) + p_\theta(\varphi + h)\right) P_\epsilon\left(\varphi, \varphi + h\right) \mathrm{d}\varphi\right\} h \mathrm{d}h \tag{2.10}$$

where $V\{\cdot\}$ is a so called valley-filling function. To obtain insight into the role of the valley-filling function, one must note that in general $\Pr\left(|\epsilon| \geq \frac{h}{2}\right)$ is a nonincreasing function of h, but the right hand side of (2.9) is not guaranteed to be monotonic. Thus, a tighter lower bound of $\Pr\left(|\epsilon| \geq \frac{h}{2}\right)$ can be obtained by capping the computed lower bound with a nonincreasing function of h. The capping operation is accomplished by the valley-filling function. The valley-filling functions was proposed by Bellini and Tartara in [52] to improve the ZZB.

In the localization problem, the unknown parameter is represented by a vector θ. Hence, it is worth to present the extension of the ZZB to vector parameters that

was derived in [39]. It lower bounds the quadratic form $\mathbf{u}^T\mathbf{\Phi}\mathbf{u}$ for any vector $\mathbf{u}$, where $\mathbf{\Phi}$ is the covariance matrix of the estimator. Lower bounding $\mathbf{u}^T\mathbf{\Phi}\mathbf{u}$ offers a flexible approach through which the total error (sum of the diagonal elements of $\mathbf{\Phi}$) or errors of specific components of $\boldsymbol{\theta}$ can be bounded. For example, for evaluation of the total error, $\mathbf{u}$ is set to be a vector of ones; for estimating the error for a specific parameter, the elements of $\mathbf{u}$ are set to zero, except the element associated with the parameter of interest, which is set to one.

An identity similar to (2.8) can be written for the vector estimation case by replacing $|\epsilon|$ with $|\mathbf{u}^T\boldsymbol{\epsilon}|$,

$$\mathbf{u}^T\mathbf{\Phi}\mathbf{u} = \mathrm{E}\left[|\mathbf{u}^T\boldsymbol{\epsilon}|^2\right] = \frac{1}{2}\int_0^\infty \Pr\left(|\mathbf{u}^T\boldsymbol{\epsilon}| \geq \frac{h}{2}\right) h dh. \tag{2.11}$$

As discussed in the scalar case, the lower bound of $\Pr\left(|\mathbf{u}^T\boldsymbol{\epsilon}| \geq \frac{h}{2}\right)$ is obtained by linking the estimation of θ with a binary hypothesis testing problem. The vector parameter θ is equal to either the vector φ or to the vector $\varphi+\delta$. The binary decision associated with an estimate $\widehat{\theta}(\mathbf{r})$ is formulated as follows:

$$\begin{aligned} &\text{Decide } H_0\text{: } \theta = \varphi && \text{if} \quad \mathbf{u}^T\hat{\theta}(\mathbf{r}) \leq \mathbf{u}^T\varphi + \frac{h}{2} \\ &\text{Decide } H_1\text{: } \theta = \varphi + \delta && \text{if} \quad \mathbf{u}^T\hat{\theta}(\mathbf{r}) \geq \mathbf{u}^T\varphi + \frac{h}{2} \end{aligned} \tag{2.12}$$

The separation between the two decision regions is provided by the line $\mathbf{u}^T\boldsymbol{\varphi} + h/2$. The probability of error for this detection problem can be lower bounded with the help of the minimum probability of error $P_\epsilon\left(\varphi, \varphi+\delta\right)$ of a binary detection problem, in which the transmitted vectors are either φ or $\varphi+\delta$. Such a minimum probability of error is obtained from the likelihood ratio test [29]

$$l\left(\mathbf{r}\right) \triangleq \ln\left[\frac{f(\mathbf{r}|\varphi)}{f(\mathbf{r}|\varphi+\delta)}\right] \underset{H_1}{\overset{H_0}{\gtrless}} 0 \tag{2.13}$$

where $f(\mathbf{r}|\boldsymbol{\varphi})$ and $f(\mathbf{r}|\boldsymbol{\varphi}+\boldsymbol{\delta})$ represent the probability density functions of the vector observations under the two hypotheses.

The ZZB for vector parameters is [39]

$$\mathbf{u}^T\boldsymbol{\Phi}\mathbf{u} \geq \frac{1}{2}\int_0^\infty h \cdot V\Bigg\{ \max_{\delta:\mathbf{u}^T\delta=h} \int_{-\infty}^{\infty} (p_\theta(\varphi) + p_\theta(\varphi+\delta)) \cdot P_\epsilon(\varphi, \varphi+\delta)d\varphi \Bigg\} \cdot dh \tag{2.14}$$

It is evident from the previous relation that the probability of error $P_\epsilon(\varphi, \varphi+\delta)$ play a key role in determining the ZZB.

CHAPTER 3

COHERENT LOCALIZATION IN PASSIVE SYSTEMS

3.1 Introduction

This chapter focuses on the passive localization of noncooperative sources, i.e., sources for which the actual signal and the time and phase of the transmitted signal are unknown to the sensors. A class of localization techniques for this case is based on time difference of arrival (TDOA). TDOA based localization can be accomplished either by formulating a joint statistic that incorporates all TDOA observations or by performing ranging between pairs of sensors and subsequently, solving a set of nonlinear equations to estimate the source location. TDOA based localization is noncoherent in the sense that it exploits the envelope, but not the phase, of signals observed at the sensors. Recent work on localization employing active sensors (i.e., sensor that transmit probing signals, such as in radar) has shown the potential for significant gains when the localization processing exploits the phase information among pairs of sensors [17]. Such techniques are refereed further on as *coherent* localization. Coherent techniques have been shown to offer great improvements in accuracy, particularly at high signal to noise ratio (SNR) [17]. This is due to the fact that the accuracy in coherent localization, as expressed through the Cramer-Rao bound, is proportional to the carrier frequency of the observed signal, whereas for noncoherent localization, the accuracy is proportional to the bandwidth of the observed signal. Accuracy also improves with the increase in the number of sensors and the angular sector of their spread (relative to the source). However, large separation between sensors yields, for a fixed number of sensors, high peak sidelobes in the coherent localization metric [54]. The aim of this Chapter is how to find the

global peak of the localization metric, and more important, to develop an analysis based on lower bounds which alleviates the search for the global peak.

3.2 System Model

Consider a radiating source located at an unknown position $\theta = [x_e, y_e]$, where θ is modeled as a continuous random variable with a known *a priori* probability density function (pdf), assumed here to be the uniform distribution $x_e,\ y_e \sim U[-D,\ D]$. This description implies that the source is known to be located somewhere in a square area of dimensions $2D \times 2D$. The signal emitted by the source has bandwidth B, and it modulates a carrier frequency f_c. The source is not cooperating with the sensors, in the sense that the timing of the transmission and the transmitted signal are unknown to the sensors. It is assumed, however, that the sensors are synchronized in both time and phase. With coherent localization, the source location is estimated from amplitude and phase measurements at the sensors. This approach is similar to measurements of signals received across a phased array for bearing estimation. In the bearing estimation problem, the source is in the far-field of the array. In the source localization problem, the source is in the near-field of the two-dimensional array formed by the sensors. In the near field, the phase and amplitude received at each sensor depend on the source location (i.e., range and bearing), not only on the bearing, as in the far field case. Since the transmission time is unknown, coherent localization of the source is performed using phase measurements relative to one of the sensors chosen as the reference sensor.

Source observations are collected by M sensors located at arbitrary coordinates $(x_k, y_k),\ k = 1, \ldots, M$. The period of time T during which these observations are collected is such that $BT \gg 1$. A figure showing the setup is presented in Figure 3.1.

Localization of the source is based on noisy observations of the signals received at the sensors and expressed as:

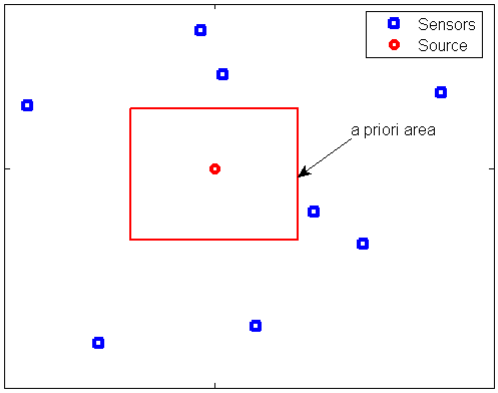

Figure 3.1 The setup for coherent passive localization

$$r_k(t) = a_k s(t - \tau_k) e^{-j2\pi f_c \tau_k} + w_k(t), \qquad k = 1, 2, \ldots, M$$
$$, 0 \leq t \leq T, \tag{3.1}$$

where s and w_k denote respectively, the transmitted signal, and additive noise at the k-th sensor. The source and the noise waveforms are sample functions of uncorrelated, zero-mean, stationary Gaussian random processes with spectral densities P_s and P_w, respectively. The spectral densities are constant across the bandwidth. The amplitude and the propagation delay of the signal received at sensor k relative to the reference sensor are denoted a_k and τ_k, respectively. Without loss of generality, the reference sensor is indexed 1. The TDOA corresponding to sensor k is related to the source and kth sensor coordinates by:

$$\tau_k = \frac{\sqrt{(x_e - x_k)^2 + (y_e - y_k)^2}}{c} - \frac{\sqrt{(x_e - x_1)^2 + (y_e - y_1)^2}}{c}, \tag{3.2}$$

where c is the signal propagation speed.

To make use of properties of the Fourier transform, the measurements are converted from the time domain to the frequency domain. The f_l Fourier coefficient of the observed signal at sensor k is given by:

$$\begin{aligned} R_k(f_l) &= \frac{1}{\sqrt{T}} \int_0^T r_k(t) e^{-j2\pi f_l t} dt \\ &= a_k S(f_l) e^{-j2\pi(f_l+f_c)\tau_k} + W_k(f_l), \qquad k = 1, 2, \ldots, M, \end{aligned} \tag{3.3}$$

where $l = 1, \ldots, N$, N is the number of frequency samples, and $S(f_l)$ and $W_k(f_l)$ are the Fourier coefficients at f_l of $s(t)$ and $w_k(t)$, respectively. For later use, we define the vectors $\mathbf{r} = [\mathbf{r}(f_1), \mathbf{r}(f_2), \ldots, \mathbf{r}(f_N)]^T$, where $\mathbf{r}(f_l) = [R_1(f_l), R_2(f_l), \ldots, R_M(f_l)]^T$. For $BT \gg 1$, any pair of Fourier coefficients is uncorrelated [55]. Because $r_k(t)$ is a Gaussian process and the Fourier transform is a linear operation, $\mathbf{r}$ has a conditional multivariate Gaussian pdf,

$$\begin{aligned} p(\mathbf{r}|\theta) = &\prod_{l=1}^{N} \det[\pi \mathbf{K}(f_l)]^{-1} \cdot \\ &\cdot \exp(-\mathbf{r}^H(f_l) \mathbf{K}^{-1}(f_l) \mathbf{r}(f_l)), \end{aligned} \tag{3.4}$$

where the covariance matrix of the Fourier coefficients at the sensors is given by

$$\begin{aligned} \mathbf{K}(f_l) &= E[\mathbf{r}(f_l)\mathbf{r}^H(f_l)] \\ &= P_s \gamma(f_l) \gamma^H(f_l) + P_w \mathbf{I}, \end{aligned} \tag{3.5}$$

and

$$\mathbf{K}^{-1}(f_l) = \frac{1}{P_w} \left(I - \frac{\frac{P_s}{P_w} \gamma(f_l) \gamma^H(f_l)}{1 + \frac{P_s}{P_w} \gamma^H(f_l) \gamma(f_l)} \right). \tag{3.6}$$

In this expression, P_s and P_w were defined previously, and the vector $\gamma(f_l) = [1, a_2 e^{-j2\pi(f_c+f_l)\tau_2}, \ldots, a_M e^{-j2\pi(f_c+f_l)\tau_M}]^T$ represents the response across the sensors to a radiated frequency component $(f_c + f_l)$. The matrix $\mathbf{I}$ is the identity matrix. The superscripts "T" and "H" denote the transpose and conjugate transpose operations, respectively.

The maximum likelihood estimate of the source location is given by the maximum of the likelihood function

$$\widehat{\theta}_{ML}(\mathbf{r}) = \arg\max_{\theta} p(\mathbf{r}|\theta) \tag{3.7}$$

where the likelihood function equals the value of the pdf at the observations $\mathbf{r}$. It can be shown that for the model defined in (3.4) and (3.5), the MLE of θ is given by the expression:

$$\begin{aligned}\hat{\theta}_{ML}(\mathbf{r}) &= \arg\max_{\theta} \sum_{l=1}^{N} |\mathbf{r}^H(f_l)\gamma(f_l)|^2 = \\ &= \arg\max_{\theta} \sum_{k=1}^{M}\sum_{i=1}^{M} a_k a_i e^{j2\pi f_c(\tau_k-\tau_i)} \cdot \sum_{l=1}^{N} R_k(f_l) R_i^*(f_l) e^{j2\pi f_l(\tau_k-\tau_i)}\end{aligned} \tag{3.8}$$

The former expression reveals the highly nonlinear nature of the MLE. Moreover, due to exploiting the phase difference information, i.e., the term $e^{j2\pi f_c(\tau_k-\tau_i)}$, the widths of the estimator's peaks are on the order of a wavelength. Thus, for searching areas of hundreds of wavelengths, the multimodal characteristic of MLE makes a challenge to find the true peak of the likelihood function. In Section 3.3, the problem of finding the maximum of the likelihood metric is solved using a hybrid deterministic global optimization algorithm.

3.3 Optimization Algorithm to Find

the Global Peak of the Localization Metric

The coherent localization problem can be formulated as an optimization problem of a suitable likelihood function. Because the peak is very narrow (order of a wavelength), a direct search based on a dense grid is impractical. A more manageable approach to find the true peak is to start with a less dense grid, and perform a local search from each grid point. It is well known in the literature that, the local optimization methods have high convergence rates, i.e., they are efficient in terms of the number of evaluations, **[56]**. Yet in order for the local optimization to find the true peak, a local search must be done for each peak of the likelihood function. Thus, this approach is also prohibitively complex computationally and timewise. An approach to circumvent these difficulties is the application of advanced global optimization (GO) algorithms. With stochastic GO algorithms, new trail points are generated randomly. Genetic algorithms or simulated annealing algorithms fall in this category [57]. A serious drawback of stochastic GO algorithms is that no formal proofs of convergence are available, and hence multiple trials are required to provide (statistical) confidence measures that the global optimum has been found [58, pp. 18]. The alternative to stochastic GO are deterministic GO algorithms, in which new trial points are generated based only on evaluations at former points. Branch and bound algorithms belong to this family [57]. Deterministic GO algorithms scan the parameter space in a systematic manner, and can be guaranteed to converge. Yet, convergence rates (number of evaluations) needed to reach required accuracy could be quite slow if the number of peaks is as high as in the coherent localization problem.

A solution to the convergent rate issue is to combine a deterministic GO algorithm with a local search algorithm. In the next subsection it is proposed a hybrid approach which combines DIRECT, a deterministic GO algorithm, and a steepest descent local search. In a two-dimensional optimization problem, such as the two-dimensional localization, DIRECT evaluates lower bounds of the function

over increasingly smaller areas. The true peak is found as the search areas become vanishingly small. The main idea of the proposed algorithm is to accelerate the convergence rate by switching a local search anytime the scale of search interval reaches the size of the carrier wavelength. This approach exploits the fact that the width of the main peak and sidelobes is of the order of the carrier wavelength.

3.3.1 Hybrid DIRECT

DIRECT (DIviding RECTangles) was developed by Jones et. al. [59] and is a modification of the Lipschitzian Optimization algorithm invented by Shubert [60]. DIRECT is a derivative free algorithm that finds the minimum of continuous function for which the rate of change is bounded [59]. DIRECT functions primarily by making exploratory moves across the parameter space by probing and subdividing hyper-rectangles that most likely contain the lowest value of the objective function.

DIRECT algorithm starts by normalizing the parameter space to a n-dimensional unit hyper-cube where n is the dimension of the parameter space, and by sampling the objective function at the center of the unit hyper-cube. In the subsequent step, a dividing strategy is performed to divide the unit hyper-cube as follows:

- sample the function at $\mathbf{b} \pm \alpha \mathbf{e}_i$, where $\mathbf{b}$ is the center of the unit hyper-cube, α equals one-third of the side length of the hypercube, and $\mathbf{e}_i$ is the ith unit vector (i.e., a vector with a one in the ith position and zero elsewhere),
- calculate $p_i = \min\{f(\mathbf{b} + \alpha \mathbf{e}_i), f(\mathbf{b} - \alpha \mathbf{e}_i)\}$
- partition along the direction with the lowest p_i and the remaining field is partitioned along the direction of the second lowest p_i and so on until all the hyper-cubes are partitioned.

From this point onwards, the algorithm focuses on hyper-rectangles that most likely contain the lowest value of the objective function, hyper-rectangles that are called potentially optimal [59].

A hyper-rectangle j is said to be potentially optimal if there exists some rate of change constant $K > 0$ such that:

$$f(\mathbf{b}_j) - K\delta_j \leq f(\mathbf{b}_i) - K\delta_i, \text{ for any } i = 1, \ldots, m$$
$$f(\mathbf{b}_j) - K\delta_j \leq f_{min} - \epsilon|f_{min}|,$$

where m denotes the number of hyper-rectangles, $\mathbf{b}_i$ and δ_i denote the center and the distance from the center to the vertices of the ith hyper-rectangle, f_{min} denotes the lowest value of the function found by the algorithm til the current iteration, and $\epsilon > 0$ is a positive constant.

The algorithm, after identification of the potentially optimal hyper-rectangles, continues by applying the dividing strategy to the identified hyper-rectangles, and repeats the two steps, i.e., the identification and the partitioning, until the number of iterations or of function evaluations is satisfied.

In Figure 3.2 are illustrated the first three iterations of DIRECT algorithm applied for a two dimensional toy example. In the first iteration, the objective function is sampled at the center of the normalized space. Next the algorithm identifies the unit square as a potentially optimal rectangle and applies the dividing strategy. In the Figure, the potentially optimal rectangles are marked with dotted pattern background. Also the center of the rectangles obtained after division are labeled with the value of the objective function at these points. Similarly, in the second iteration, the algorithm identifies the rectangle with center labeled number 2 as a potentially optimal rectangle, and applies the dividing strategy to it. In the third iteration, the algorithm identifies the rectangles with centers labeled number 2 and

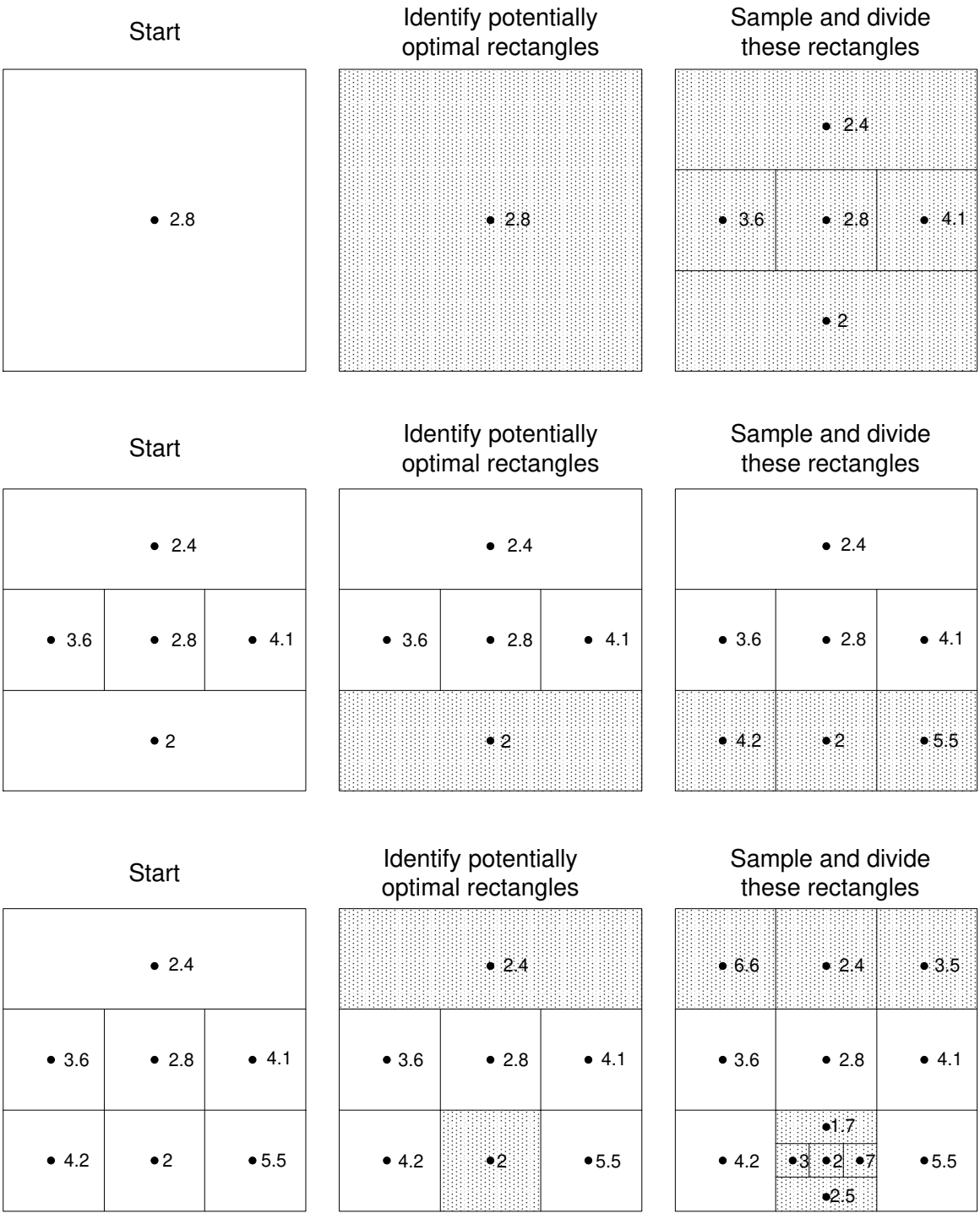

Figure 3.2 The first three iterations of DIRECT algorithm

2.5 as potentially optimal rectangles, and applies the dividing strategy to them. This process is repeated until the stopping condition is satisfied.

Because DIRECT scans the parameter space in a semi-blind manner, i.e., it doesn't use characteristics of the objective function like gradient, its convergence rates (number of evaluations) needed to reach a required accuracy could be quite slow. A required accuracy is necessary for the coherent localization problem where the sidelobes compete with the main lobe of the likelihood metric, [44]. To improve the convergence rate a switch to a local search can be performed as soon as the potentially optimal rectangles reach the size of the carrier wavelength. This approach exploits that the width of the main peak and sidelobes for the coherent localization problem is of the order of the carrier wavelength. The local search is performed using a steepest descent approach that is discussed next. Starting from the center of a potentially optimal rectangle that has a size smaller than the carrier wavelength, the gradient of the objective function is estimated by computing new values at small separations from the center, and finding the difference from the objective function at the center point. These values allow the direction of steepest descent to be computed. The function chooses a starting step length of 1/10 of a wavelength of the carrier signal; this value is chosen partly for computational convenience, partly to ensure that the initial step is substantial shorter than the ¼ wavelength oscillation rate which is the shortest-wavelength variation possible in the likelihood. The algorithm then examines the objective function one step length away from the current search point in the direction of steepest descent and compares it to the objective function at the current search point. If the objective function one step away is smaller, then the new location becomes the current search point, and the process repeats, including the calculation of a new gradient to correct the direction of steepest descent.

If, in contrast, the objective function one step away is higher, then the step length is too long for the geometry in the vicinity of the current point; the current

point is not changed, and the gradient is not recalculated, but the step length is divided in half. The iteration then returns to evaluating the objective function at the prospective new point. The reason for this particular ordering of processes is to keep the step length as long as possible for as much of the calculation as possible, to avoid excessive iteration. As long as steps of a given size are not overshooting the range of validity of the local gradient estimate, they are retained; only when the local curvature becomes too variable is the step length shortened. Shortening the step length also determines when the search terminates; when the step length is reduced to a prescribed value, the steepest descent approach halts and declares the current search point to be the terminal point of the search.

In the next subsection are presented numerical results based on the implementation of H-DIRECT and DIRECT.

3.3.2 Implementation of the Optimization Algorithm

In this section, numerical examples are provided to illustrate the effectiveness of DIRECT and H-DIRECT for the source localization problem. DIRECT and H-DIRECT are tested for a setup with a source that emits an unknown signal with a 1 GHz carrier frequency and with a 200 kHz bandwidth. The emitted signal is collected by 8 sensors located arbitrarily around the source. The position of the source is unknown to the sensors, yet it is positioned at the coordinates [0.035, 0.055], and the searching area is 10×10 meters around the source. This choice was done such that the position is off the grid.

In Figure 3.3 are presented how DIRECT and H-DIRECT sampled the parameter space in order to find the global optimum. Both algorithms were stopped after the same number of function evaluations. Comparing the two figures one can observe that H-DIRECT samples the searching area more dens than DIRECT. This is because DIRECT spends more function evaluations in finding local optima than

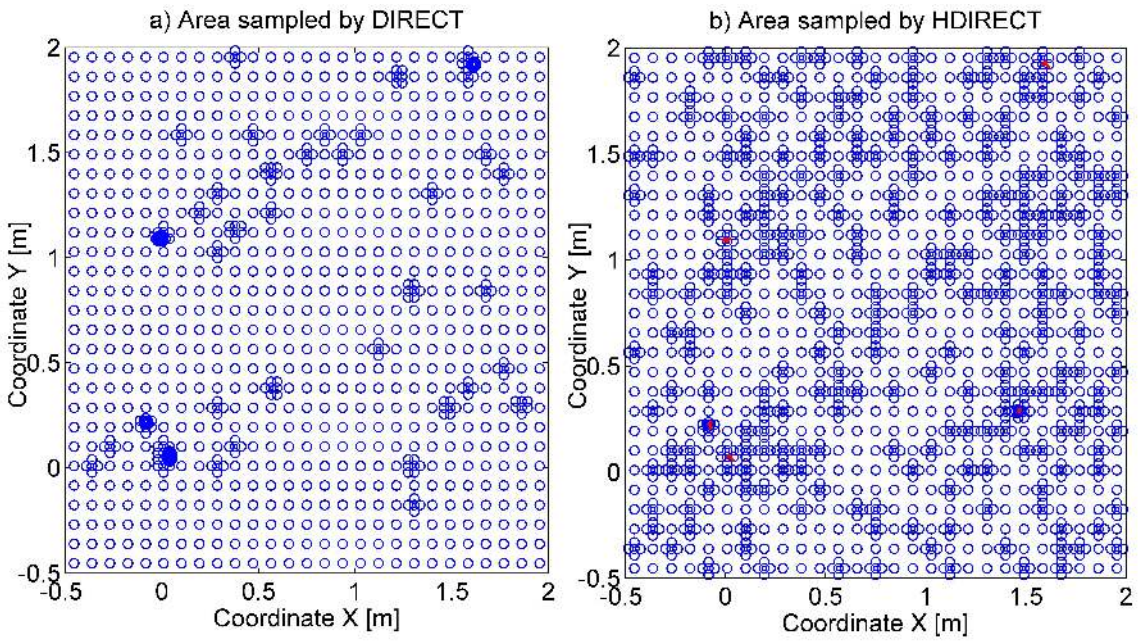

Figure 3.3 Searching area sampled by the two algorithms: DIRECT (left Figure) and H-DIRECT (right Figure). For the same number of function evaluations, H-DIRECT samples the searching area more dens than DIRECT.

H-DIRECT. A zoom around the position of the source, reveals the low convergence rate of DIRECT compared with H-DIRECT, Figure 3.4.

In Figure 3.5, the contour of the likelihood function is plotted, contour that was obtained using a very fine grid of 1 cm. The main lobe corresponding to the position of the source and three highest sidelobes are encircled. Comparing Figure 3.5 to Figure 3.3, one can observe that DIRECT and H-DIRECT can identify the main lobe and the three sidelobes of the likelihood function. Thus, the two algorithms are not stuck on some local optima.

Figure 3.6 shows the number of function evaluations required by DIRECT and H-DIRECT to converge to the global optimum of the localization likelihood function for the localization setup. H-DIRECT provides a reduction in the number of function evaluations by a factor of 2 compared to DIRECT. Moreover, the proposed algorithm compared to an exhaustive grid search performed for a grid space of 1 cm over the same searching area, results in 2 orders of magnitude of savings in function evaluations.

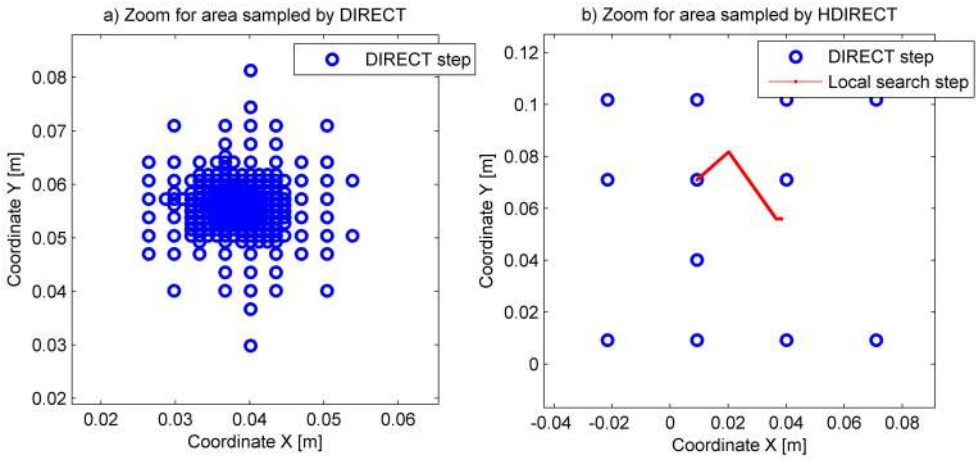

Figure 3.4 Zoom around source location of the searching areas sampled by the two algorithms: DIRECT (left Figure) and H-DIRECT (right Figure). DIRECT spends more function evaluations in finding local optima than H-DIRECT.

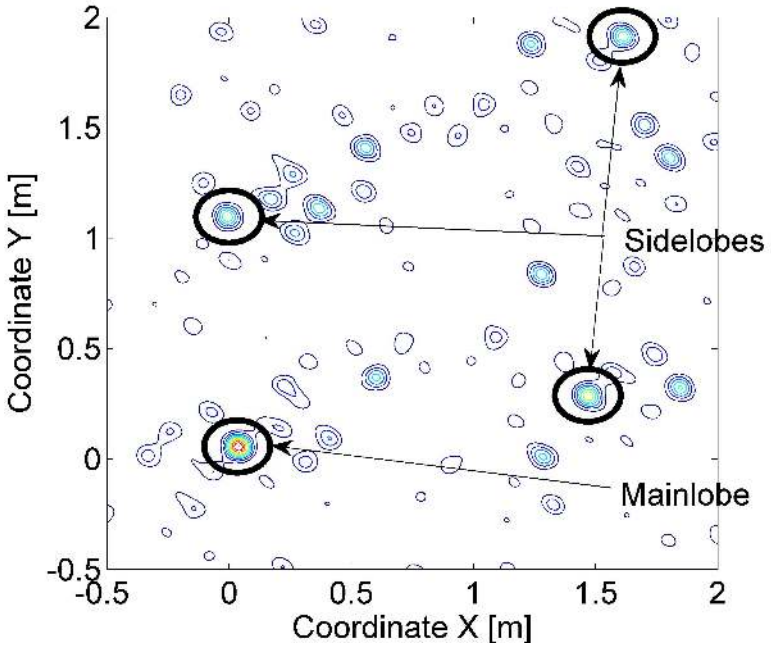

Figure 3.5 Contour of the likelihood function for the coherent localization problem. The main lobe corresponding to the position of the source and three highest sidelobes are encircled.

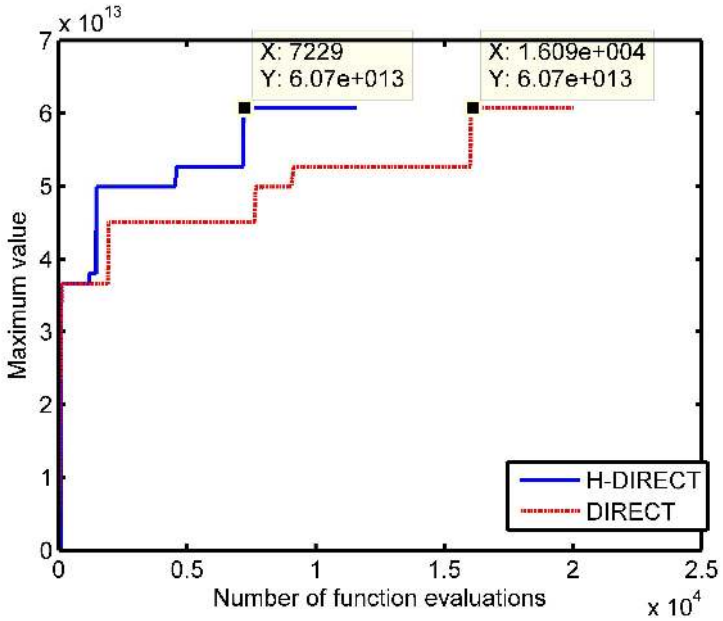

Figure 3.6 Number of function evaluations for DIRECT and H-DIRECT for finding the global optimum of the coherent localization problem

In order to predict the performance of MLE for different SNRs, Monte Carlo simulations need to be run. However, this is time consuming even with H-DIRECT algorithm. To alleviate this disadvantage, an analysis can be made based on a lower bound.

3.4 Cramer-Rao Lower Bound for Coherent Localization Estimation in Passive Systems

In the literature, one of the most popular bounds used to predict the performance of the MLE is the Cramer Rao lower bound (CRLB), [29]. The justification of using CRLB resides in that the MLE approaches the CRLB arbitrarily close for very long observations.

The CRLB of parameter estimated θ is given by [29]

$$C_{CRLB}(\theta) = \mathbf{J}^{-1}(\theta) \tag{3.9}$$

where

$$\mathbf{J}(\theta) \triangleq E_{\mathbf{r}|\theta}\left[\frac{\partial}{\partial\theta}\log\, p\left(\mathbf{r}|\theta\right)\left(\frac{\partial}{\partial\theta}\log\, p\left(\mathbf{r}|\theta\right)\right)^{T}\right] \tag{3.10}$$

is the Fisher information matrix (FIM). $p\left(\mathbf{r}|\theta\right)$ is the conditional pdf of $\mathbf{r}$ given θ and it is defined in (3.4), $E_{\mathbf{r}|\theta}\left[\cdot\right]$ stands for expectation with respect to $p\left(\mathbf{r}|\theta\right)$. In Appendix **??**, the following CRLB for passive coherent localization is derived

$$C_{CRLB} = \frac{c^2}{8\pi^2 BT\alpha f_c^2\left(1+\frac{B^2}{12f_c^2}\right)}\cdot g \tag{3.11}$$

where

$$\alpha = \frac{\left(\frac{P_s}{P_w}\sum_{k=1}^{M} a_k^2\right)^2}{1+\left(\frac{P_s}{P_w}\sum_{k=1}^{M} a_k^2\right)} \tag{3.12}$$

P_s and P_w are the power spectral densities of the transmitted signal and of the noise, T is the duration of observations, B is the bandwidth, f_c is the carrier frequency, and $a_k,\ k=1,\ldots,M$ are the attenuations. The term g incorporates the target's position with respect to the positions of the sensors, term known in the literature as geometric dilution of precision (GDOP) [61].

From (3.11) expression, it can be noted that for narrowband signals (i.e., $B \ll f_c$), the CRLB for estimating coherently the location coordinates $[x_e,\, y_e]$ is inverse proportionally with SNR (α), with carrier frequency (f_c), and with the number of samples (BT). Coherent localizations can provide accuracies proportional to the carrier frequency, due to the fact that the estimator exploits the phase differences information from pairs of sensors.

The CRLB, being a local bound error performance, i.e., it represents the performance of estimators only for small errors, doesn't capture the effect of sidelobes, and it can provide too optimistic performances. The effect of sidelobes over the performance of the estimator can be predicted by the ZZB.

3.5 Ziv-Zakai Lower Bound for Coherent Localization Estimation in Passive Systems

Recall from previous Chapter that the extended ZZB for vector parameter estimation in the case of equally likely hypotheses is given by

$$\mathbf{u}^T\mathbf{\Phi}\mathbf{u} \geq \int_0^\infty h \cdot V\left\{ \max_{\delta:\mathbf{u}^T\delta=h} \int_{\mathbf{\Theta}} \min[p_\theta(\varphi), p_\theta(\varphi+\delta)] \cdot P_\epsilon(\varphi, \varphi+\delta)d\varphi \right\} \cdot dh \tag{3.13}$$

where $V\{\cdot\}$ is the valley-filling function, and $\theta \in \mathbf{\Theta}$. Assuming uniform, *a priori* pdf's in the interval $[-D, D]$ for the x, y coordinates of the emitting source, equation (3.13) can be specialized as follows

$$\mathbf{u}^T\mathbf{\Phi}\mathbf{u} \geq \int_0^{2D} \frac{h}{4D^2} \cdot \left\{ \max_{\delta:\mathbf{u}^T\delta=h} \int_{\mathbf{\Theta}} P_\epsilon(\varphi, \varphi+\delta)d\varphi \right\} dh \tag{3.14}$$

As can be observed from (3.14), the main part of the bound is represented by $P_\epsilon(\varphi, \varphi+\delta)$. A closed form for $P_\epsilon(\varphi, \varphi+\delta)$ doesn't exist, however an approximation of P_ϵ can be obtained using Chernoff's formula [29, pp 125]:

$$P_\epsilon(\varphi, \varphi+\delta) \approx \frac{1}{2}\exp\left(\mu(s_m) + \frac{s_m^2}{2}\ddot{\mu}(s_m)\right) \cdot Q\left(s_m\sqrt{\ddot{\mu}(s_m)}\right) + \tag{3.15}$$

$$+ \frac{1}{2}\exp\left(\mu(s_m) + \frac{(1-s_m)^2}{2}\ddot{\mu}(s_m)\right) \cdot Q\left((1-s_m)\sqrt{\ddot{\mu}(s_m)}\right), \tag{3.16}$$

where $\mu(s)$ is the semi-invariant moment generating function, $\ddot{\mu}(s)$ is the second derivative of $\mu(s)$ with respect to s, s_m is the point for which $\dot{\mu}(s_m) = 0$, and $Q(z)$ is

the Gaussian integral

$$Q(z) = \int_z^\infty \frac{1}{\sqrt{2\pi}} e^{-v^2/2} dv$$

The semi-invariant moment generating function $\mu(s)$ is defined [29, pp 119]

$$\mu(s) = \ln \int p(\mathbf{r}|\varphi + \delta)^s p(\mathbf{r}|\varphi)^{1-s} d\mathbf{R} \tag{3.17}$$

Substituting the expression for $p(\mathbf{r}|\theta)$ given in (3.4) into (3.17), and using the result from [62, pp 47], the semi-invariant moment generating function can be rewritten as follows

$$\begin{aligned} \mu(s) = -\frac{1}{2} \sum_{l=1}^{N} \ln \big(& \det[\mathbf{K}(f_l)]^{-s} \det[\mathbf{K}_\delta(f_l)]^{-(1-s)} \\ & \cdot \det[s\mathbf{K}(f_l, \tau) + (1-s)\mathbf{K}_\delta(f_l)] \big) \end{aligned} \tag{3.18}$$

where

$$\begin{aligned} \mathbf{K}_\delta(f_l) &= P_s \gamma_\delta(f_l) {\gamma_\delta}^H(f_l) + P_w \mathbf{I} \\ \gamma_\delta(f_l) &= [1, \ldots, a_M e^{-j2\pi(f_l + f_c)(\tau_M + d_M)}]^T \\ d_k &= \frac{1}{c} \left(\sqrt{(x_e + \delta_x - x_k)^2 + (y_e + \delta_y - y_k)^2} - \right. \\ &\quad \left. - \sqrt{(x_e + \delta_x - x_1)^2 + (y_e + \delta_y - y_1)^2} \right) - \\ &\quad - \frac{1}{c} \left(\sqrt{(x_e - x_k)^2 + (y_e - y_k)^2} - \right. \\ &\quad \left. - \sqrt{(x_e - x_1)^2 + (y_e - y_1)^2} \right), \quad k = 2, \ldots, M \end{aligned} \tag{3.19}$$

The first two determinants from equation (3.18) can be easily calculated using the matrix formula given in [4], and they are given by

$$\det[\mathbf{K}(f_l)] = P_w^M \left(1 + \frac{P_s}{P_w} \beta \right) = \det[\mathbf{K}_\delta(f_l)] \tag{3.20}$$

where

$$\beta = \left(1 + \sum_{k=2}^{M} a_k^2\right) \tag{3.21}$$

The derivation of the third determinant can be done using the approach in [63]. After some algebra, the following expression is obtained for the third determinant

$$\det[s\mathbf{K}(f_l) + (1-s)\mathbf{K}_\delta(f_l)] = P_w^M \left(1 + \frac{P_s}{P_w}\beta + s(1-s)\left(\frac{P_s}{P_w}\right)^2 \left(\beta^2 - g(f_l)\right)\right) \tag{3.22}$$

where

$$g(f_l) = \frac{|\gamma_\delta^H(f_l)\gamma(f_l)|^2}{\beta^2}$$

and $|\cdot|$ denotes the absolute value.

Substitution of (3.20) and (3.22) into (3.18) gives

$$\mu(s) = -\sum_{l=1}^{N} \ln\left(1 + s(1-s)\alpha\left(1 - g(f_l)\right)\right) \tag{3.23}$$

where

$$\alpha = \frac{\beta^2\left(\frac{P_s}{P_w}\right)^2}{1 + \beta\left(\frac{P_s}{P_w}\right)}. \tag{3.24}$$

Differentiating with respect to s yields

$$\dot{\mu}(s) = -\sum_{l=1}^{N} \frac{(1-2s)\,\alpha\left(1 - g(f_l)\right)}{1 + s(1-s)\alpha\left(1 - g(f_l)\right)} \tag{3.25}$$

$$\ddot{\mu}(s) = \sum_{l=1}^{N}\left[\left(\frac{(1-2s)\,\alpha\left(1 - g(f_l)\right)}{1 + s(1-s)\alpha\left(1 - g(f_l)\right)}\right)^2 + \frac{2\alpha\left(1 - g(f_l)\right)}{1 + s(1-s)\alpha\left(1 - g(f_l)\right)}\right]. \tag{3.26}$$

Solving the equation $\dot{\mu}(s) = 0$, results in $s = \frac{1}{2}$. For $s = \frac{1}{2}$, equations (3.23) and (3.26) reduce to

$$\begin{aligned}\mu\left(\frac{1}{2}\right) =& -\sum_{l=1}^{N} \ln\left(1+\frac{1}{4}\alpha\left(1-g(f_l)\right)\right) \xrightarrow{BT\gg 1} \\ & -T\int_{-B/2}^{B/2} \ln\left(1+\frac{1}{4}\alpha\left(1-g(f)\right)\right) df \\ \ddot{\mu}\left(\frac{1}{2}\right) =& \sum_{l=1}^{N} \frac{2\alpha\left(1-g(f_l)\right)}{1+\frac{1}{4}\alpha\left(1-g(f_l)\right)} \xrightarrow{BT\gg 1} \\ & T\int_{-B/2}^{B/2} \frac{2\alpha\left(1-g(f)\right)}{1+\frac{1}{4}\alpha\left(1-g(f)\right)} df. \end{aligned} \tag{3.27}$$

Using the notation

$$\xi(f) = \frac{1}{4}\alpha\left(1-g(f)\right),$$

$\mu(\frac{1}{2})$ and $\ddot{\mu}(\frac{1}{2})$ have the following forms

$$\begin{aligned}\mu(\frac{1}{2}) &= -T\int_{-B/2}^{B/2} \ln\left(1+\xi(f)\right) df, \\ \ddot{\mu}(\frac{1}{2}) &= T\int_{-B/2}^{B/2} 8\frac{\xi(f)}{1+\xi(f)} df. \end{aligned} \tag{3.28}$$

Using (3.28) and the following inequalities

$$\begin{aligned}\ln(1+z) - z &\le \frac{1}{2}z^2, \ \text{ for } 0 \le z \le 1 \\ \frac{z}{1+z} &\le z, \ \text{ for } 0 \le z \le 1 \end{aligned} \tag{3.29}$$

in (3.16), $P_\epsilon(\varphi, \varphi+\delta)$ is lower bounded by:

$$P_\epsilon(\varphi, \varphi+\delta) \ge \exp\left(-T\int_F \frac{1}{2}\xi^2(f) df\right) \cdot Q\left(\sqrt{2T\int_F \xi(f) df}\right) \tag{3.30}$$

It is noted that $P_\epsilon(\varphi, \varphi+\delta)$ doesn't depend on φ, but only on δ.

The final version of the ZZB lower bound for location estimate is:

$$\mathbf{u}^T\mathbf{\Phi u} \geq \frac{1}{4D^2}\int_0^{2D} h \cdot \left\{ \max_{\delta:\mathbf{u}^T\delta=h} (2D-u_1\delta_1)(2D-u_2\delta_2) \right.$$
$$\left. \cdot \exp\left(-T\int_F \frac{1}{2}\xi^2(f)df\right) Q\left(\sqrt{2T\int_F \xi(f)df}\right)\right\} dh, \tag{3.31}$$

where

$$\xi(f) = \frac{1}{4}\alpha\left(1 - \frac{|{\gamma_\delta}^H(f)\gamma(f)|^2}{\beta^2}\right),$$
$$\alpha = \frac{\beta^2\left(\frac{P_s(f)}{P_w(f)}\right)^2}{1+\beta\left(\frac{P_s(f)}{P_w(f)}\right)}, \text{ and } \quad \beta = \left(1+\sum_{k=2}^{M} a_k^2\right).$$

3.6 Numerical Examples

In this section, numerical examples are provided to illustrate the ZZB for various cases of the source localization problem. The numerical results show the ZZB parameterized by the carrier frequency, bandwidth, and number of sensors. The setup has sensors equally spaced on a circle with a source located at the center of the circle. The duration of the observation was taken to be $T = 4.3$ milliseconds.

In Figure 3.6, the ZZB obtained by numerical integration of (3.31) is plotted versus the SNR per sensor, P_s/P_w. The CRLB and the root mean square error (RMSE) of the MLE of the source location are also plotted for reference. The CRLB for the coherent passive localization is derived in Appendix **??**. The RMSE of the MLE is computed from one thousand simulations of a sequence of raised cosine pulses. The various metrics were calculated for eight sensors, bandwidth $B = 200$ kHz, and for a carrier frequency $f_c = 100$ MHz. The *a priori* interval for the coordinates of the source is set to a square with a side equal to 50 m. From the figure, it can be observed that the ZZB versus SNR can be divided into three regions. For low SNR, the ZZB reaches a plateau equal to the standard deviation of the *a priori* pdf of the source location, computed as $\sqrt{\frac{D^2}{3}} = \frac{25}{\sqrt{3}}$. In this region performance is dominated

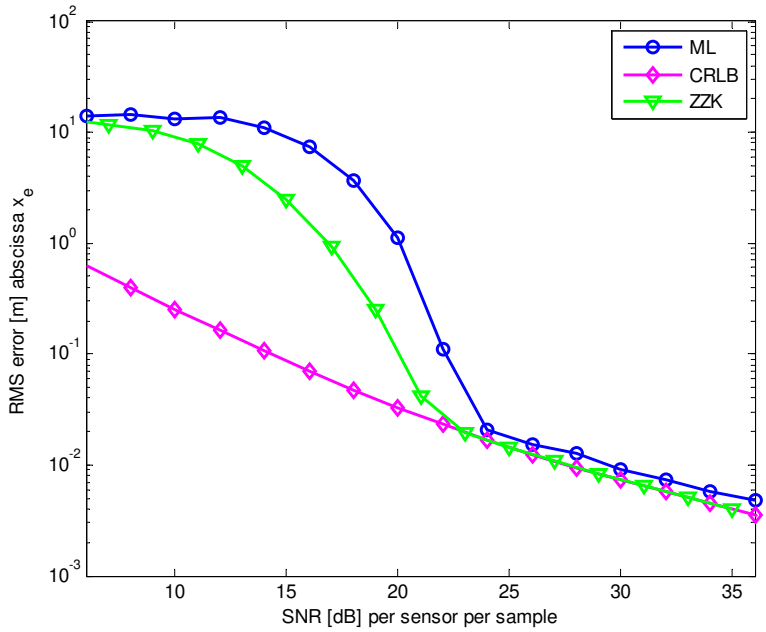

Figure 3.7 ZZB for passive coherent localization plotted versus SNR. ZZB is tight to the performance of MLE over the whole SNR range.

by noise, hence the localization error is limited only by the *a priori* information. For high SNR, the ZZB coincides with the CRLB, indicating that the noise errors are too small to cast the estimate outside the main lobe of the estimation metric. This region is the ambiguity free region. Between the two SNR extremes is the ambiguity region, in which the location estimator is affected by ambiguities created by sidelobes of the localization metric, [54].

In Figure 3.8, the ZZB of the error in estimating the abscissa x_e of the source is presented for different carrier frequencies. The results presented in the figure were obtained for eight sensors and $B = 200$ kHz signal bandwidth. The *a priori* interval for the abscissa x_e of the narrowband source was set to [-250 m, 250 m] around the real abscissa. One can observe that if the SNR is high enough, localization accuracy improves with the carrier frequency. The exception is in the ambiguity region in which the performance of the estimator at $f_c = 100$ MHz may outperform the performance at $f_c = 1$ GHz. This result can be explained due to the increase in sidelobes with the

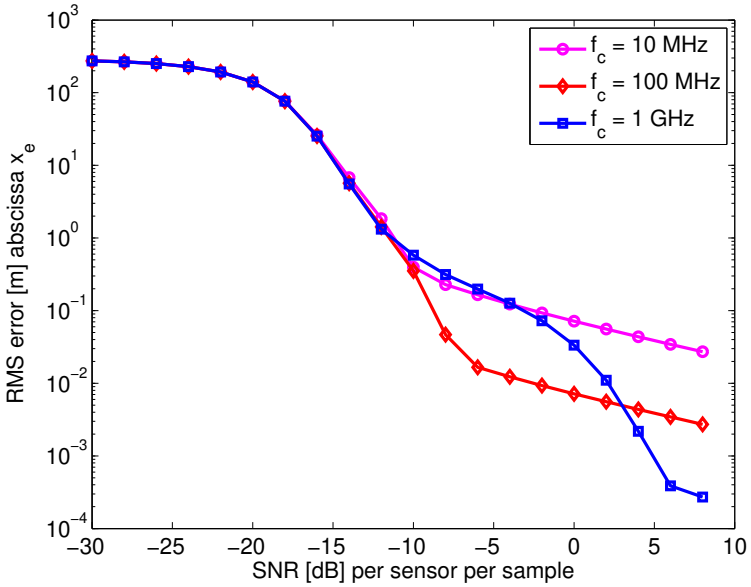

Figure 3.8 ZZB computed for different carrier frequencies. Increasing the carrier frequency increases the accuracy at high SNR, but also increases the ambiguity region.

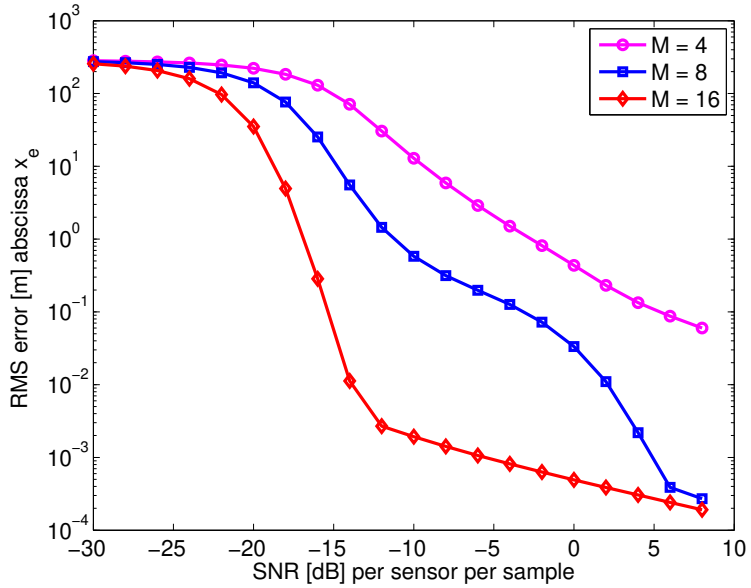

Figure 3.9 ZZB computed for different number of sensors. Increasing the number of sensors reduces the effect of sidelobes

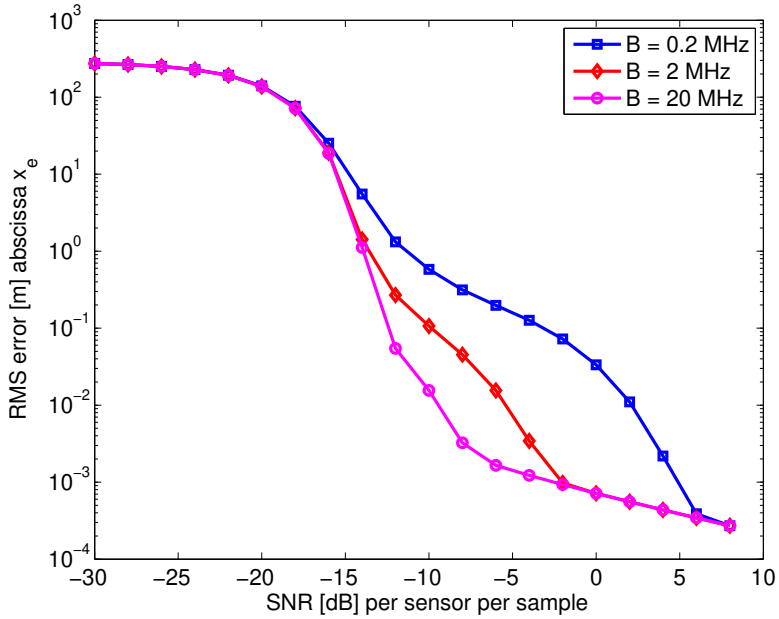

Figure 3.10 ZZB computed for different bandwidths. The effect of sidelobes can be reduced by increasing the bandwidth.

carrier frequency. The effect of sidelobes in the localization metric can be reduced by increasing the number of sensors. This is illustrated in Figure 3.9. The effect of bandwidth on localization is shown in Figure 3.10. An increase in bandwidth causes a reduction in the sidelobes leading to smaller errors in the ambiguity region. This is due to the fact that the transmitted pulse autocorrelation function serves as the envelope of the localization metric. This envelope, which becomes narrower with the increase in bandwidth, forces the sidelobes to decay faster.

In summary, the ZZB provides a smart way to analyze coherent localization performance at the full range of SNR values and parameterized by the quantities of interest such as carrier frequency, signal bandwidth, and number of sensors. Numerical examples demonstrate that the bound provides results close to the MLE over the whole SNR range. Three SNR regions are distinguishable for the bound. At low SNR, performance is dominated by noise with false peaks popping up anywhere in the a priori parameter space of the source location. As the SNR increases, a transition

region is observed in which performance is dominated by the peak sidelobes of the localization metric. The performance at high SNR is ambiguity free, and the ZZB coincides with the CRLB.

CHAPTER 4

COHERENT LOCALIZATION IN ACTIVE SYSTEMS

In Chapter 3, the coherent localization performed by passive sensors was analyzed with ZZB. In this chapter, a similar analysis is done for coherent localization performed by MIMO radar systems. MIMO radar systems represent active systems employing multiple antennas, and can transmit multiple waveforms, via its antennas, and process jointly echos received at multiple received antennas.

4.1 System Model

Similar to the passive case, a target is considered located at an unknown position $\theta = [x_e, y_e]$, where the unknown coordinates are assumed to be uniform distributed $x_e,\ y_e \sim U[-D,\ D]$. The target is radiated by M transmitting radars arbitrarily located at coordinates $\mathbf{T}_i = [x_{ti}, y_{ti}]$, $i = 1, \ldots, M$, with a set of orthogonal signals, s_i. For the active systems, the transmitted signals are assumed to be deterministic signals, versus the assumption made for passive systems where, the transmitted signal was assumed to be stochastic. Moreover, it is assumed that the orthogonality between different transmitted signals is maintained for all relevant delays. The transmitted signals have bandwidth B, and they modulate a carrier frequency f_c. The signals scattered by the target are collected by N sensors placed at arbitrary positions $\mathbf{R}_k = [x_{rk}, y_{rk}]$, $k = 1, \ldots, N$. The transmitting radars, and the sensors are assumed to be synchronous in time and phase. The period of time T during which the observations are collected is such that $BT \gg 1$. Based on the noisy observations collected, the location of the target is estimated coherently i.e., the location is estimated from amplitude and phase measurements.

The noisy observations of the signals received at the sensors are expressed by:

$$r_k(t) = \sum_{i=1}^{M} a_{i,k} s_i(t - \tau_{i,k}) e^{-j2\pi f_c \tau_{i,k}} + w_k(t) \tag{4.1}$$

where s_i and w_k denote respectively, the signal transmitted by the i-th transmitting radar, and additive noise at the k-th sensor. The transmitted signals are deterministic signals with power P_{si}, $i = 1, \ldots, M$. The noise waveforms are sample functions of uncorrelated, zero-mean, stationary Gaussian random processes with spectral density P_w, respectively. The spectral densities are constant across the bandwidth. The amplitude and the propagation delay of the signal transmitted by the i-th transmitting radar and received at k-th sensor are denoted $a_{i,k}$ and $\tau_{i,k}$, respectively. It is assumed that the amplitudes $a_{i,k}$ are known or can be estimated based on a priori rough information on the target location. The propagation delay $\tau_{i,k}$ is the sum of the time delays from radar i to the target and from target to sensor k. Using $\rho_{ti} = \|\mathbf{T}_i - \theta\|$ for the distance between the transmitting radar at $\mathbf{T}_i$ and the target, and $\rho_{rk} = \|\mathbf{R}_k - \theta\|$ for the distance between the target and the receiving radar located at $\mathbf{R}_k$, $\tau_{i,k}$ can be expressed as:

$$\tau_{i,k} = \frac{1}{c}(\rho_{ti} + \rho_{rk}), \tag{4.2}$$

where c is the signal propagation speed.

Analysis in the frequency domain is more convenient than in the time domain because in the frequency domain the time delays appear in the argument of the complex exponential function. To make use of properties of the Fourier transform, the time domain measurements are converted to the frequency domain. The f_l Fourier coefficient of the observed signal at sensor k is given by:

$$R_k(f_l) = \frac{1}{\sqrt{T}} \int_0^T r_k(t)\, e^{-j2\pi f_l t} dt = \\ = \sum_{i=1}^{M} a_{i,k} S_i(f_l) e^{-j2\pi(f_l+f_c)\tau_{i,k}} + W_k(f_l) \tag{4.3}$$

where $l = 1, \ldots, L$, L is the number of frequency samples, and $S_i(f_l)$ and $W_k(f_l)$ are the Fourier coefficients at f_l of $s_i(t)$ and $w_k(t)$, respectively. For simplicity, the following notation is used $\mathbf{r} = [\mathbf{r}^T(f_1), \mathbf{r}^T(f_2), \ldots, \mathbf{r}^T(f_L)]^T$, where $\mathbf{r}(f_l) = [R_1(f_l), R_2(f_l), \ldots, R_N(f_l)]^T$. For $BT \gg 1$, any pair of Fourier coefficients is uncorrelated [55]. Because $r_k(t)$ is a Gaussian process and the Fourier transform is a linear operation, $\mathbf{r}$ has a conditional multivariate Gaussian pdf,

$$p(\mathbf{r}|\theta) = \prod_{l=1}^{L} \frac{1}{\det(\pi \mathbf{K}(f_l))} \\ \cdot \exp\left\{ -([\mathbf{r}(f_l) - \gamma(f_l)]^H \boldsymbol{K}^{-1}(f_l)([\mathbf{r}(f_l) - \gamma(f_l)] \right\} \tag{4.4}$$

where

$$\gamma(f_l) = \left[\sum_{i=1}^{M} a_{i,1} S_i(f_l) e^{-j2\pi(f_l+f_c)\tau_{i,1}}, \ldots, \sum_{i=1}^{M} a_{i,N} S_i(f_l) e^{-j2\pi(f_l+f_c)\tau_{i,N}} \right]^T \tag{4.5}$$

represents the response across the sensors to a radiated frequency component $(f_c + f_l)$, and $\mathbf{K}(f_l) = P_w(f_l)\mathbf{I}$ represents the covariance matrix of the Fourier coefficients at the sensors. The matrix $\mathbf{I}$ is the identity matrix. The superscripts "T" and "H" denote the transpose and conjugate transpose operations, respectively.

The maximum likelihood estimate of the source location is given by the maximum of the likelihood function

$$\widehat{\theta}_{ML}(\mathbf{r}) = \arg\max_{\theta} p(\mathbf{r}|\theta) \tag{4.6}$$

where the likelihood function equals the value of the pdf at the observations $\mathbf{r}$. It can be shown that for the model defined in (4.4), the MLE of θ is given by the expression:

$$\hat{\theta}_{ML}(\mathbf{r}) = \arg\max_{\theta} \sum_{k=1}^{N} \sum_{i=1}^{M} a_{i,k}^{*} e^{j2\pi f_c \tau_{i,k}} \cdot \sum_{l=1}^{L} R_k(f_l) S_i^{*}(f_l) e^{j2\pi f_l \tau_{i,k}} \tag{4.7}$$

The term $e^{j2\pi f_c \tau_{i,k}}$ that is the phase information reveals the coherent nature of the estimator. It is well known that a linear phased array in which the elements are highly thinned, has a beampattern with large sidelobes. In particular, when the elements of the array are randomly spaced at intervals of the order of 10's or 100's of wavelengths, the beampattern has random peak sidelobes [64]. Recent work on coherent MIMO radar based in a setting of widely spaced transmitters and receivers also shows the presence of large peak sidelobes [54]. This motivates the derivation of the ZZB on the coherent active localization performance, as presented in the next section.

4.2 Ziv-Zakai Lower Bound for Coherent Localization Estimation in Active Systems

Assuming uniform *a priori* pdf's in the interval $[-D,\ D]$ for the x_e, y_e coordinates of the target, the general expression of ZZB (2.14) can be specialized as follows

$$\mathbf{u}^T \mathbf{\Phi} \mathbf{u} \geq \int_0^{2D} \frac{h}{4D^2} \cdot \left\{ \max_{\delta : \mathbf{u}^T \delta = h} \int_{\mathbf{\Theta}} P_\epsilon(\varphi, \varphi + \delta) d\varphi \right\} dh \tag{4.8}$$

As can be observed from Expression (4.8), the main part of the bound is represented by $P_\epsilon(\varphi, \varphi + \delta)$. The optimum test for a binary hypothesis problem is known to be the likelihood ratio test, but evaluating the performance of the test does not always result in tractable expressions. When exact calculation of the probability of error is not possible, an asymptotic approximation can be applied instead, [62]. Using this approach, the following approximation for $P_\epsilon(\varphi, \varphi + \delta)$ is obtained [29, pp 125]:

$$P_e(\varphi, \varphi+\delta) = \exp\left(\mu(s_m) + \frac{s_m^2}{2}\ddot{\mu}(s_m)\right) Q\left(s_m\sqrt{\ddot{\mu}(s_m)}\right) \tag{4.9}$$

where $\mu(s)$ is the semi-invariant moment generating function of the likelihood ratio test associated with the binary hypothesis problem between φ and $\varphi+\delta$, $\ddot{\mu}(s)$ is the second derivative of $\mu(s)$ with respect to s, s_m is the point for which $\dot{\mu}(s_m) = 0$, and $Q(z)$ is the Gaussian integral

$$Q(z) = \int_z^\infty \frac{1}{\sqrt{2\pi}} e^{-v^2/2} dv$$

The semi-invariant moment generating function $\mu(s)$ can be expressed [29, pp 119]

$$\mu(s) = \ln \int p(\mathbf{r}|\varphi+\delta)^s p(\mathbf{r}|\varphi)^{1-s} d\mathbf{R} \tag{4.10}$$

Substituting the expression for $p(\mathbf{r}|\theta)$ given in (4.4) into (4.10), and using the result from [62, pp 47], the semi-invariant moment generating function can be rewritten as follows

$$\mu(s) = -\frac{s(1-s)}{2} \cdot \sum_{l=1}^{L} \frac{1}{P_w(f_l)} [\gamma_{(\mathbf{1})}(f_l) - \gamma_{(\mathbf{0})}(f_l)]^H [\gamma_{(\mathbf{1})}(f_l) - \gamma_{(\mathbf{0})}(f_l)] \tag{4.11}$$

where

$$\gamma_{(\mathbf{0})}(f_l) = \left[\sum_{i=1}^{M} a_{i,1} S_i(f_l) e^{-j2\pi(f_l+f_c)\tilde{\tau}_{i,1}}, \ldots, \sum_{i=1}^{M} a_{i,N} S_i(f_l) e^{-j2\pi(f_l+f_c)\tilde{\tau}_{i,N}}\right]^T \tag{4.12}$$

and

$$\gamma_{(\mathbf{1})}(f_l) = \left[\sum_{i=1}^{M} a_{i,1} S_i(f_l) e^{-j2\pi(f_l+f_c)(\tilde{\tau}_{i,1}+d_{i,1})}, \ldots, \sum_{i=1}^{M} a_{i,N} S_i(f_l) e^{-j2\pi(f_l+f_c)(\tilde{\tau}_{i,N}+d_{i,N})} \right]^T \tag{4.13}$$

In these expressions, $d_{i,k}$ represents the difference in propagation delays along the paths i-$\varphi+\delta$-k and i-φ-k. The term $d_{i,k}$ is given by:

$$d_{i,k} = \frac{1}{c}(\rho_{ti1} + \rho_{rk1} - \rho_{ti0} - \rho_{rk0})$$

where $\rho_{ti1} = \|\mathbf{T}_i - \varphi + \delta\|$, $\rho_{rk1} = \|\mathbf{R}_k - \varphi + \delta\|$, $\rho_{ti0} = \|\mathbf{T}_i - \varphi\|$, and $\rho_{rk} = \|\mathbf{R}_k - \varphi\|$. Because φ represents the true target location and $\varphi+\delta$ represents an erroneous target location, it follows that $d_{i,k}$ are time delay terms associated with erroneous target locations.

Differentiating equation (4.11) with respect to s yields:

$$\dot{\mu}(s) = -\frac{1-2s}{2} \cdot \sum_{l=1}^{L} \frac{1}{P_w(f_l)} [\gamma_{(\mathbf{1})}(f_l) - \gamma_{(\mathbf{0})}(f_l)]^H [\gamma_{(\mathbf{1})}(f_l) - \gamma_{(\mathbf{0})}(f_l)] \tag{4.14}$$

Differentiating once again,

$$\ddot{\mu}(s) = \sum_{l=1}^{L} \frac{1}{P_w(f_l)} [\gamma_{(\mathbf{1})}(f_l) - \gamma_{(\mathbf{0})}(f_l)]^H [\gamma_{(\mathbf{1})}(f_l) - \gamma_{(\mathbf{0})}(f_l)] \tag{4.15}$$

Solving $\dot{\mu}(s_m) = 0$, yields $s_m = \frac{1}{2}$. Substituting $\mu(s_m)$, $\ddot{\mu}(s_m)$ and $s_m = \frac{1}{2}$ into (4.9), results in:

$$P_e(\varphi, \varphi+\delta) = Q\left(\frac{1}{2}\sqrt{\ddot{\mu}\left(\frac{1}{2}\right)}\right) \tag{4.16}$$

Using the fact that the transmitted signals are orthogonal to each other, and $BT \gg 1$, $\ddot{\mu}(s_m)$ is:

$$\ddot{\mu}\left(\frac{1}{2}\right) = 2BT\sum_{k=1}^{N}\sum_{i=1}^{M} a_{i,k}^2 \frac{P_{si}}{P_w}\left[1 - \frac{\sin(\pi B d_{i,k})}{\pi B d_{i,k}}\cos(2\pi f_c d_{i,k})\right] \tag{4.17}$$

The final version of the ZZB lower bound for the location estimate is:

$$\begin{aligned}\mathbf{u}^T\Phi\mathbf{u} =& \frac{1}{4D^2}\cdot\int_0^{2D} h\left\{\max_{\delta:\mathbf{u}^T\delta=h}\right. \\ & \left.(2D-u_1\delta_1)(2D-u_2\delta_2)Q\left(\frac{1}{2}\sqrt{\ddot{\mu}\left(\frac{1}{2}\right)}\right)\right\}dh\end{aligned} \tag{4.18}$$

Note that $\ddot{\mu}\left(\frac{1}{2}\right)$ in (4.17) depends on the distance h between hypotheses through the terms $d_{i,k}$. Further insight can be gained by observing that the ZZB decreases with the probability of error $P_e(\varphi, \varphi+\delta)$ (see (4.8)) and that $P_e(\varphi, \varphi+\delta)$ is monotonically decreasing with the argument of the Gaussian integral, i.e., with $\ddot{\mu}\left(\frac{1}{2}\right)$. A closer inspection of $\ddot{\mu}\left(\frac{1}{2}\right)$ in ((4.17)) is then warranted. For a transmitter-receiver pair i-k, the factor $2BTa_{i,k}^2\frac{P_{si}}{P_w}$ serves as an SNR term. Not surprisingly, increasing the SNR, reduces the MSE of localization. More interesting is the factor $\psi(\delta)$,

$$\psi(\delta) = \sum_{k=1}^{N}\sum_{i=1}^{M}\frac{\sin(\pi B d_{i,k})}{\pi B d_{i,k}}\cos(2\pi f_c d_{i,k}) \tag{4.19}$$

This factor has peaks at time delays $d_{i,k}$ that are multiples of $1/f_c$. Each peak represents a location associated with an increased probability of error. Thus peaks of $\psi(\delta)$ correspond to ambiguities marked by peaks sidelobes in the localization metric (4.7). Increasing the carrier frequency increases the density of ambiguities over an area, and indirectly the MSE for SNR regions where the ambiguities dominate. The term $\frac{\sin(\pi B d_{i,k})}{\pi B d_{i,k}}$ corresponds to the autocorrelation of a transmitted pulse (assumed rectangular). This term caps the effect of ambiguities, particularly away from the mainlobe of the localization metric. The effect of ambiguities is reduced by increasing the bandwidth B of the transmitted signals. This observation is consistent with [65].

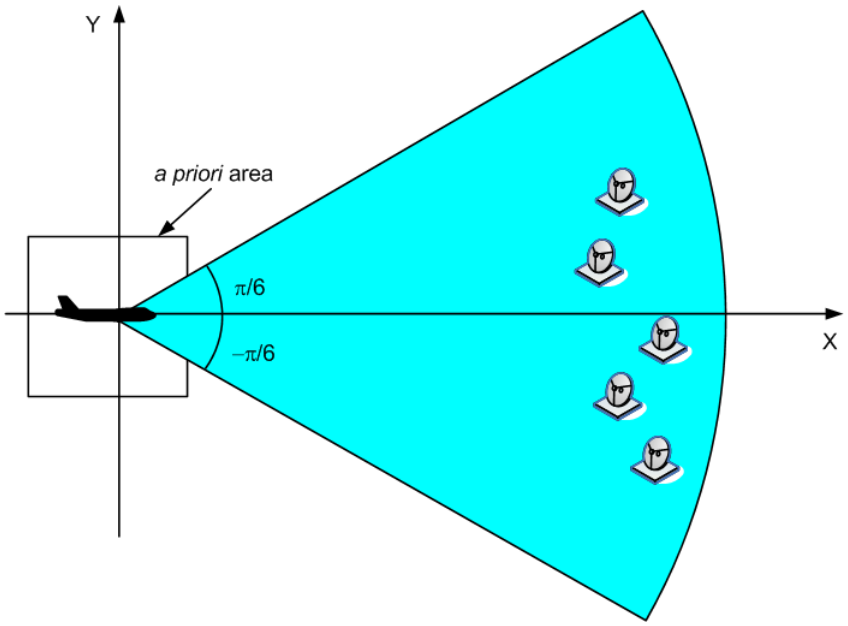

Figure 4.1 Setup configuration of the MIMO radar system with antennas distributed in a sector.

Ambiguity sidelobes affect the ZZB when they are large enough to compete with the mainlobe of the localization metric. Increasing the number of transmitting stations M and receiving stations N, reduces the effect of ambiguities relative to the mainlobe. To explain that, we note that each transmitter-receiver pair has its own pattern of ambiguities. Ambiguities impact performance when ambiguities from multiple transmitter-receiver pairs happen to build up at a specific location. Increasing the number of radars leads to a stronger mainlobe and requires that a larger number of sidelobes build up to compete with the mainlobe. Since the sidelobe build up from multiple transmitter-receiver pairs is a random event, the chances of a large number of sidelobes lining up at one location are small. Thus performance improves with an increase in the number of radars.

4.3 Numerical Examples

The numerical results were obtained for a setup in which the target was positioned in the center of the coordinate system. The transmitting and receiving radars were

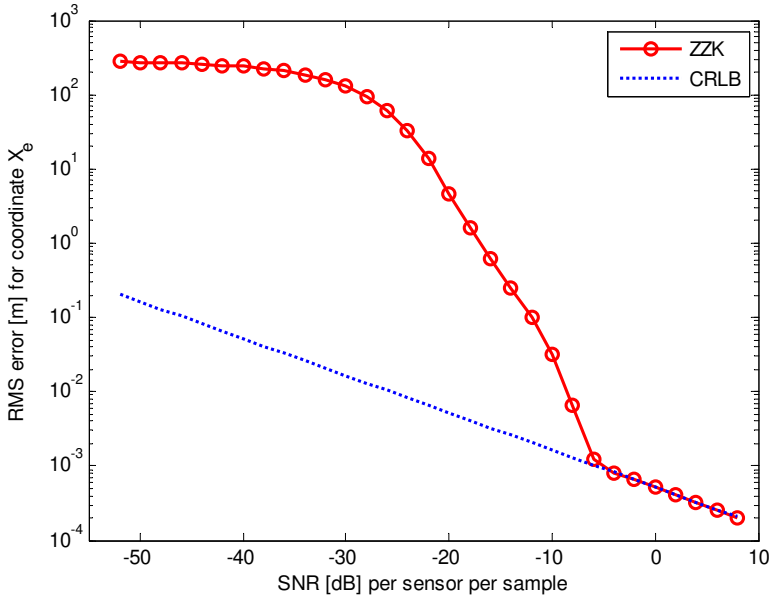

Figure 4.2 ZZK for active coherent localization plotted versus SNR. At high SNR, ZZB coincides with CRLB.

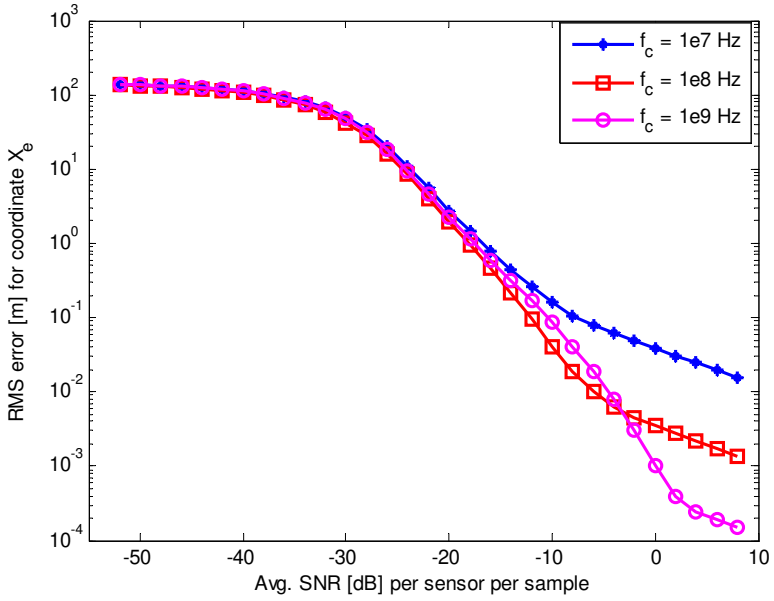

Figure 4.3 ZZB computed for different carrier frequencies. Localization accuracy improves with the carrier frequency at high SNR

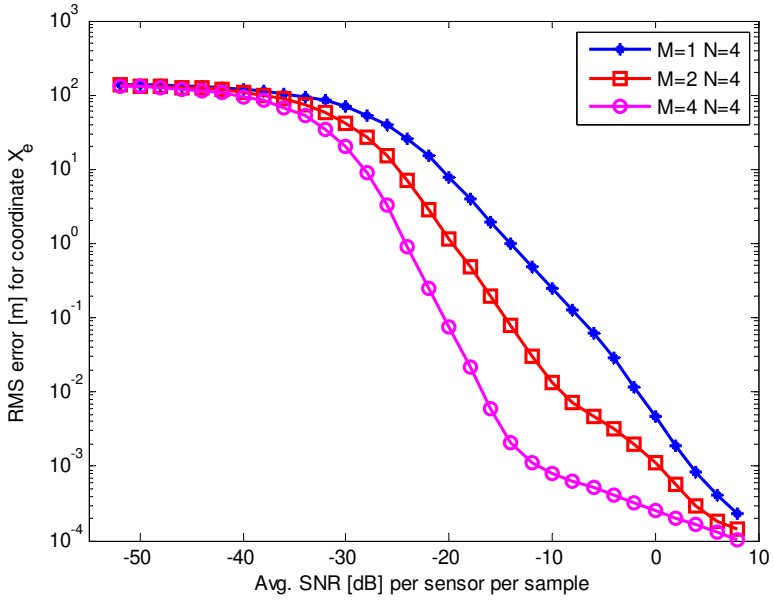

Figure 4.4 ZZB computed for different radar configurations. Localization accuracy improves with the increase in the number of antennas

distributed randomly in a sector with center at the origin of the axes $(0, 0)$ and with a central angle of $\pi/3$ radians. The ZZB was computed numerically by averaging over 30 random setups (different radar configurations). The setup is shown in Figure 4.1. The duration of the observation T was taken such that $BT = 625$ samples, where B is the bandwidth in Hz.

In Figure 4.2, the ZZB obtained by numerical integration of (4.18) is plotted versus the SNR, SNR$= \frac{P_{si}}{P_w}$ for a 2×4 MIMO configuration (two transmit and four receive antennas) and transmitted signals with bandwidth $B = 200$ kHz and carrier $f_c = 1$ GHz. The CRLB of the target location is also plotted for reference. The *a priori* interval for the coordinates of the source is set to a square with a side equal to 1 km. From the figure it can be observed that the ZZB versus SNR can be divided into three regions. For low SNR, the ZZB reaches a plateau equal to the standard deviation of the *a priori* pdf of the source location, computed as $\sqrt{\frac{D^2}{3}} = \frac{500}{\sqrt{3}}$. In this region performance is dominated by noise, hence the localization error is limited

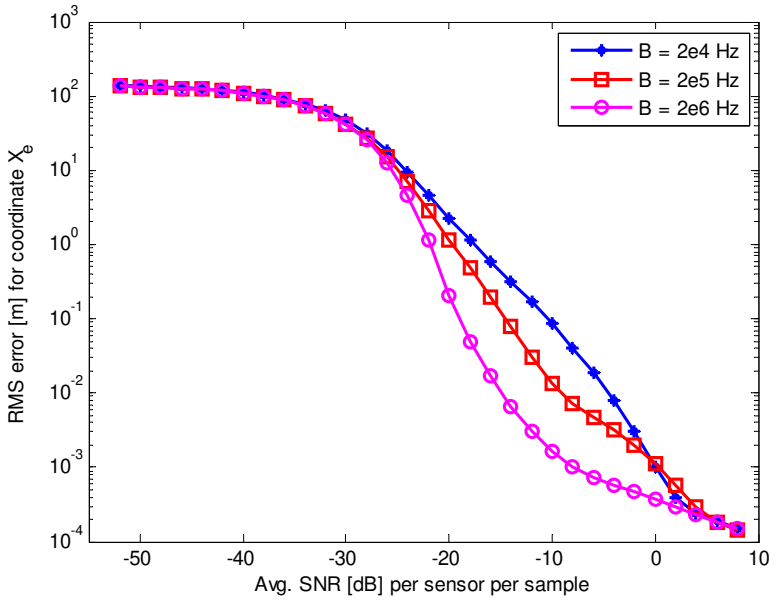

Figure 4.5 ZZB computed for different bandwidths. The effect of sidelobes can be reduced by increasing the bandwidth.

only by the *a priori* information. For high SNR, the ZZB merges with the CRLB, indicating that the noise errors are too small to cast the estimate outside the mainlobe of the localization metric. This region is the ambiguity free region. Between the two SNR extremes, is the ambiguity region, in which the location estimator is affected by ambiguities created by sidelobes of the localization metric, [54].

In Figure 4.3, the ZZB of the error in estimating the abscissa x_e of the source is presented for different carrier frequencies. The results presented in the figure were obtained for a 2×4 MIMO system and $B = 200$ kHz signal bandwidth. The *a priori* interval for the abscissa x_e of the narrowband source was set to [-500 m, 500 m] around the real abscissa. One can observe that if the SNR is high enough, localization accuracy improves with the carrier frequency. As predicted by the discussion in the preceding section, in the ambiguity region, the performance degrades with increasing carrier frequency. This result is explained by the increase in sidelobes with the carrier frequency. The effect of sidelobes in the localization metric can be reduced

by increasing the number of sensors. This is illustrated in Figure 4.4. The effect of bandwidth on localization is shown in Figure 4.5. An increase in bandwidth leads to a reduction in the sidelobes, leading to smaller errors in the ambiguity region. This is due to the fact that the transmitted pulse autocorrelation function serves as the envelope of the localization metric. This envelope, which becomes narrower with the increase in bandwidth, forces the sidelobes to decay faster.

CHAPTER 5

NONCOHERENT LOCALIZATION OF A MOVING TARGET IN ACTIVE SYSTEMS

This chapter focuses on the problem of estimating both the location and the velocity of a target in distributed MIMO radar systems. MIMO radar systems represent radar systems employing multiple antennas, and can transmit multiple waveforms, via its antennas, and process jointly echos received at multiple received antennas. MIMO radar systems were suggested with co-located and with distributed antennas [66, 67]. MIMO radar with distributed antennas exploits spatial diversity [68], whereas MIMO radar with co-located antennas exploits waveform diversity [69].

A problem related to the estimation of both the location and the velocity is the estimation of range and range rate. Similar to coherent localization problem, the estimation of range and range rate is a nonlinear problem, for which the estimation metric is often multimodal. For the joint estimation of range and range rate, the likelihood function in a noise-free environment is proportional to the ambiguity function (AF) [46]. The AF is a metric that displays the inherent tradeoff between the ability to estimate the range (time delay) and range rate (Doppler) of a moving target. The AF can provide insights about ambiguities in estimating the target parameters. Masking the detection of other targets represents another undesirable effect of sidelobes in the likelihood function [70]. The design of ambiguity functions with near "ideal[1]" properties has been one of the main preoccupations of the radar community [71–76].

Even though the AF is a very useful tool, it is not informative about the behavior of an estimator as a function of SNR as is the ZZB. Thus, in the next sections, the ZZB for target's delay and Doppler estimation is derived. Furthermore, this

[1]An ideal AF is a delta function located at the origin of delay-Doppler plan and zero elsewhere.

derivation is extended to the problem of estimating target's location and velocity in a distributed MIMO radar system. An asymptotic analysis of the location-velocity estimation problem for a distributed MIMO radar was presented in [77,78]. However, the threshold phenomena has not been analyzed. The derivation performed in this chapter shows that there is a direct relationship between the ZZB and the AF thus, new waveforms for MIMO radar can be analyzed or designed using the derived ZZB. Moreover, the results obtained in the sequel can be applied to study the performance of the estimator as a function of different system parameters. Comparison between the ZZB and the MSE of the maximum likelihood estimate (MLE) obtained through simulations demonstrate that the bound is tight in all SNR regions.

5.1 System Model

Consider a MIMO radar system with M transmitters and N receivers located at arbitrary coordinates (x_{ti}, y_{ti}), $i = 1, \ldots, M$, and (x_{rk}, y_{rk}), $k = 1, \ldots, N$, respectively. Assume a target located at an unknown location $(x_0,\ y_0)$ and moving at an unknown velocity $(v_x,\ v_y)$. The target reflectivity is assumed to obey a Swerling Case 1 model, and has a complex valued Gaussian probability density function. The target reflectivity is further assumed to be independent between different pairs of transmit-receive elements. Let the ith element emit a waveform with complex envelope $\sqrt{E/M}s_i(t)$, where $\int |s_i(t)|^2 dt = 1$, and E is the energy. The normalization by the number of transmit antennas ensures that the total output power is independent of the number of transmit antennas. The noisy observations gathered by a receiver represent a sum of delayed and Doppler shifted versions of the transmitted signals. Each receiver collects L uncorrelated samples with a sampling interval of Δt. The lth sample at receiver kth can be expressed

$$r_k(t_l) = \sum_{i=1}^{M} a_{ik}\sqrt{\frac{E}{M}}s_i(t_l - \tau_{ik})\, e^{j2\pi f_{ik}t_l} + w_k(t_l) \tag{5.1}$$

where a_{ik} is the reflectivity coefficient of the target, and τ_{ik} and f_{ik} are the delay and Doppler shift, respectively, corresponding to the i, k transmit-receive pair. The additive noise term $w_k(t_l)$ is assumed to be stationary, white, complex Gaussian with zero-mean and variance σ_w^2.

The reflectivity coefficients of the target are modeled as independent, complex-valued, normal random variables with zero-mean and variance σ_α^2 ($a_{ik} \sim CN(0, \sigma_\alpha^2)$). The time delay τ_{ik} is proportional to the distance traveled by the transmitted signal i to the target, and from the target to receiver k, and it is given in the sampled signal domain

$$\tau_{ik} = \frac{1}{c\Delta t}\left(\sqrt{(x_{ti}-x_t)^2+(y_{ti}-y_t)^2}+\sqrt{(x_{rk}-x_t)^2+(y_{rk}-y_t)^2}\right) \tag{5.2}$$

where c is the speed of light. The Doppler shift f_{ik} is defined also in the sampled signal domain as a function of the unknown target's location and velocity,

$$f_{ik} = \frac{v_x}{\lambda}\Delta t\left(\cos\phi_i+\cos\phi_k\right)+\frac{v_y}{\lambda}\Delta t\left(\sin\phi_i+\sin\phi_k\right) \tag{5.3}$$

where λ is the wavelength, and ϕ_i and ϕ_k are bearing angles of the target measured with respect to the x axis at transmitting radar i and receiving radar k, respectively. Estimates of the location and velocity of the target can be obtained from the noisy measurements.

In the next section, the ZZB for target's delay and Doppler estimation is derived.

5.2 SISO Radar Analysis

A SISO radar is formed by single, collocated transmit and receive antenna. As stipulated in Sec. 5.1, the target is illuminated with a known waveform. The echo from the target consists of a noisy, time delayed and Doppler-shifted version of the

transmitted waveform. The radar's goal is to estimate the target's time delay (τ) and Doppler shift (f). The aim is to find an expression for the bound on the variance of the estimate $\theta = [\tau,\ f]^T$ and to explore links between the bound and the radar's AF.

The delay and Doppler shift are modeled as random variables with an uniform *a priori* distribtion, $\tau \sim U[0,\ T]$, $f \sim U[0, \Omega]$. In this case, the bound (2.14) can be specialized as follows:

$$\mathbf{u}^T \mathbf{\Phi} \mathbf{u} \geq \int_0^\infty \frac{h}{T\Omega} \cdot \left\{ \max_{\boldsymbol{\delta}:\mathbf{u}^T\boldsymbol{\delta}=h} \int_{\boldsymbol{\Theta}} P_\epsilon(\boldsymbol{\varphi}, \boldsymbol{\varphi}+\boldsymbol{\delta}) \mathrm{d}\boldsymbol{\varphi} \right\} \mathrm{d}h \tag{5.4}$$

In Inequality (5.4), the probability of error $P_\epsilon(\boldsymbol{\varphi}, \boldsymbol{\varphi}+\boldsymbol{\delta})$ is associated with the detection problem in which, under hypothesis H_0, the estimated parameter $\boldsymbol{\theta} = \boldsymbol{\varphi} = [\tau,\ f]^T$, and under hypothesis H_1, $\boldsymbol{\theta} = \boldsymbol{\varphi} + \boldsymbol{\delta} = [\tau + \tau_\delta,\ f + f_\delta]^T$. Error events occur when the likelihood ratio has opposite sign to that associated with the hypotheses. The probability of error is given by

$$P_\epsilon(\boldsymbol{\varphi}, \boldsymbol{\varphi}+\boldsymbol{\delta}) = \frac{1}{2} P_\epsilon(l(\mathbf{r}) < 0 | H_1) + \frac{1}{2} P_\epsilon(l(\mathbf{r}) > 0 | H_0). \tag{5.5}$$

To evaluate the probability of error, we need to examine the likelihood ratio test used to discriminate between $\boldsymbol{\varphi}$ and $\boldsymbol{\varphi} + \boldsymbol{\delta}$. To this end, define the observations vector, $\mathbf{r} = [r(t_1), \ldots, r(t_L)]^T$ and the signal vectors $\mathbf{s}_{(m)} = \left[s\left(t_1 - \tau - m\tau_\delta\right) e^{j2\pi(f+mf_\delta)t_1}, \ldots, s\left(t_L - \tau - m\tau_\delta\right) e^{j2\pi(f+mf_\delta)t_L} \right]^T$ for $m = 0, 1$, corresponding to hypotheses H_0 and H_1, respectively. Recalling (5.1), the signal model for the detection problem is given by

$$\mathbf{r} = \sqrt{E} a \mathbf{s}_{(m)} + \mathbf{w} \tag{5.6}$$

where $a \sim CN(0, \sigma_\alpha^2)$ and $\mathbf{w} \sim CN(\mathbf{0}, \sigma_w^2 \mathbf{I})$. The log-likelihood ratio test (2.13) for the detection problem is computed with the help of the following Lemma.

Lemma: Given the vector observations model (5.6) the likelihood ratio test is given by

$$l\left(\mathbf{r}\right)=\frac{E}{\sigma_w^2\left(E+\frac{\sigma_w^2}{\sigma_a^2}\right)}\mathbf{r}^H\left(\mathbf{s}_{(1)}\mathbf{s}_{(1)}^H-\mathbf{s}_{(0)}\mathbf{s}_{(0)}^H\right)\mathbf{r}\underset{H_0}{\overset{H_1}{\gtrless}}0 \tag{5.7}$$

Proof. See Appendix B. □

From Equation (5.7), the optimal detector discriminates between the squared output of a matched filter corresponding to a target response with delay τ and Doppler f and the squared output of a matched filter corresponding to a target response with delay $\tau+\tau_\delta$ and Doppler $f+f_\delta$.

In order to compute $P_\epsilon(\boldsymbol{\varphi},\boldsymbol{\varphi}+\boldsymbol{\delta})$, the distribution of the likelihood ratio test $l\left(\mathbf{r}\right)$ needs to be determined. From Expression (5.7), $l\left(\mathbf{r}\right)$ is a central, indefinite quadratic form in complex Gaussian random variables. It is central because $\mathrm{E}[\mathbf{r}]=0$, and indefinite since $\mathbf{s}_{(1)}\mathbf{s}_{(1)}^H-\mathbf{s}_{(0)}\mathbf{s}_{(0)}^H$ can have positive and negative eigenvalues. Based on this information, and following a characteristic function approach, the following closed form of $P_\epsilon(\boldsymbol{\varphi},\boldsymbol{\varphi}+\boldsymbol{\delta})$ is derived in Appendix C:

$$P_\epsilon(\boldsymbol{\delta})=\frac{1}{2}-\frac{\mathrm{SNR}\left(1-\Psi\left(\tau_\delta,f_\delta\right)\right)}{2\sqrt{\left(\mathrm{SNR}^2\left(1-\Psi\left(\tau_\delta,f_\delta\right)\right)+4\mathrm{SNR}+4\right)\cdot\left(1-\Psi\left(\tau_\delta,f_\delta\right)\right)}}, \tag{5.8}$$

where

$$\Psi\left(\tau_\delta,f_\delta\right)=\left|\mathbf{s}_{(0)}^H\mathbf{s}_{(1)}\right|^2 \tag{5.9}$$

represents a sampled version of the Woodward ambiguity function, and $\mathrm{SNR}=E\sigma_a^2/\sigma_w^2$. The probability of error $P_e(\boldsymbol{\delta})$ is a non-increasing function of the SNR. Moreover, the probablity of error is a function of the AF. For a fixed SNR, the

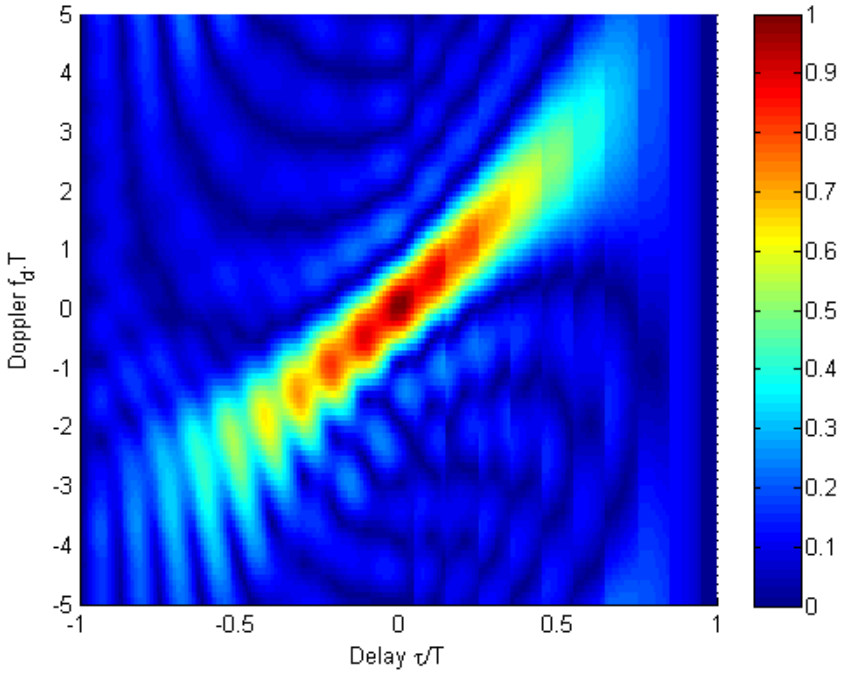

Figure 5.1 Ambiguity function of a single LFM pulse with time bandwidth product = 5.

behavior of the probability of error follows that of the AF. For example, when the AF peaks $\Psi(\tau_\delta, f_\delta) = 1$, the error probability peaks at $P_\epsilon(\boldsymbol{\delta}) = 0.5$ regardless of the SNR. At the other extreme, when there is no ambiguity, $\Psi(\tau_\delta, f_\delta) = 0$, the error is inverse proportional to the SNR, $P_e(\boldsymbol{\delta}) = 1/(\mathrm{SNR} + 2)$. We conclude that through the probability of error of binary decisions, the ZZB is determined by both the SNR and the AF. The ZZB for delay-Doppler estimation in SISO radar is given by substituting (5.8) in (5.4).

Numerical Results

In this section, numerical results are presented to illustrate the application of the ZZB to SISO radar. Several scenarios are considered in which the transmitted waveforms are linear frequency modulation (LFM) pulses. Note that LFM is a pulse compression technique employed in radar to obtain high range resolution while providing good

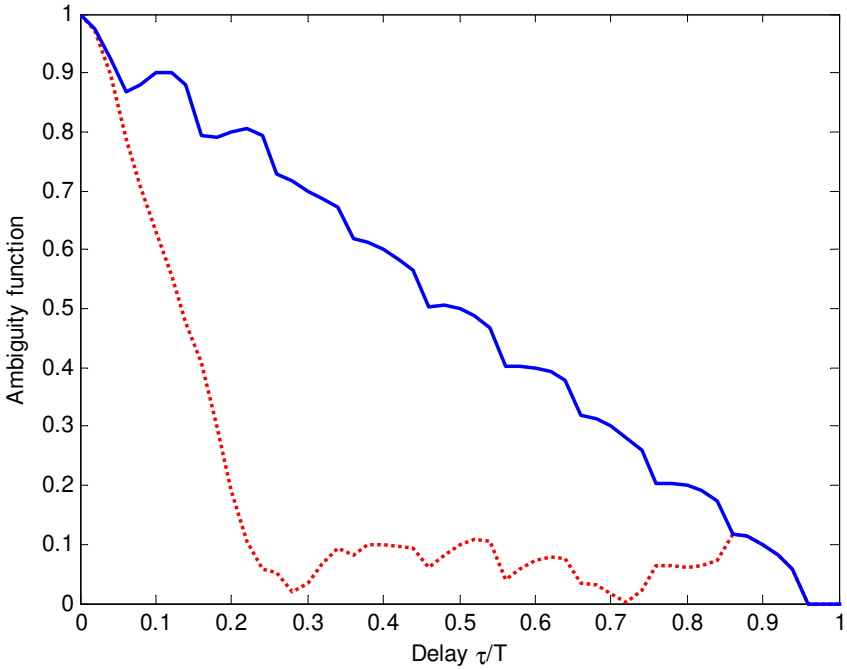

Figure 5.2 Zero-Doppler cut of the AF of an LFM pulse (dotted line) and the cut through the ridge of the AF (solid line).

Doppler tolerance, [79]. The LFM pulse used to generate the data in this part has duration T and time bandwidth product 5. The AF of a single LFM pulse is a diagonal ridge above the delay-Doppler plane, and is illustrated in Figure 5.1. The delay axis is normalized to the pulse duration T, and the Doppler axis is scaled by the pulse duration.

In Figure 5.2 the zero-Doppler cut of the AF of the LFM pulse (dotted line) and the cut through the ridge of the AF (solid line) are shown. The zero-Doppler cut shows the effect of pulse compression, which reduces the response from the duration T of the transmitted pulse to approximately $T/5$. The figure also shows that the system response is high for mismatched values of Doppler and delay. These high sidelobes are expected to result in high probabilities of error. The link between the ambiguity function and the probability of error is evident by comparing Figure 5.2

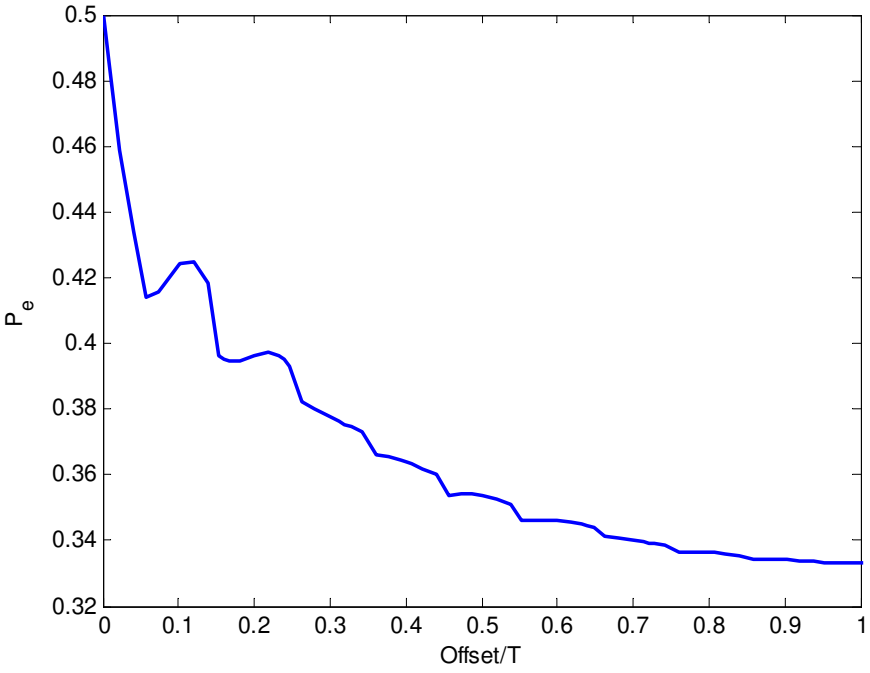

Figure 5.3 Probability of error for range estimation with an LFM pulse. The behavior of the probability of error follows that of the AF.

with Figure 5.3, with the latter representing the probability of error for an LFM pulse at SNR = 10 dB. The SNR is defined as SNR $= E\sigma_\alpha^2/\sigma_w^2$.

It can be observed that the probability of error has maxima that coincide with the peaks of the mainlobe and sidelobes of the AF. This can be explained by noting that the maxima of the AF, which indicate high correlation between the observed signal and the signal matched at the receiver, translate into ambiguous decisions, and implicitly cause an increase in the probability of error. In particular, when the time delay between the two hypotheses vanishes, it is impossible to distinguish between them, hence the probability of error $P_e = 0.5$. It is also apparent in the figures that minima of the probability of error coincide with nulls of the AF. However, the minima of the probability of error are not equal to zero due to the effect of noise, which induces a nonzero probability of error. Yet, the minima decrease with an increase in SNR, as

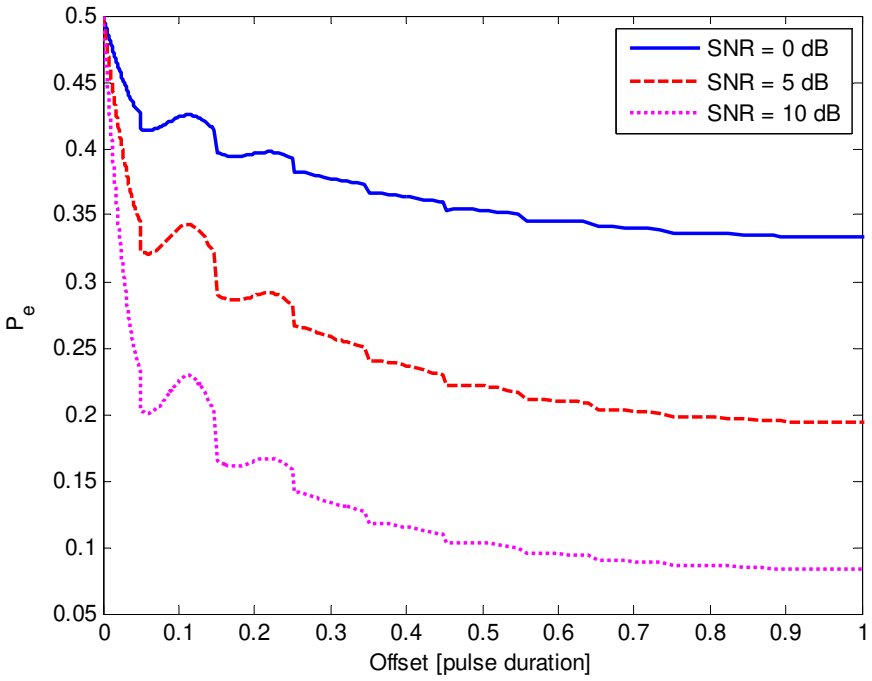

Figure 5.4 Probability of error in estimating range using 1 LFM pulse for different SNR. Increasing SNR induces a decrease in the error probability.

can be seen in Figure 5.4. It is also observed from Figure 5.4 that the locations of the maxima does not depend on the SNR.

Doppler resolution depends on the waveform duration. To improve Doppler resolution, a coherent pulse train can be transmitted rather than a single pulse. The ambiguity function of a coherent train of 5 identical LFM pulses with pulse repetition interval (PRI) (duration between consecutive pulses) $2T$, where T is the pulse duration, is plotted in Figure 5.5. As before, individual LFM pulses have time bandwidth product equal to 5. Note that range ambiguities occur at multiples of PRI, and Doppler ambiguities occur at multiples of 1/PRI. These ambiguities can lead to large errors in estimating the delay-Doppler parameters as can be observed from Figure 5.6 and Figure 5.8. Figure 5.6 shows that the probability of error has peaks at $2T$ time offset intervals. This is the same time interval as between the spurious peaks of the AF of the coherent pulse train in 5.5. The multiple peak sidelobes in the

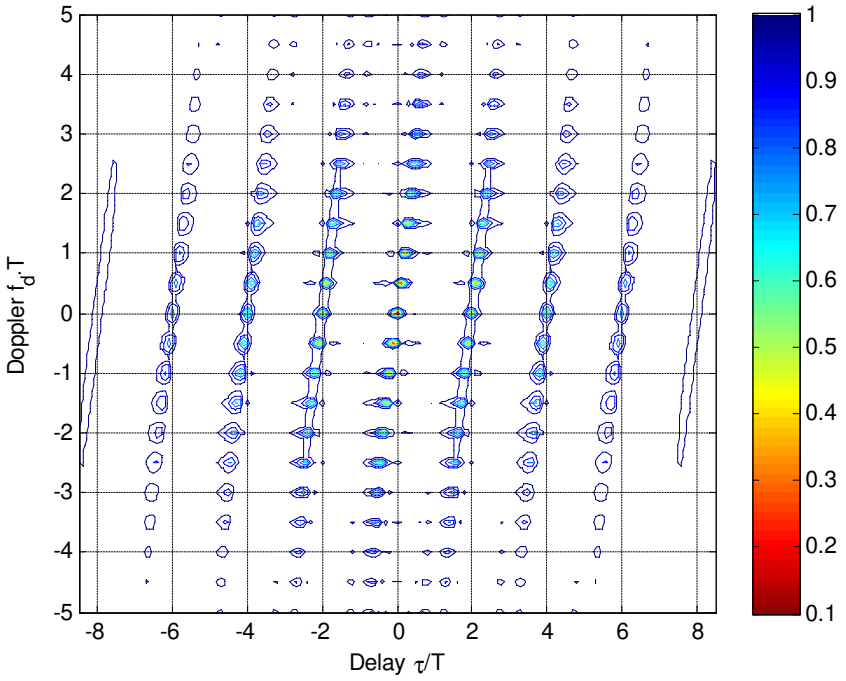

Figure 5.5 Ambiguity function of a coherent train of 5 LFM pulses

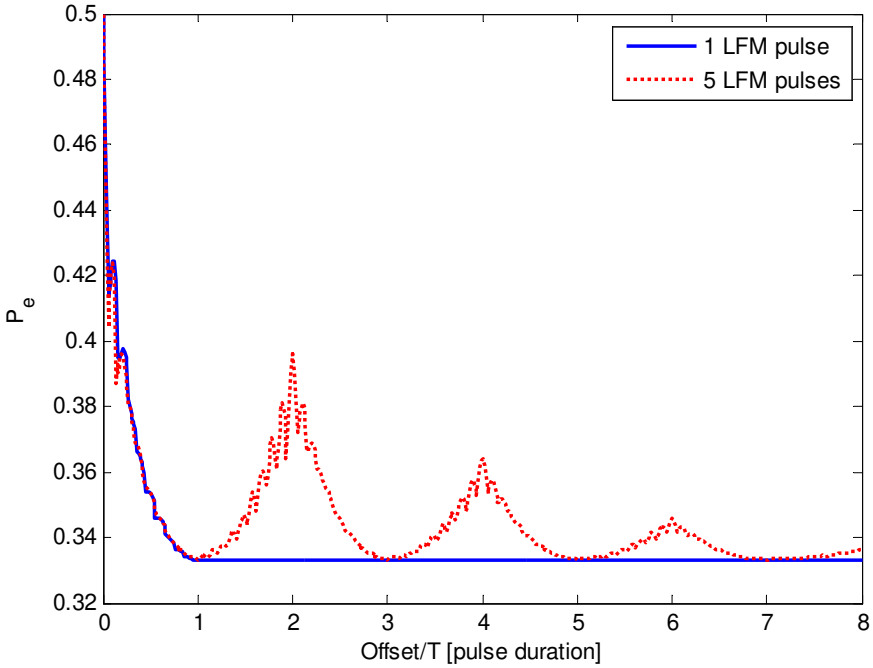

Figure 5.6 Probability of error in estimating range using 1 LFM pulse and 5 LFM pulses

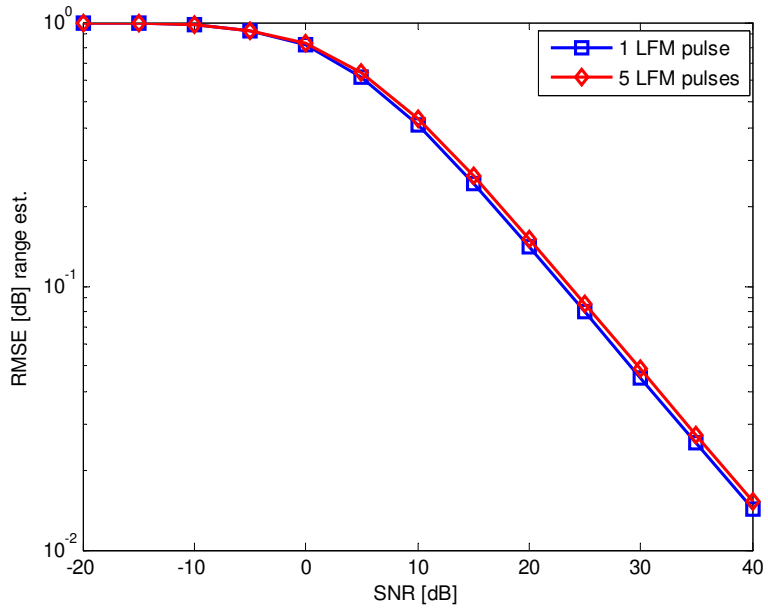

Figure 5.7 ZZB of estimating range using 1 LFM pulse and 5 LFM pulses. Increasing the number of pulses leads to an increase in the number of ambiguities that translates in an increase in the range estimation error.

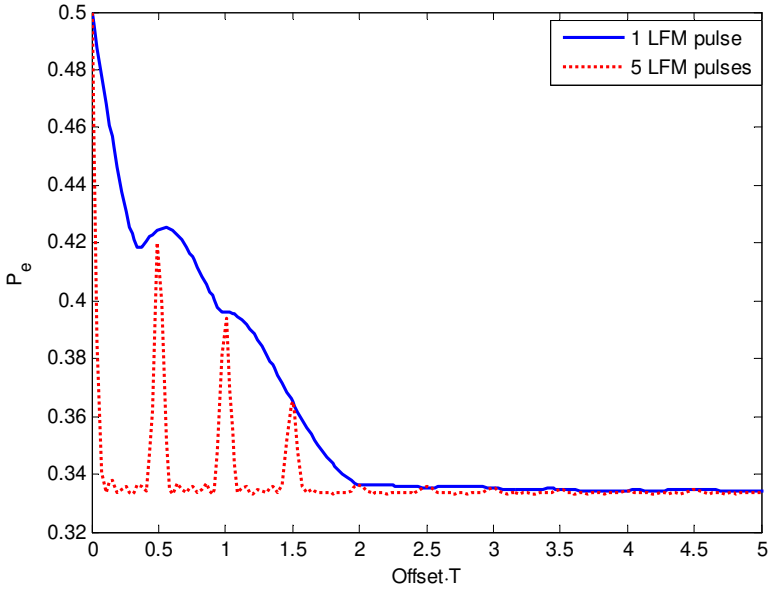

Figure 5.8 Probability of error in estimating Doppler using 1 LFM pulse and 5 LFM pulses.

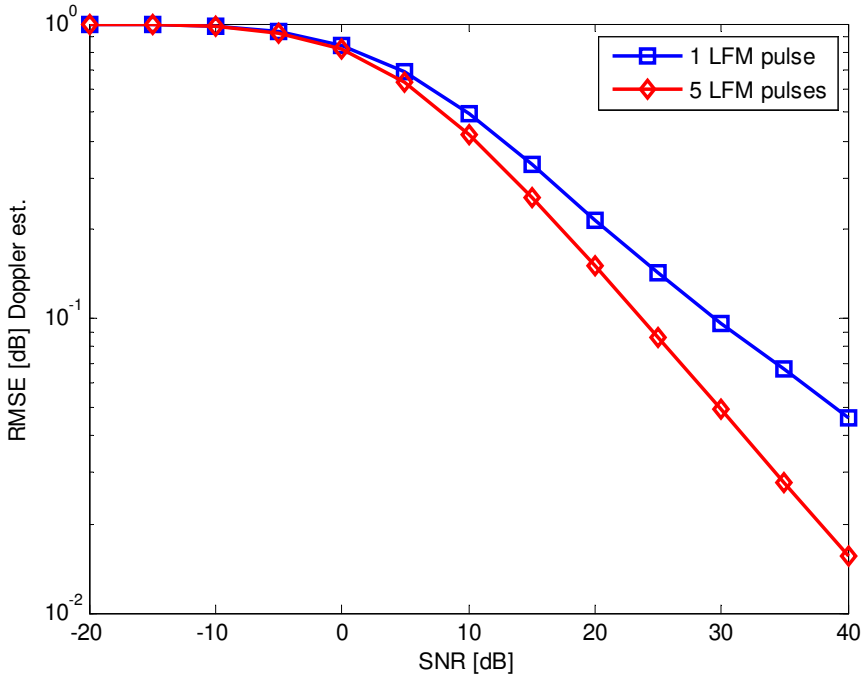

Figure 5.9 ZZB of estimating Doppler using 1 LFM pulse and 5 LFM pulses. Increasing the number of pulses leads to an increase in the number of ambiguities, yet leads to an increase in the duration of observation that translates in a decrease of the Doppler estimation error.

AF of the coherent pulse train increase the MSE of the time delay estimation relative to the single pulse case. This is shown in 5.7. An opposite effect occurs in Doppler estimation, where the longer duration observation reduces the MSE. In Figure 5.8, the probability of error for the pulse train has a main peak narrower by a factor of 10 compared to the single pulse. This factor corresponds to the time duration $10T$ of the pulse sequence. Improved Doppler estimation performance for the pulse train is evident in 5.9.

The AF has served as a classical tool for radar signal design since its introduction in the 1950's. The preceding discussion demonstrates that the ZZB analysis can serve as an alternative to the AF as a tool for radar design. In fact, the ZZB analysis has two advantages over the AF analysis: (1) it integrates the effect of delay-Doppler sidelobes into a single figure of merit, the joint delay-Doppler estimation error, (2) it accounts for the effect of noise, while the ambiguity function does not.

5.3 MIMO Radar Analysis

MIMO radar systems represent radar systems employing multiple antennas, that transmit multiple waveforms, and process jointly the echos received at receiving antennas. Because MIMO radars employ multiple antennas, not only the time delays and the Doppler shifts associated with each pair transmitter-target-receiver can be estimated, but also target's location and velocity can be estimated by processing jointly all the noisy observations, [78]. In this section, the previous analysis is extended to the problem of estimating target's location ($[x_0,\, y_0]$) and velocity ($[v_x,\, v_y]$) with MIMO radar systems, more specifically the ZZB on the variance of the estimate $\boldsymbol{\theta} = [x_0,\, y_0,\, v_x,\, v_y]^T$ is derived.

To derive the ZZB for the problem of estimating target's location and velocity, we start from the ZZB for vector parameters (2.14), and specialize for the case where

the target's coordinates and velocity components are modeled as random variables with a uniform *a priori* distribution, $x_0,\, y_0 \sim U[0,\, D]$, $v_x\,, v_y \sim U[0, V]$

$$\mathbf{u}^T \mathbf{\Phi} \mathbf{u} \geq \int_0^{\infty} \frac{h}{D^2 V^2} \cdot \cdot \left\{ \max_{\boldsymbol{\delta}: \mathbf{u}^T \boldsymbol{\delta} = h} \int_{\boldsymbol{\Theta}} P_\epsilon(\boldsymbol{\varphi}, \boldsymbol{\varphi} + \boldsymbol{\delta}) \mathrm{d}\boldsymbol{\varphi} \right\} \mathrm{d}h \tag{5.10}$$

In (5.10), the probability of error $P_\epsilon(\boldsymbol{\varphi}, \boldsymbol{\varphi} + \boldsymbol{\delta})$ is associated with the detection problem in which, under hypothesis H_0, the estimated parameter $\boldsymbol{\theta} = \boldsymbol{\varphi} = [x_0,\, y_0,\, v_x,\, v_y]^T$, and under hypothesis H_1, $\boldsymbol{\theta} = \boldsymbol{\varphi} + \boldsymbol{\delta} = [x_0 + x_\delta,\, y_0 + y_\delta,\, v_x + v_{\delta x},\, v_y + v_{\delta y}]^T$. Similar to the SISO case, $P_\epsilon(\boldsymbol{\varphi}, \boldsymbol{\varphi} + \boldsymbol{\delta})$ is determined based on the distribution of the likelihood ratio test that discriminates between hypothesis H_0, and hypothesis H_1 (see Equation (5.5)). Next, the error probability is computed.

Under the two hypotheses, the observations collected by receiver kth can be written as

$$r_{(m)k}\left(t_l\right) = \sum_{i=1}^{M} a_{ik} \sqrt{\frac{E}{M}} s_{(m)ik}(t_l) + w_k\left(t_l\right) \;\; l = 1, ..., L \tag{5.11}$$

where m takes values 0 and 1 corresponding to hypotheses H_0 or H_1, $s_{(m)ik}\left(t_l\right) = s_i\left(t_l - \tau_{ik} - m \cdot \tau_{\delta ik}\right) e^{j2\pi(f_{ik} + m \cdot f_{\delta ik})t}$, and $\tau_{\delta ik}$ and $f_{\delta ik}$ represent the difference in delay and Doppler shift between the two hypotheses, respectively,

$$\begin{aligned} \tau_{\delta ik} =& \frac{1}{c} \left(\sqrt{\left(x_{ti} - x_0 - x_\delta\right)^2 + \left(y_{ti} - y_0 - y_\delta\right)^2} \right. \\ & \left. + \sqrt{\left(x_{rk} - x_0 - x_\delta\right)^2 + \left(y_{rk} - y_0 - y_\delta\right)^2} \right) \\ & - \frac{1}{c} \left(\sqrt{\left(x_{ti} - x_0\right)^2 + \left(y_{ti} - y_0\right)^2} + \sqrt{\left(x_{rk} - x_0\right)^2 + \left(y_{rk} - y_0\right)^2} \right) \end{aligned} \tag{5.12}$$

and

$$\delta f_{ik} = \frac{v_x + v_{\delta x}}{\lambda} \left(\cos\left(\phi_i + \phi_{\delta i}\right) + \cos\left(\phi_k + \phi_{\delta k}\right)\right) +$$
$$+ \frac{v_y + v_{\delta y}}{\lambda} \left(\sin\left(\phi_i + \phi_{\delta i}\right) + \sin\left(\phi_k + \phi_{\delta k}\right)\right) - \tag{5.13}$$
$$- \frac{v_x}{\lambda} \left(\cos\phi_i + \cos\phi_k\right) - \frac{v_y}{\lambda} \left(\sin\phi_i + \sin\phi_k\right) \tag{5.14}$$

The detailed steps are omitted here due to space considerations, but it can be shown that, under the independence assumption between the target's reflectivity coefficients (see Equation (5.1)), the distributions of the vector observations, conditioned on the estimated parameters and averaged over the distributions of the target reflectivity are:

$$f_{(m)}(\mathbf{r}|\boldsymbol{\varphi} + m\boldsymbol{\delta}) = c' \exp\left\{-\frac{1}{\sigma_w^2}\left\|\mathbf{r}\right\|^2\right\} \cdot \exp\left\{\frac{\frac{E}{M}}{\sigma_w^2(\frac{E}{M} + \frac{\sigma_w^2}{\sigma_\alpha^2})}\left\|\mathbf{z}_{(m)}\right\|^2\right\}$$

where $\mathbf{r} = [r_{11}(t_1), ..., r_{11}(t_L), r_{21}(t_1), ..., r_{MN}(t_L)]^T$, $r_{ik}(t_l) = r_k(t_l)$, $\mathbf{z}_{(m)} = [z_{(m)11}, ..., z_{(m)MN}]^T$, $z_{(m)ik} = \sum_{l=1}^{L} r_k(t_l) s_i^*(t_l - \tau_{ik} - m\tau_{\delta ik}) e^{-j2\pi(f_{ik} + m f_{\delta ik})t_l}$, and c' is a constant which doesn't depend on the estimated parameter. If we make the notation $\mathbf{s}_{(m)ik} = [s_{(m)ik}(t_1), ..., s_{(m)ik}(t_L)]^T$, from the distribution of the received signals, we can write the log likelihood ratio test (2.13) as

$$l(\mathbf{r}) = \ln\left[\frac{f(\mathbf{r}|H_1)}{f(\mathbf{r}|H_0)}\right] = \frac{\frac{E}{M}}{\sigma_w^2(\frac{E}{M} + \frac{\sigma_w^2}{\sigma_\alpha^2})}\left(\left\|\mathbf{z}_{(1)}\right\|^2 - \left\|\mathbf{z}_{(0)}\right\|^2\right) =$$
$$= \frac{\frac{E}{M}}{\sigma_w^2(\frac{E}{M} + \frac{\sigma_w^2}{\sigma_\alpha^2})} \mathbf{r}^H (\mathbf{Q}_{(1)} - \mathbf{Q}_{(0)}) \mathbf{r} \underset{H_0}{\overset{H_1}{\gtrless}} 0 \tag{5.15}$$

where $\mathbf{Q}_{(m)} = \text{diag}(\mathbf{s}_{(m)11}\mathbf{s}_{(m)11}^H, \mathbf{s}_{(m)21}\mathbf{s}_{(m)21}^H, \cdots, \mathbf{s}_{(m)MN}\mathbf{s}_{(m)MN}^H)$ is a block diagonal matrix. By inspection of (5.15) and of $\mathbf{z}_{(m)}$, the log likelihood ratio test is a noncoherent processor, that functions by combining the output of MN matched

filters. Note that, with suitable normalization, a single term $|z_{(m)ik}|^2$ has a χ_2^2 (chi-square with two degrees of freedom) distribution, and $||\mathbf{z}_{(m)}||^2$ has the statistical properties of a χ_{2MN}^2 random variable. The $2MN$ degrees of freedom provides the improvement in target detection and position estimation of MIMO radar systems as observed in [67, 78].

Next, the distribution of the log likelihood ratio test will be computed in order to determine the error probability $P_\epsilon(\boldsymbol{\varphi}, \boldsymbol{\varphi} + \boldsymbol{\delta})$ (see (5.5)). The distribution of the random variable $l' = \mathbf{r}^H(Q_{(1)} - Q_{(0)})\mathbf{r}$ is a central, indefinite quadratic form in complex Gaussian random variables, with the characteristic function of the form

$$G_{l'}(s) = \frac{1}{\det(I - js\boldsymbol{\Sigma}^H(\mathbf{Q}_{(1)} - \mathbf{Q}_{(0)}))} = \prod_{n=1}^{N_\lambda}(1 - js\lambda_n)^{-\mu_n} \tag{5.16}$$

where $\boldsymbol{\Sigma} = \mathrm{E}[\mathbf{r}\mathbf{r}^{\mathbf{H}}]$, and λ_n with $n = 1, \ldots, N_\lambda$ are the distinct non-zero eigenvalues of the matrix $\boldsymbol{\Sigma}(\mathbf{Q}_{(1)} - \mathbf{Q}_{(0)})$ with multiplicities $\mu_1, \ldots, \mu_{N_\lambda}$. The quantity N_λ denotes the number of distinct non-zero eigenvalues.

Note that the probabilities $P_\epsilon(l(\mathbf{r}) < 0|H_1)$ and $P_\epsilon(l(\mathbf{r}) > 0|H_0)$ which form the error probability $P_\epsilon(\boldsymbol{\varphi}, \boldsymbol{\varphi} + \boldsymbol{\delta})$ (see (5.5)) are given by

$$P_\epsilon(l(\mathbf{r}) < 0|H_1) = \frac{1}{2\pi}\int_{-\infty}^{0}\int_{-\infty}^{\infty} G_{l'}(s)e^{-jsl'}dsdl' \tag{5.17}$$

$$P_\epsilon(l(\mathbf{r}) > 0|H_0) = \frac{1}{2\pi}\int_{0}^{\infty}\int_{-\infty}^{\infty} G_{l'}(s)e^{-jsl'}dsdl' \tag{5.18}$$

The eigenvalues of the matrix $\boldsymbol{\Sigma}(\mathbf{Q}_{(1)} - \mathbf{Q}_{(0)})$ can be calculated by noting that the eigenvalues of a block diagonal matrix are those of the matrices which form the block diagonal matrix [80]. Next, the eigenvalues for one matrix from the block diagonal matrix (e.g., $\mathbf{Y}_{ik} = \boldsymbol{\Sigma}_k^H(\mathbf{s}_{(1)ik}\mathbf{s}_{(1)ik}^H - \mathbf{s}_{(0)ik}\mathbf{s}_{(0)ik}^H)$ where $\boldsymbol{\Sigma}_k$ is the covariance

matrix of $\mathbf{r}_k$) are determined. Because the matrix $\left(\mathbf{s}_{(1)ik}\mathbf{s}_{(1)ik}^H - \mathbf{s}_{(0)ik}\mathbf{s}_{(0)ik}^H\right)$ has rank two, $\mathbf{Y}_{ik}$ being the product of two matrices, has also rank two[2] (see [81, Appendix A]). Thus, $\mathbf{Y}_{ik}$ has two distinct non-zero eigenvalues $\lambda_{ik}^+ > 0$ and $\lambda_{ik}^- < 0$, which can be determined from Bcher's formula [82]:

$$\lambda_{ik}^2 + e_1\lambda_{ik} + e_2 = 0 \tag{5.19}$$

where $e_1 = -\mathrm{Tr}\{\mathbf{Y}_{ik}\}$ and $e_2 = -\frac{1}{2}(e_1\mathrm{Tr}\{\mathbf{Y}_{ik}\} + \mathrm{Tr}\{\mathbf{Y}_{ik}^2\})$. After evaluation of the traces, the coefficients of the quadratic polynomial are given by:

$$\begin{aligned} e_1 &= -\frac{E}{M}\sigma_\alpha^2\left(\mathbf{\Psi}_{(1)ik}^H\mathbf{\Psi}_{(1)ik} - \mathbf{\Psi}_{(0)ik}^H\mathbf{\Psi}_{(0)ik}\right) \\ e_2 &= -\frac{E}{M}\sigma_\alpha^2\sigma_w^2(\mathbf{\Psi}_{(1)ik}^H\mathbf{\Psi}_{(1)ik} + \mathbf{\Psi}_{(0)ik}^H\mathbf{\Psi}_{(0)ik} - \psi_{(01)ik}\mathbf{\Psi}_{(1)ik}^H\mathbf{\Psi}_{(0)ik} - \\ &\quad - \psi_{(01)ik}^*\mathbf{\Psi}_{(0)ik}^H\mathbf{\Psi}_{(1)ik}) - \sigma_w^4(1 - |\psi_{(01)ik}|^2) \end{aligned} \tag{5.20}$$

where

$$\begin{aligned} \mathbf{\Psi}_{(1)ik} &= [\psi_{(1)1ik},\, \psi_{(1)2ik}, \ldots, \psi_{(1)Mik}]^T \\ \mathbf{\Psi}_{(0)ik} &= [\psi_{(0)1ik},\, \psi_{(0)2ik}, \ldots, \psi_{(0)Mik}]^T \\ \psi_{(1)jik} &= \mathbf{s}_{(1)jk}^H\mathbf{s}_{(1)ik} \\ \psi_{(0)jik} &= \mathbf{s}_{(0)jk}^H\mathbf{s}_{(0)ik} \\ \psi_{(01)ik} &= \mathbf{s}_{(0)ik}^H\mathbf{s}_{(1)ik} \end{aligned}$$

The term $\psi_{(01)ik}$ represents the sampled version of the ambiguity function, the terms $\psi_{(1)jik}$, $\psi_{(0)jik}$, with $j \neq i$ represent sampled versions of cross-ambiguity functions, that take place between different transmitted signals and matched filter

[2]The covariance matrix $\mathbf{\Sigma}_k$ is a full rank matrix, and rank $(\mathbf{AB}) \leq \min(\mathrm{rank}(\mathbf{A}), \mathrm{rank}(\mathbf{B}))$.

signals, and $\psi_{(1)iik} = \psi_{(0)iik} = 1$. Remember that, the ambiguity function measures the correlation between the same signals for different delay-Doppler shifts. The cross-ambiguity function represents a generalization of the ambiguity function, i.e., it measures the correlation between two different signals for different delay-Doppler shifts.

A special case for MIMO radar systems is when different delays and Doppler shifts don't affect the orthogonality between transmitted signals, i.e., the cross-ambiguity function terms are equal to zero. For this case, the coefficients of the quadratic polynomial are

$$\begin{aligned} e_{1o} &= -\frac{E}{M}\sigma_\alpha^2\left(1 - |\psi_{(01)ik}|^2\right) \\ e_{2o} &= -\frac{E}{M}\sigma_\alpha^2\sigma_w^2(1 - |\psi_{(01)ik}|^2) - \sigma_w^4(1 - |\psi_{(01)ik}|^2) \end{aligned} \tag{5.21}$$

It was shown in [83] that, for radar systems where the transmit and receive antennas are not collocated, the ambiguity function depends on the positions of the transmitting antenna, the receiving antenna, and the target. Thus, for practical cases of MIMO radar systems, the ambiguity functions and the cross-ambiguity functions are distinct due to the randomness of the antennas positions. This leads to distinct eigenvalues. For this situation[3], a partial fraction expansion can be applied to the characteristic function yielding

$$G_{l'}(s) = \sum_{n=1}^{MN}\left[\frac{c_n^-}{(1 - js\lambda_n^-)} + \frac{c_n^+}{(1 - js\lambda_n^+)}\right] \tag{5.22}$$

where

[3]For the situation when the eigenvalues have different multiplicities the characteristic function can be calculated accordingly [84], however it complicates notation.

$$c_n^- = \prod_{\substack{k=1 \\ k\neq n}}^{MN} \frac{\lambda_n^-}{\lambda_n^- - \lambda_k^-} \prod_{k=1}^{MN} \frac{\lambda_n^-}{\lambda_n^- - \lambda_k^+} \tag{5.23}$$

$$c_n^+ = \prod_{k=1}^{MN} \frac{\lambda_n^+}{\lambda_n^+ - \lambda_k^-} \prod_{\substack{k=1 \\ k\neq n}}^{MN} \frac{\lambda_n^+}{\lambda_n^+ - \lambda_k^+}, \tag{5.24}$$

Based on (5.17), the error probability $P_\epsilon(l(\mathbf{r}) < 0|H_1)$ is

$$\begin{aligned} P_\epsilon(l(\mathbf{r}) < 0|H_1) &= \frac{1}{2\pi} \int_{-\infty}^{0} \int_{-\infty}^{\infty} G_{l'}(s) e^{-jsl'} ds dl' \\ &= \sum_{n=1}^{MN} \left[c_n^- \frac{1}{2\pi} \int_{-\infty}^{0} \int_{-\infty}^{\infty} \frac{e^{-jsl'}}{(1 - js\lambda_n^-)} ds dl' + \right. \\ &\left. + \, c_n^+ \frac{1}{2\pi} \int_{-\infty}^{0} \int_{-\infty}^{\infty} \frac{e^{-jsl'}}{(1 - js\lambda_n^+)} ds dl' \right] = \\ &= \sum_{n=1}^{MN} c_n^- \end{aligned} \tag{5.25}$$

In the last equality we used $\int_{-\infty}^{\infty} \frac{e^{-jsl'}}{(1-js\lambda_n^-)} ds = -2\pi e^{-l'/\lambda_n^-}/\lambda_n^-$, $\int_{-\infty}^{\infty} \frac{e^{-jsl'}}{(1-js\lambda_n^+)} ds = 0$, and $\int_{-\infty}^{0} -e^{-l'/\lambda_n^-}/\lambda_n^- dl' = 1$, [85, 3.382 ET I 118(4)].

Replacing (5.25) into (5.5) gives the following closed form for the probability of error $P_\epsilon(\boldsymbol{\varphi}, \boldsymbol{\varphi} + \boldsymbol{\delta})$

$$P_\epsilon(\boldsymbol{\varphi}, \boldsymbol{\varphi} + \boldsymbol{\delta}) = \sum_{n=1}^{MN} c_n^- = \sum_{n=1}^{MN} \left(\prod_{\substack{k=1 \\ k\neq n}}^{MN} \frac{\lambda_n^-}{\lambda_n^- - \lambda_k^-} \prod_{k=1}^{MN} \frac{\lambda_n^-}{\lambda_n^- - \lambda_k^+} \right) \tag{5.26}$$

In the case of a single collocated transmitter and receiver, the expression in (5.26) reduces to (5.8).

From (5.26), the $P_\epsilon(\boldsymbol{\varphi}, \boldsymbol{\varphi} + \boldsymbol{\delta})$ is determined by the product between the number of transmitting antennas and the number of receiving antennas, and by the eigenvalues

of the matrix $\mathbf{\Sigma}(\mathbf{Q}_{(1)}-\mathbf{Q}_{(0)})$ (reminder: $\mathbf{\Sigma}$ is the covariance matrix of $\mathbf{r}$). Furthermore, through the eigenvalues λ_n, the error probability depends on all the ambiguity functions and the cross-ambiguity functions corresponding to all pairs transmitter-target-receiver (see (5.19) and (5.20)). Thus, the ZZB which is obtained by replacing (5.26) into (5.10) provides a more complete analysis than the recently defined MIMO radar ambiguity function [86] because, in addition of considering the ambiguity and cross-ambiguity functions, the ZZB considers also the effect of noise.

Numerical Results

In this section, numerical results will be presented in order to support the theoretical derivations of the ZZB done for the MIMO radar systems. The numerical results follow a setup in which the target is positioned in the center of the coordinate system. The transmitting and receiving antennas are distributed randomly in a sector with center at the origin of the axes $(0, 0)$ and with a central angle of $\pi/6$ radians. The setup is shown in Figure 5.10. Each transmitting antenna transmits orthogonal coded orthogonal frequency division multiplexing (COFDM) pulses. COFDM that are presented in Appendix D, are a set of waveforms suitable for MIMO radar systems with widely separated antennas due to their orthogonality properties. Each CODFM pulse consists of sixteen OFDM symbols each with sixteen subcarriers.

In Figure 5.11, the ZZB of the error in estimating the abscissa x_t and the velocity v_x are plotted versus the SNR, $\text{SNR} = \frac{E\sigma_\alpha^2}{\sigma_w^2}$, for a 2×3 MIMO configuration (two transmit and three receive antennas). The CRLB and MLE of the target's location and velocity are also plotted for reference. From the figure it can be observed that the ZZB versus SNR can be divided into three regions. For low SNR, the ZZB reaches a plateau and the performance is dominated by noise. For high SNR, the ZZB merges with the CRLB, indicating that the noise errors are too small to cast the estimate outside the mainlobe of the estimation metric. This region is the

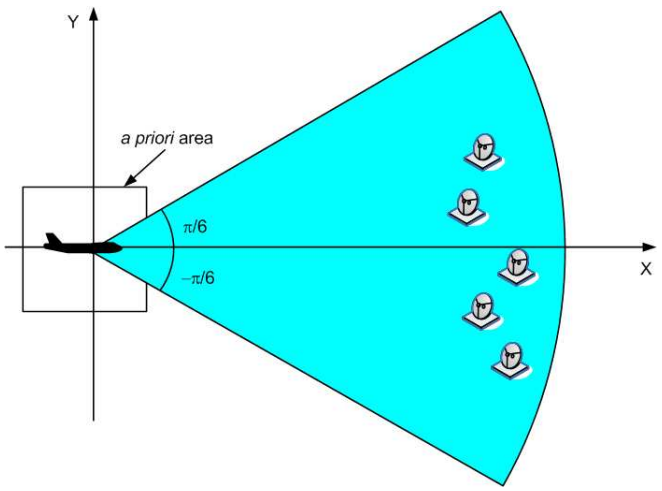

Figure 5.10 Setup configuration of the MIMO radar system with antennas distributed in a sector.

ambiguity free region. Between the two SNR extremes, is the ambiguity region, in which the estimator is affected by ambiguities created by sidelobes of the ambiguity and cross-ambiguity functions.

Figure 5.12 shows the MSE of estimating parameter x_t for different SNR values and different number of transmit and receive antennas. We see that increasing the number of antennas in the system results in the reduction of the estimation error. From the SISO analysis, it was noted that the error probability has maxima corresponding to the sidelobes of the ambiguity function. For MIMO radar systems, the estimation performance is affected when the sidelobes of the ambiguity functions and cross-ambiguity functions from multiple transmitter-receiver pairs happen to build up at a specific location and velocity. Increasing the number of radars leads to a stronger mainlobe and requires that a larger number of sidelobes build up to compete with the mainlobe. Because each transmitter-receiver pair has its own pattern of ambiguity functions, the chances of a large number of sidelobes lining up at one location are small. Thus performance improves with an increase in the number of radars.

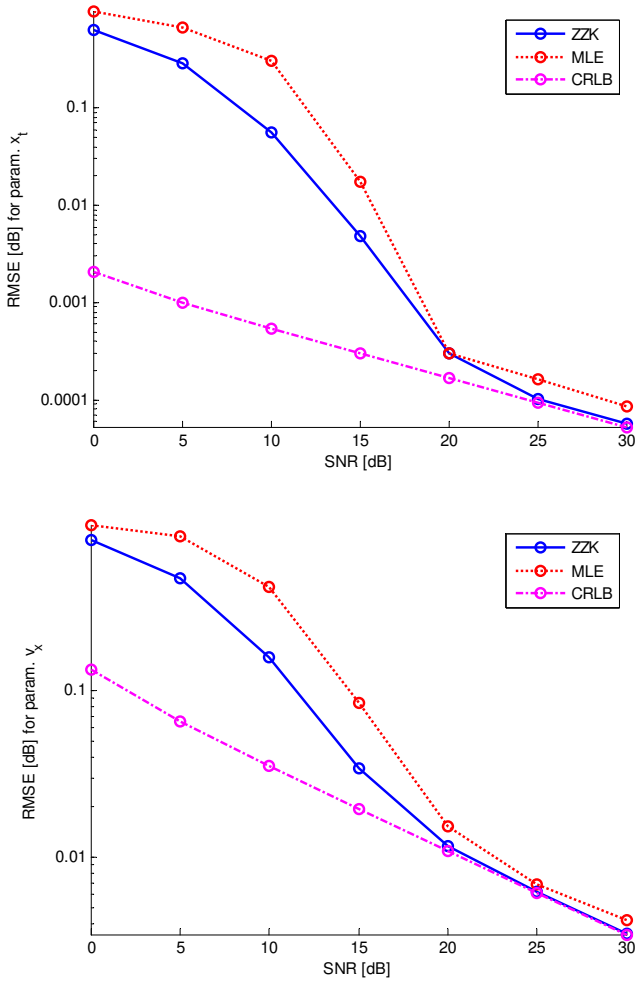

Figure 5.11 ZZB, MLE, and CRLB for estimating location (top) and velocity (bottom)

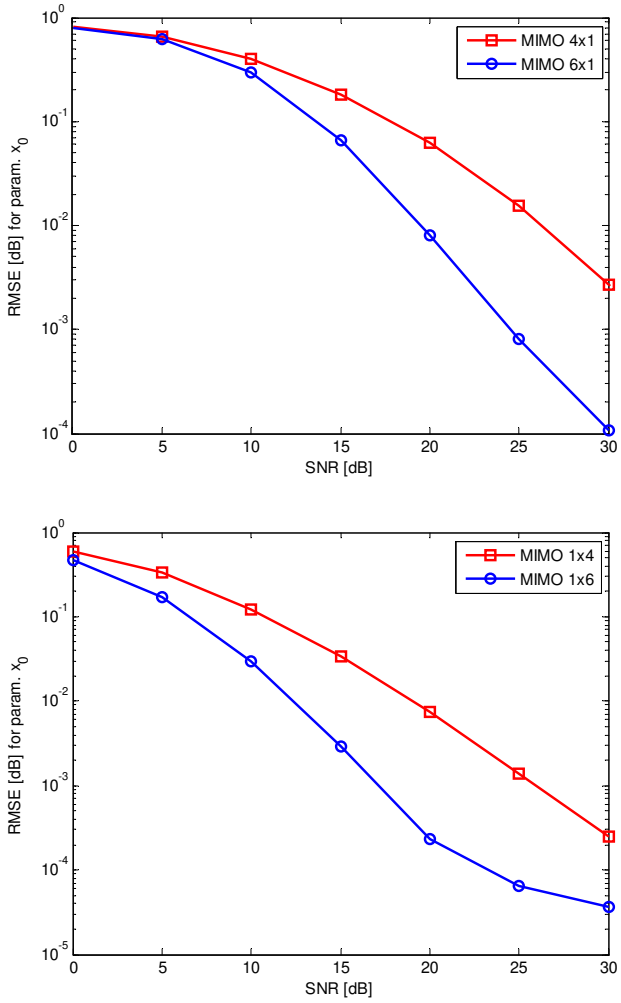

Figure 5.12 RMSE for different number of transmitters (top) and for different number of receivers (bottom)

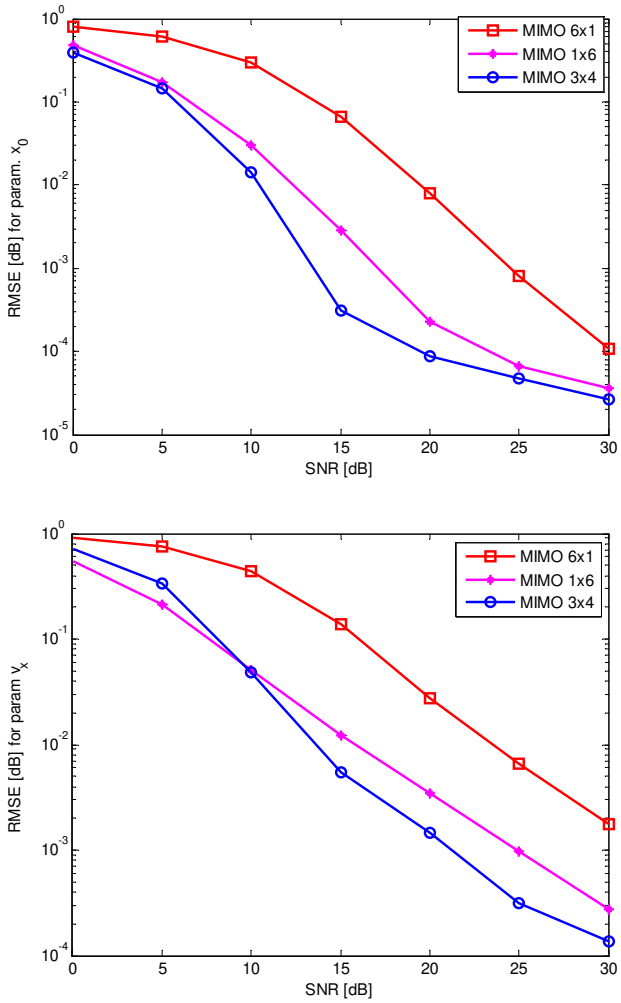

Figure 5.13 ZZB for different configurations

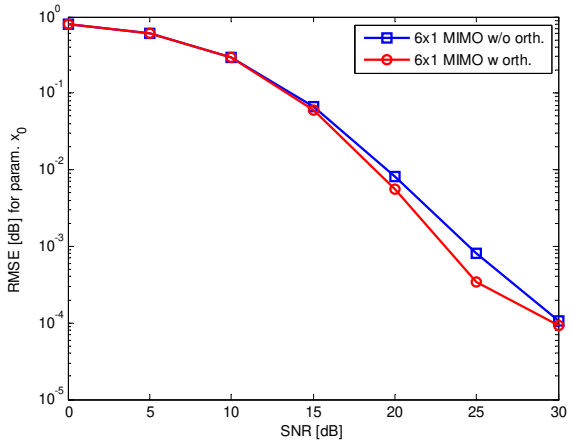

Figure 5.14 The effect of interference between transmitted signals over the estimation performance

Figure 5.13 shows the performance of MIMO radar systems for different configurations of transmit-receive antennas when the number of antennas per system is kept constant. The 6x1 MIMO radar system has the worst performance between all the systems analyzed due to the normalization done to maintain the same average transmitted energy. Another reason for poorer performance is that the system with more transmitting antennas is affected by higher interferences which are created at receivers between different transmitted signals. The 3x4 MIMO radar system provides the best performance between all the systems analyzed, since the performance is determined by the product between the number of transmitting antennas and the number of receiving antennas.

In MIMO radar systems, due to the wide separation between antennas, the transmitted waveforms propagate along different paths and arrive at sensors with different delays and Doppler shifts. As a result, the orthogonality of the transmitted signals is lost, and the received signals start to be correlated and to engender interferences. The effect of the interferences between the transmitted signals over the system performance can be evaluated based on (5.20) and (5.21), and it is exemplified in Figure 5.14 for a 6x1 MIMO radar.

CHAPTER 6

CONCLUSIONS AND FUTURE WORK

In the framework of this dissertation work, lower bounds on coherent target localization in passive and active systems were derived. For coherent passive localization the CRLB was derived. The CRLB shows that coherent localizations offer high accuracies i.e., proportional with the carrier frequency of the observed signal. However, the likelihood function is a highly nonlinear function, and a global optimization algorithm needs to be used in order to find the global maximum of the likelihood function. A hybrid global deterministic algorithm was proposed. Even with global optimization algorithms, to analyze the system performance for different system parameters and range of SNR is time consuming. The derived ZZB provides a convenient tool to assess the localization performance for different system parameters. Numerical examples demonstrate that, the ZZB gives results close to the MLE over the whole SNR range.

The ZZB was also used to derive a lower bound on the MSE of estimating the location and the velocity of a target with a MIMO radar system. The derived bound can serve as an alternative to the AF as a tool for radar design. It is shown that, the ZZB analysis has two advantages over the AF analysis: (1) it integrates the effect of delay-Doppler sidelobes into a single figure of merit, the joint delay-Doppler estimation error, (2) it accounts for the effect of noise, while the ambiguity function does not. The bound is a convenient tool for analyzing the estimator's performance for different waveforms and for different systems parameters.

A new type of orthogonal waveforms was proposed for MIMO radar systems. Utilizing the ZZB, it was shown that the new waveforms provide good interference suppression.

High precision in the system parameters are required for coherent localization systems to provide high accuracies. Thus, it is desired to investigate the effect of small errors in the system e.g., uncertainties in the position of sensors, over the localization performance. This analysis can be done by incorporating the mismatches into the system model and assessing the system performance with the use of a lower bound.

Estimation algorithms with reduced sidelobes is a vital point in implementing the coherent localization systems practical.

The ZZB as an alternative to AF provides endless research topics from waveform design, to design radar systems for specific applications.

APPENDIX A

CRAMER RAO LOWER BOUND FOR COHERENT PASSIVE LOCALIZATION

In this Appendix, the CRLB for coherent passive localization is derived.

The CRLB of parameter estimated θ is given by [87]

$$C_{CRLB}(\theta) = \mathbf{J}^{-1}(\theta) \tag{A.1}$$

where

$$\mathbf{J}(\theta) \triangleq E_{\mathbf{r}|\theta}\left[\frac{\partial}{\partial\theta}\log p(\mathbf{r}|\theta)\left(\frac{\partial}{\partial\theta}\log p(\mathbf{r}|\theta)\right)^{T}\right] \tag{A.2}$$

is the Fisher information matrix (FIM). $p(\mathbf{r}|\theta)$ is the conditional pdf of $\mathbf{r}$ given θ and it is defined in (3.4), $E_{\mathbf{r}|\theta}[\cdot]$ stands for expectation with respect to $p(\mathbf{r}|\theta)$. Because the received signal is a function of TDOA, τ_k, using the chain rule, the CRLB can be expressed as:

$$\mathbf{C}_{CRLB}(\theta) = \mathbf{G}^{-T}\mathbf{J}^{-1}(\tau)\mathbf{G}^{-1} \tag{A.3}$$

where

$$\mathbf{G} = \begin{bmatrix} \frac{\partial\tau_2}{\partial x_e} & \frac{\partial\tau_3}{\partial x_e} & \cdots & \frac{\partial\tau_M}{\partial x_e} \\ \frac{\partial\tau_2}{\partial y_e} & \frac{\partial\tau_3}{\partial y_e} & \cdots & \frac{\partial\tau_M}{\partial y_e} \end{bmatrix}^{T} \tag{A.4}$$

and $\mathbf{J}(\tau)$ is the FIM for the unknown vector $\tau = [\tau_2, \ldots, \tau_M]^T$.

For simplicity, the following notations are used:

$$\frac{\partial \tau_k}{\partial x_e} = \frac{1}{c}\left(\frac{x_e - x_0}{\sqrt{(x_e - x_0)^2 + (y_e - y_0)^2}} - \frac{x_e - x_k}{\sqrt{(x_e - x_k)^2 + (y_e - y_k)^2}}\right) = \frac{d_{xk}}{c} \quad \text{(A.5)}$$

$$\frac{\partial \tau_k}{\partial y_e} = \frac{1}{c}\left(\frac{y_e - y_0}{\sqrt{(x_e - x_0)^2 + (y_e - y_0)^2}} - \frac{y_e - y_k}{\sqrt{(x_e - x_k)^2 + (y_e - y_k)^2}}\right) = \frac{d_{yk}}{c} \quad \text{(A.6)}$$

Starting from the general expression of the FIM for a complex Gaussian pdf which is given in [87, pp 525] and reproduced here (using our notation),

$$J_{ij}(\tau) = \sum_{l=1}^{N} \mathrm{Tr}\left[\mathbf{K}^{-1}(f_l)\frac{\partial \mathbf{K}(f_l)}{\partial \tau_i}\mathbf{K}^{-1}(f_l)\frac{\partial \mathbf{K}(f_l)}{\partial \tau_j}\right] + 2Re\left[\frac{\partial \mu^H}{\partial \tau_i}\mathbf{K}^{-1}(f_l)\frac{\partial \mu}{\partial \tau_j}\right] \quad \text{(A.7)}$$

the elements of the FIM $\mathbf{J}(\tau)$ can be expressed as:

$$J_{ij}(\tau) = -\sum_{l=1}^{N} \mathrm{Tr}\left[\frac{\partial \mathbf{K}(f_l)}{\partial \tau_i}\frac{\partial \mathbf{K}^{-1}(f_l)}{\partial \tau_j}\right] \quad \text{(A.8)}$$

where it was used that the mean of $\mathbf{r}$ is zero ($\mu = 0$) and $\mathbf{A}^{-1}\frac{\partial \mathbf{A}}{\partial \tau}\mathbf{A}^{-1} = -\frac{\partial \mathbf{A}^{-1}}{\partial \tau}$.

Using the following property

$$\mathrm{Tr}(\partial A) = \partial(\mathrm{Tr}(A)) \quad \text{(A.9)}$$

equation (A.8) can be transformed to:

$$J_{ij}(\tau) = \sum_{l=1}^{N} \frac{\partial^2}{\partial v_i \partial u_j}\mathrm{Tr}\left(\mathbf{K}_{\mathbf{v}}^{-1}(f_l)\,\mathbf{K}_{\mathbf{u}}(f_l)\right)\Big|_{\mathbf{v}=\mathbf{u}=\tau} \quad \text{(A.10)}$$

Replacing (3.5) and (3.6) into (A.10), and performing the derivations yields

$$J_{ij}(\tau) = \begin{cases} \sum_{l=1}^{N} \sum_{\substack{k=2 \\ k\neq i}}^{M} 8\pi^2 (f_l + f_c)^2 \alpha \frac{a_i^2 a_k^2}{\beta^2} & i = j \\ -\sum_{l=1}^{N} 8\pi^2 (f_l + f_c)^2 \alpha \frac{a_i^2 a_j^2}{\beta^2} & i \neq j \end{cases} \tag{A.11}$$

where

$$\alpha = \frac{\beta^2 \left(\frac{P_s}{P_w}\right)^2}{1 + \beta \left(\frac{P_s}{P_w}\right)} \tag{A.12}$$

$$\beta = \sum_{k=1}^{M} a_k^2. \tag{A.13}$$

Using the fact that $BT \gg 1$, the summation in (A.11) can be replaced by integration. Thus, the elements of the $\mathbf{J}(\tau)$ are given by:

$$J_{ij}(\tau) = \begin{cases} T \int_{-B/2}^{B/2} \sum_{\substack{k=2 \\ k\neq i}}^{M} 8\pi^2 (f + f_c)^2 \frac{\alpha}{\beta^2} a_i^2 a_k^2 df & i = j \\ -T \int_{-B/2}^{B/2} 8\pi^2 (f + f_c)^2 \frac{\alpha}{\beta^2} a_i^2 a_j^2 df & i \neq j \end{cases} \tag{A.14}$$

Performing the integrations in (A.14) and replacing the result in (A.3), it follows that the CRLB is given by

$$C_{CRLB} = \frac{c^2}{8\pi^2 BT\alpha f_c^2 \left(1 + \frac{B^2}{12 f_c^2}\right)} \frac{\beta^2}{q_{11}q_{22} - q_{12}q_{21}} \begin{bmatrix} q_{22} & -q_{21} \\ -q_{12} & q_{11} \end{bmatrix} \tag{A.15}$$

where

$$q_{11} = \sum_{k=2}^{M} a_k^2 d_{xk}^2 + \sum_{k=2}^{M}\sum_{l=2}^{M} a_k^2 a_l^2 d_{xk}^2 - \sum_{k=2}^{M}\sum_{l=2}^{M} a_k^2 a_l^2 d_{xk} d_{xl} \tag{A.16}$$

$$q_{12} = q_{21} = \sum_{k=2}^{M} a_k^2 d_{xk} d_{yk} + \sum_{k=2}^{M}\sum_{l=2}^{M} a_k^2 a_l^2 d_{xk} d_{yk} - \sum_{k=2}^{M}\sum_{l=2}^{M} a_k^2 a_l^2 d_{xk} d_{yl} \tag{A.17}$$

$$q_{22} = \sum_{k=2}^{M} a_k^2 d_{yk}^2 + \sum_{k=2}^{M}\sum_{l=2}^{M} a_k^2 a_l^2 d_{yk}^2 - \sum_{k=2}^{M}\sum_{l=2}^{M} a_k^2 a_l^2 d_{yk} d_{yl}. \tag{A.18}$$

Or, using the notation

$$g = \frac{\beta^2}{q_{11}q_{22} - q_{12}q_{21}} \begin{bmatrix} q_{22} & -q_{21} \\ -q_{12} & q_{11} \end{bmatrix}$$

the CRLB can be expressed as

$$C_{CRLB} = \frac{c^2}{8\pi^2 BT\alpha f_c^2 \left(1 + \frac{B^2}{12 f_c^2}\right)} \cdot g \tag{A.19}$$

From last expression, it can be noted that for narrowband signals (i.e., $B \ll f_c$), the CRLB for estimating coherently the location coordinates $[x_e, y_e]$ is inverse proportionally with SNR (α), with carrier frequency (f_c), and with the duration of observations (BT). Also, the term g incorporates the target's position with respect to the positions of the sensors, term known in the literature as geometric dilution of precision (GDOP) [61].

APPENDIX B

PROOF OF LEMMA 1

In this appendix the log-likelihood ratio test is computed (2.13) for the SISO scenario.

From (5.6), the distributions of the vector observations, under the two hypotheses, conditioned on the parameters τ and f and averaged over the distributions of the target reflectivity are:

$$\begin{aligned}
f_{(m)}(\mathbf{r}|\tau,f) &= \int f_{(m)}\left(\mathbf{r}|\tau,f,a\right)\cdot f\left(a\right)\mathrm{d}a \\
&= \int c_1 \exp\left\{-\frac{1}{\sigma_w^2}\sum_{l=1}^{L}\left|r\left(t_l\right)-\sqrt{E}as\left(t_l-\tau-m\tau_\delta\right)e^{j2\pi(f+mf_\delta)t_l}\right|^2\right\}\cdot \\
&\quad \cdot f\left(a\right)\mathrm{d}a = \\
&= \int c_1 \exp\left\{-\frac{1}{\sigma_w^2}\sum_{l=1}^{L}\left(\left|r\left(t_l\right)\right|^2\right.\right. \\
&\quad -\sqrt{E}a^* r\left(t_l\right)s^*\left(t_l-\tau-m\tau_\delta\right)e^{-j2\pi(f+mf_\delta)t_l}- \\
&\quad -\sqrt{E}a r^*\left(t_l\right)s\left(t_l-\tau-m\tau_\delta\right)e^{j2\pi(f+mf_\delta)t_l}+ \\
&\quad \left.\left.+E\left|a\right|^2\left|s\left(t_l-\tau-m\tau_\delta\right)\right|^2\right)\right\}f\left(a\right)\mathrm{d}a
\end{aligned}$$

Completing the square of the integrand,

$$f_{(m)}(\mathbf{r}|\tau, f) = c_2 \exp\left(-\frac{1}{\sigma_w^2}\|\mathbf{r}\|^2\right) \cdot \exp\left\{\frac{E}{\sigma_w^2\left(E+\frac{\sigma_w^2}{\sigma_a^2}\right)}\left|\sum_{l=1}^{L} r(t_l)\, s^*(t_l-\tau-m\tau_\delta)\, e^{-j2\pi(f+m\delta f_\delta)t_l}\right|^2\right\}. \tag{B.1}$$

$$\cdot \int \exp\left\{-\frac{1}{\sigma_w^2}\left|\sqrt{\frac{E}{\left(E+\frac{\sigma_w^2}{\sigma_a^2}\right)}}\sum_{l=1}^{L} r(t_l)\, s^*(t_l-\tau-m\tau_\delta)\, e^{-j2\pi(f+mf_\delta)t_l} - \right.\right.$$
$$\left.\left. -\sqrt{E+\frac{\sigma_w^2}{\sigma_a^2}}a\right|^2\right\} \mathrm{d}a \tag{B.2}$$

Performing the integration,

$$f_{(m)}(\mathbf{r}|\tau, f) = c_3 \exp\left(-\frac{1}{\sigma_w^2}\|\mathbf{r}\|^2\right) \cdot \exp\left\{\frac{E}{\sigma_w^2\left(E+\frac{\sigma_w^2}{\sigma_a^2}\right)}\left|\sum_{l=1}^{L} r(t_l)\, s^*(t_l-\tau-m\tau_\delta)\, e^{-j2\pi(f+mf_\delta)t_l}\right|^2\right\}$$

In these expressions, c_1, c_2, and c_3 are constants that do not depend on the unknown parameters $\boldsymbol{\varphi}$, $\boldsymbol{\varphi}+\boldsymbol{\delta}$. Substituting the last expression in (2.13) yields the following likelihood ratio test:

$$l(\mathbf{r}) = \frac{E}{\sigma_w^2\left(E+\frac{\sigma_w^2}{\sigma_a^2}\right)}\mathbf{r}^H\left(\mathbf{s}_{(1)}\mathbf{s}_{(1)}^H - \mathbf{s}_{(0)}\mathbf{s}_{(0)}^H\right)\mathbf{r} \underset{H_0}{\overset{H_1}{\gtrless}} 0 \tag{B.3}$$

where $\mathbf{s}_{(m)} = \left[s(t_1-\tau-m\tau_\delta)\, e^{j2\pi(f+mf_\delta)t_1}, \ldots, s(t_L-\tau-m\tau_\delta)\, e^{j2\pi(f+mf_\delta)t_L}\right]^T$.

APPENDIX C

DERIVATION OF PROBABILITY OF ERROR

To derive an expression for the probability of error of binary hypothesis testing (5.5), it is first necessary to determine the statistical properties of the random variable $l' = \mathbf{r}^H \left(\mathbf{s}_{(1)}\mathbf{s}_{(1)}^H - \mathbf{s}_{(0)}\mathbf{s}_{(0)}^H \right) \mathbf{r}$, which appears in the likelihood ratio test (5.7). Since $\mathbf{r}$ is multivariate complex Gaussian (due to the target reflectivity and noise), the distribution of l' is a central, indefinite quadratic form in complex Gaussian random variables. It is central since $\mathrm{E}[\mathbf{r}] = 0$, and indefinite since $\mathbf{s}_{(1)}\mathbf{s}_{(1)}^H - \mathbf{s}_{(0)}\mathbf{s}_{(0)}^H$ can have positive and negative eigenvalues. The characteristic function of a central quadratic form is [88]

$$G_{l'}(s) = \frac{1}{\det\left(I - js\boldsymbol{\Sigma}^H \left(\mathbf{s}_{(1)}\mathbf{s}_{(1)}^H - \mathbf{s}_{(0)}\mathbf{s}_{(0)}^H \right) \right)} = \prod_{n=1}^{N_\lambda} \frac{1}{(1 - js\lambda_n)^{\mu_n}} \tag{C.1}$$

where $\boldsymbol{\Sigma}$ is the covariance matrix of $\mathbf{r}$, $\boldsymbol{\Sigma} = \mathrm{E}[\mathbf{r}\mathbf{r}^{\mathbf{H}}] = E\sigma_a^2 \mathbf{s}_{(0)}\mathbf{s}_{(0)}^H + \sigma_w^2 I$. The terms λ_n, $n = 1, \ldots, N_\lambda$, are the distinct non-zero eigenvalues of the matrix $\mathbf{Y} = \boldsymbol{\Sigma}^H \left(\mathbf{s}_{(1)}\mathbf{s}_{(1)}^H - \mathbf{s}_{(0)}\mathbf{s}_{(0)}^H \right)$; μ_n are the multiplicities of the eigenvalues λ_n. Since the matrix $\left(\mathbf{s}_{(1)}\mathbf{s}_{(1)}^H - \mathbf{s}_{(0)}\mathbf{s}_{(0)}^H \right)$ has rank two, $\mathbf{Y}$ being the product of two matrices, has also rank two[1] (see [81, Appendix A]). Thus, $\mathbf{Y}$ has two distinct non-zero eigenvalues $\lambda^+ > 0 \,\mathtt{and}\, \lambda^- < 0$, which can be determined from Bôcher's formula [82]:

$$\lambda^2 + e_1\lambda + e_2 = 0 \tag{C.2}$$

where $e_1 = -\mathrm{Tr}\{\mathbf{Y}\}$, $e_2 = -\frac{1}{2}(e_1 \mathrm{Tr}\{\mathbf{Y}\} + \mathrm{Tr}\{\mathbf{Y}^2\})$, and $\mathrm{Tr}\{\cdot\}$ represents trace. After some straightforward algebra operations, these parameters can be expressed

[1] The covariance matrix $\boldsymbol{\Sigma}$ is a full rank matrix, and $\mathrm{rank}\,(\mathbf{AB}) \leq \min\left(\mathrm{rank}\,(\mathbf{A}), \mathrm{rank}\,(\mathbf{B})\right)$.

$$e_1 = -E\sigma_a^2 \left(1 - \Psi\left(\tau_\delta, f_\delta\right)\right)$$
$$e_2 = -E\sigma_a^2\sigma_w^2 \left(1 - \Psi\left(\tau_\delta, f_\delta\right)\right) - \sigma_w^4 \left(1 - \Psi\left(\tau_\delta, f_\delta\right)\right). \tag{C.3}$$

where

$$\Psi\left(\tau_\delta, f_\delta\right) = \left|\mathbf{s}_{(0)}^H \mathbf{s}_{(1)}\right|^2 = \left|\sum_{l=1}^{L} s\left(t_l\right) s^*\left(t_l - \tau_\delta\right) e^{-j2\pi f_\delta t_l}\right|^2 \tag{C.4}$$

is a sampled version of the ambiguity function [89].

From the characteristic function of the random variable l', we can determine its cumulative distribution function, and implicitly $P_\epsilon(l(\mathbf{r}) < 0|H_1)$,

$$\begin{aligned} P_\epsilon(l(\mathbf{r}) < 0|H_1) =& \frac{1}{2\pi}\int_{-\infty}^{0}\int_{-\infty}^{\infty} G_{l'}(s) e^{-jsl'} ds dl' \\ =& \frac{1}{2\pi}\int_{-\infty}^{0}\int_{-\infty}^{\infty} \left(\frac{1}{(1-js\lambda^+)}\frac{1}{(1-js\lambda^-)}\right) e^{-jsl'} ds dl' \\ =& \frac{1}{2\pi}\int_{-\infty}^{0}\int_{-\infty}^{\infty} \left(\frac{\frac{\lambda^+}{\lambda^+-\lambda^-}}{(1-js\lambda^+)} + \frac{\frac{\lambda^-}{\lambda^--\lambda^+}}{(1-js\lambda^-)}\right) e^{-jsl'} ds dl' \\ =& \frac{\lambda^-}{\lambda^- - \lambda^+} \end{aligned} \tag{C.5}$$

The third equality was obtained with the help of partial fraction expansion. In the last equality, we used $\int_{-\infty}^{\infty} \frac{e^{-jsl'}}{(1-js\lambda^-)} ds = -2\pi e^{-l'/\lambda^-}/\lambda^-$, $\int_{-\infty}^{\infty} \frac{e^{-jsl'}}{(1-js\lambda^+)} ds = 0$, and $\int_{-\infty}^{0} -e^{-l'/\lambda^-}/\lambda^- dl' = 1$, [85, 3.382 ET I 118(4)]. The following closed form of the probability of error is obtained after substituting in (C.5) the solutions of the quadratic equation (C.2), and using the notation $E\sigma_\alpha^2/\sigma_w^2 = \mathrm{SNR}$

$$P_\epsilon(\boldsymbol{\delta}) = \frac{1}{2} - \frac{\mathrm{SNR}\left(1 - \Psi\left(\tau_\delta, f_\delta\right)\right)}{2\sqrt{\left(\mathrm{SNR}^2\left(1 - \Psi\left(\tau_\delta, f_\delta\right)\right) + 4\mathrm{SNR} + 4\right) \cdot \left(1 - \Psi\left(\tau_\delta, f_\delta\right)\right)}},$$

APPENDIX D

CODED OFDM WAVEFORMS

In the distributed MIMO radars, due to the wide-separation between antennas, the transmitted waveforms propagate along different paths to the target, and from the target to receive antennas. As a result the transmitted signals are being received with uncorrelated amplitude and phase, and with different delays and Doppler shifts. Even if the transmitted waveforms are orthogonal upon transmission, the orthogonality property is lost at the receivers. In such case, received signals will interfere with each other leading to degraded performance in the MIMO radar. It is necessary to design waveforms that maintain orthogonality under a wide range of sensor locations. A naive solution to this problem is a frequency division multiple access (FDMA) approach, where each transmitter is allocated a frequency channel. Because each waveform has to be wideband for high range-delay accuracy, this approach is very wasteful in its bandwidth utilization. We seek techniques that allow the waveforms to overlap in frequency. In this appendix, we introduce orthogonal frequency division multiplexing (OFDM) based waveforms for MIMO radar, referred to as *Coded OFDM* waveforms.

A spread spectrum OFDM radar waveform is obtained by modulating orthogonal subcarriers with a polyphase code or any other type of spreading code. In communication, such signals are known as *multicarrier CDMA (MC-CDMA)* [90]. Frequency spreading leads to improved spectral utilization in the sense that its power spectral density sidelobes are lower than that of polyphase waveforms. The power spectral density (PSD) of an OFDM signal with S subcarriers and duration T, has a nearly rectangular shape with a bandwidth of S/T. Spectral sidelobes of OFDM symbols occur each $1/T$. Compare that to the PSD of a signal of the same duration

T, and spread by modulating it with S short pulses (chips) of duration T/S each. The PSD of this waveform is a squared sinc function with a null-to-null bandwidth of $2S/T$. For such a pulse, the spectral sidelobes occur each S/T. It follows that within one spectral sidelobe of the time domain waveform, there are S spectral sidelobes of the frequency domain waveform, leading to a much faster decay of the spectral sidelobes in the latter.

Levanon designed a radar waveform consisting of a sequence of S OFDM symbols, where each symbol consists of S subcarriers [91]. Each subcarrier is modulated by a P4 symbol (P4 symbols are the digital version of linear frequency modulated signals). Multifrequency Complementary Phase Coded (MCPC) waveform, as he named it, is constructed by using all the cyclic time shifts of a P4 symbol to modulate the OFDM subcarriers. It is shown in [91] that , the MCPC waveform has an ambiguity function that does not exhibit the ambiguity ridge in the time - Doppler domain. The ambiguity ridge is found in the ambiguity functions of P4 sequences. This advantage of MCPC codes over the P4 codes is obtained because all the different cyclic time shifts of a P4 sequence forms a complementary set, and so, MCPC codes are complementary both in the time and frequency domains. A set of S sequences $\Gamma = \{\gamma_1, \gamma_2, \ldots, \gamma_S\}$, each of length K, is called a complementary set, if the sum of the aperiodic autocorrelation functions of all sequences from the set is zero for all non-zero shifts p, i.e.,

$$Z(p) = \sum_{i=0}^{S-1} \sum_{j=0}^{K-1-p} \gamma_i(j)\gamma_i^*(j+p) = \begin{cases} \sum_{i=0}^{S-1} R_i(0) & p = 0 \\ 0 & p \neq 0 \end{cases} \tag{D.1}$$

where $|\gamma_i(j)| = 1$ for any $i = 1 \ldots S$ and $j = 1 \ldots K$ and R_i denotes the autocorrelation function for sequence γ_i.

The improved spectral efficiency and ambiguity function properties, make OFDM based signals an attractive alternative for the design of radar waveforms. To extend

this design to MIMO radar, it is necessary to add the requirement that the waveforms are orthogonal. Any design of a radar system with multiple transmit antennas in which each transmitter sends a different waveform, requires that the receivers have the ability to separate these waveforms. The easiest way to achieve separability of the waveforms is to design the waveforms orthogonal, and to perform matched filtering at the receiver. In MIMO radar with widely separated antennas, the problem is compounded by the fact that the waveforms may reach the receive sensors with marked different delays. This requires waveforms that have low cross correlations over a range of time delays.

Here, we seek to stick with OFDM based waveforms to capitalize on their advantages as discussed above. Hence, orthogonality is required waveforms, where each waveform is constituted by a set of sequences. Each sequence corresponds to a subcarrier in the sequence of OFDM symbols.

Two complementary sets of binary elements, $\overline{\Gamma} = [\overline{\gamma}_1, \overline{\gamma}_2, \ldots, \overline{\gamma}_M]$ and $\widetilde{\Gamma} = [\widetilde{\gamma}_1, \widetilde{\gamma}_2, \ldots, \widetilde{\gamma}_L]$, are called mates if [92]:

1. The two sets have the same number of sequences, $M = L$
2. The sequence $\overline{\gamma}_i$ has the same length N as sequence $\widetilde{\gamma}_i$, for any $1 \leq i \leq M$
3. The sum of the crosscorrelations is zero for all lags, i.e.,

$$Y(p) = \sum_{i=0}^{M-1} \sum_{j=0}^{N-1-p} \overline{\gamma}_i(j)\widetilde{\gamma}_i^*(j+p) = 0, \qquad \forall p \tag{D.2}$$

A collection of sets of sequences is said to be of mutually orthogonal complementary sets if any two sets in the collection are mates to each other [92] .

Recapping, it is possible to construct mutually orthogonal complementary sets and apply them to modulate subcarriers of a sequence of OFDM symbols. Each set corresponds to a radar waveform. This enables the design of OFDM based

waveforms for MIMO radar. However, this process departed from the original MCPC waveforms that are complementary both in time and frequency domains. Yet, the mutually orthogonal complementary sets maintain complementarity only in one domain. To recapture the complementary property in the time and frequency domains, we employ the algorithm proposed by Zhang et. al., [93]. The algorithm, originally proposed for creating MC-CDMA spreading sequences, generates binary mutually orthogonal sequences that are complementary in two dimensions, time and frequency. The authors refer to these sequences as two dimensional combined complementary sequences. The proposed algorithm has some limitations in generating the sets. For example, to generate J orthogonal sets (i.e., J orthogonal waveforms), the minimum number of subcarriers is $2J$ and the required length of each sequence is J^2. For comparison, Tseng, [92], showed that to generate J mutually orthogonal sets complementary only in the time domain, the minimum number of subcarriers required is J and the shortest sequence length is $J/2$. Clearly, the collection of mutually orthogonal sets complementary in time and frequency is smaller than the collection of mutually orthogonal sets complementary only in time. Yet the former have important advantages for MIMO radar.

In view of the former discussion, we propose coded OFDM radar waveforms that form a collection of on generating mutually orthogonal sets that are complementary in the time and frequency domains. We utilize the algorithm in [93] to generate the sets, and apply them to modulate sequences of OFDM symbols. The general structure of a coded OFDM waveform is shown in Figure D: $S_1,\ S_2,\ S_3,\ S_4$ denote the OFDM symbols, $f_1,\ f_2,\ f_3,\ f_4$ denote the subcarriers, and $\gamma_{l,m}$ represents the modulation of the l-th subcarrier in the m-th OFDM symbol. Coded OFDM pulses are different from MCPC pulses [91] in several respects: (1) Coded OFDM has binary elements, whereas MCPC has polyphase elements, (2) sequences of coded OFDM subcarriers

are not necessarily cyclic time shifted versions of each other, (3) most important, coded OFDM waveforms are mutually orthogonal.

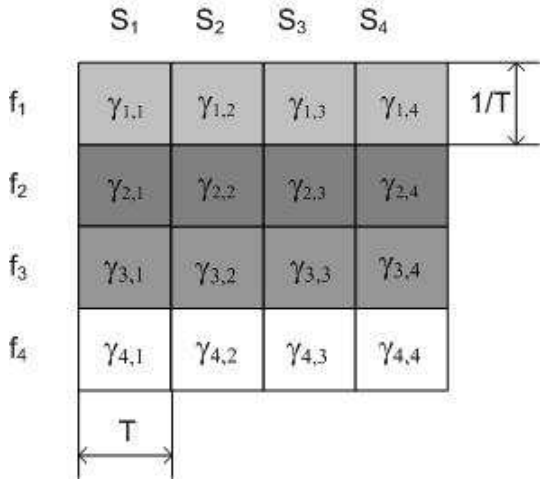

Figure D.1 Structure of a COFDM pulse with $S = 4$.

REFERENCES

[1] Y. H. Hu and D. Li, "Energy based collaborative source localization using acoustic micro-sensor array," *EURASIP J. Appl. Signal Process.*, no. 4, pp. 321–337, Aug. 2003.

[2] X. Sheng and Y. H. Hu, "Maximum likelihood multiple-source localization using acoustic energy measurements with wireless sensor networks," *IEEE Transactions on Signal Processing*, vol. 53, no. 1, pp. 44–53, Jan. 2005.

[3] D. Blatt and A. O. Hero, "Energy-based sensor network source localization via projection onto convex sets," *IEEE Transactions on Signal Processing*, vol. 54, no. 9, pp. 3614–3619, Sep. 2006.

[4] K. C. Ho and M. Sun, "Passive Source Localization Using Time Differences of Arrival and Gain Ratios of Arrival," *IEEE Transactions on Signal Processing*, vol. 56, no. 2, pp. 464–477, Feb. 2008.

[5] K. W. Cheung, H. C. So, W. K. Ma, and Y. T. Chan, "Least squares algorithms for time-of-arrival-based mobile location," *IEEE Transactions on Signal Processing*, vol. 52, no. 4, pp. 1121–1130, Apr. 2004.

[6] Y. Qi, H. Kobayashi, and H. Suda, "On time-of-arrival positioning in a multipath environment," *IEEE Transactions on Vehicular Technology*, vol. 55, no. 5, pp. 1516–1526, Sep. 2006.

[7] Y. T. Chan, W. Y. Tsui, H. C. So, and P. Ching, "Time-of-arrival based localization under NLOS conditions," *IEEE Transactions on Vehicular Technology*, vol. 55, no. 1, pp. 17–24, Jan. 2006.

[8] W. A. Gardner and C. K. Chen, "Signal-selective time-difference-of-arrival estimation for passive location of man-made signal sources in highly corruptive environments. I. Theory and method," *IEEE Transactions on Signal Processing*, vol. 40, no. 5, pp. 1168–1184, May 1992.

[9] C. K. Chen and W. A. Gardner, "Signal-selective time-difference of arrival estimation for passive location of man-made signal sources in highly corruptive environments. II. Algorithms and performance," *IEEE Transactions on Signal Processing*, vol. 40, no. 5, pp. 1185–1197, May 1992.

[10] F. Gustafsson and F. Gunnarsson, "Positioning using time-difference of arrival measurements," in *Proc. IEEE International Conference on Acoustics, Speech, and Signal Processing,(ICASSP'03)*, vol. 6, Hong Kong, China, Apr. 2003, pp. 553–556.

[11] R. Klukas and M. Fattouche, "Line-of-sight angle of arrival estimation in the outdoor multipath environment," *IEEE Transactions on Vehicular Technology*, vol. 47, no. 1, pp. 342–351, Feb. 1998.

[12] A. Pages-Zamora, J. Vidal, and D. Brooks, "Closed-form solution for positioning based on angle of arrival measurements," in *Proc. 13th IEEE Int. Symp. Personal, Indoor and Mobile Radio Commun.*, Lisbon, Portugal, Sep. 2002, pp. 1522–1526.

[13] A. Sayed, A. Tarighat, and N. Khajehnouri, "Network-based wireless location: challenges faced in developing techniques for accurate wireless location information," *IEEE Signal Processing Magazine*, vol. 22, no. 4, pp. 24–40, Jul. 2005.

[14] P. Rong and M. L. Sichitiu, "Angle of arrival localization for wireless sensor networks," in *Proc. IEEE 3rd Annual IEEE Communications Society on Sensor and Ad Hoc Communications and Networks (SECON'06)*, Sep. 2006, pp. 374–382.

[15] T. S. Rappaport, *Wireless communications: principles and practice*, 2nd ed. Englewood Cliffs, NJ: Prentice Hall PTR, 2002.

[16] K. Yu, I. Sharp, and Y. J. Guo, *Ground-based wireless positioning.* Chichester, West Sussex, UK: John Wiley and Sons Ltd., 2009.

[17] N. H. Lehmann, A. M. Haimovich, R. S. Blum, and L. J. Cimini, "High resolution capabilities of MIMO radar," in *Proc. 40ed Asilomar Conference on Signals, Systems and Computers*, Pacific Grove, CA, Oct. 2006, pp. 25–30.

[18] A. J. Weiss and E. Weinstein, "Fundamental limitations in passive time delay estimation - Part I: Narrow-band systems," *IEEE Transactions on Acoustics, Speech and Signal Processing*, vol. 31, no. 2, pp. 472–486, Apr. 1983.

[19] ——, "Fundamental limitations in passive time delay estimation - Part II: Wide-band systems," *IEEE Transactions on Acoustics, Speech and Signal Processing*, vol. 32, no. 5, pp. 1064–1078, Oct. 1984.

[20] B. M. Sadler, L. Huang, and Z. Xu, "Ziv-Zakai time delay estimation bound for ultra-wideband signals," in *Proc. IEEE International Conference on Acoustics, Speech, and Signal Processing,(ICASSP'07)*, vol. 3, Apr. 2007, pp. 549–552.

[21] D. Dardari, C. C. Chong, and M. Z. Win, "Threshold-based time-of-arrival estimators in UWB dense multipath channels," *IEEE Transactions on Communications*, vol. 56, no. 8, pp. 1366–1378, Aug. 2008.

[22] B. M. Sadler, N. Liu, and Z. Xu, "Ziv-Zakai Bounds on Time Delay Estimation in Unknown Convolutive Random Channels," *IEEE Transactions on Signal Processing*, vol. 58, no. 5, pp. 2729–2745, May 2010.

[23] N. Liu, Z. Xu, and B. M. Sadler, "Ziv-Zakai Time-Delay Estimation Bounds for Frequency-Hopping Waveforms Under Frequency-Selective Fading," *IEEE Transactions on Signal Processing*, vol. 58, no. 12, pp. 6400–6406, Dec. 2010.

[24] B. M. Sadler and R. J. Kozick, "A survey of time delay estimation performance bounds," in *Fourth IEEE Workshop on Sensor Array and Multichannel Processing*, Jul. 2006, pp. 282–288.

[25] K. L. Bell, Y. Ephraim, and H. L. V. Trees, "Explicit Ziv-Zakai lower bound for bearing estimation," *IEEE Transactions on Signal Processing*, vol. 44, no. 11, pp. 2810–2824, Nov. 1996.

[26] F. Athley, "Threshold region performance of maximum likelihood direction of arrival estimators," *IEEE Transactions on Signal Processing*, vol. 53, no. 4, pp. 1359–1373, Apr. 2005.

[27] C. D. Richmond, "Capon algorithm mean-squared error threshold SNR prediction and probability of resolution," *IEEE Transactions on Signal Processing*, vol. 53, no. 8, pp. 2748–2764, Aug. 2005.

[28] ——, "Mean-squared error and threshold SNR prediction of maximum-likelihood signal parameter estimation with estimated colored noise covariances," *IEEE Transactions on Information Theory*, vol. 52, no. 5, pp. 2146–2164, May 2006.

[29] H. L. V. Trees, *Detection, Estimation, and Modulation Theory, Part I.* New York, NY: John Wiley and Sons, 2001.

[30] E. W. Barankin, "Locally best unbiased estimates," *Ann. Math. Stat.*, vol. 20, no. 4, pp. 477–501, 1949.

[31] R. McAulay and E. Hofstetter, "Barankin bounds on parameter estimation," *IEEE Transactions on Information Theory*, vol. 17, no. 6, pp. 669–676, 1971.

[32] L. Knockaert, "The Barankin bound and threshold behavior in frequency estimation," *IEEE Transactions on Signal Processing*, vol. 45, no. 9, pp. 2398–2401, Sep. 1997.

[33] J. Tabrikian and J. L. Krolik, "Barankin bounds for source localization in an uncertain ocean environment," *IEEE Transactions on Signal Processing*, vol. 47, no. 11, pp. 2917–2927, Nov. 1999.

[34] A. Pinkus and J. Tabrikian, "Barankin Bound for Range and Doppler Estimation Using Orthogonal Signal Transmission," in *IEEE Conference on Radar*, Apr. 2006, pp. 94–99.

[35] P. S. La Rosa, A. Renaux, and A. Nehorai, "Barankin Bound for Multiple Change-Point Estimation," in *2nd IEEE International Workshop on Computational Advances in Multi-Sensor Adaptive Processing, (CAMPSAP '07)*, St. Thomas, VI, Dec. 2007, pp. 37–40.

[36] E. Naftali and N. C. Makris, "Necessary conditions for a maximum likelihood estimate to become asymptotically unbiased and attain the Cramer-Rao lower bound. Part I. General approach with an application to time-delay and Doppler shift estimation." *Journal of the Acoustical Society of America*, vol. 110, no. 4, pp. 1917–1930, Oct. 2001.

[37] A. Thode, M. Zanolin, E. Naftali, I. Ingram, P. Ratilal, and N. C. Makris, "Necessary conditions for a maximum likelihood estimate to become asymptotically unbiased and attain the Cramer-Rao lower bound. Part II. Range and depth localization of a sound source in an ocean waveguide," *The Journal of the Acoustical Society of America*, vol. 112, pp. 1890–1910, 2002.

[38] J. Ziv and M. Zakai, "Some lower bounds on signal parameter estimation," *IEEE Transactions on Information Theory*, vol. 15, no. 3, pp. 386–391, May 1969.

[39] K. L. Bell, Y. Steinberg, Y. Ephraim, and H. L. V. Trees, "Extended Ziv-Zakai lower bound for vector parameter estimation," *IEEE Transactions on Information Theory*, vol. 43, no. 2, pp. 624–637, Mar. 1997.

[40] K. L. Bell, "Performance Bounds in Parameter Estimation with Application to Bearing Estimation," Ph.D. dissertation, George Mason University, Fairfax, VA, 1995.

[41] W. Xu, "Performance bounds on matched-field methods for source localization and estimation of ocean environmental parameters," Ph.D. dissertation, Massachusetts Institute of Technology, Cambridge, MA, 2001.

[42] W. Xu, A. B. Baggeroer, and H. Schmidt, "Performance Analysis for Matched-Field Source Localization: Simulations and Experimental Results," *IEEE Journal of Oceanic Engineering*, vol. 31, no. 2, pp. 325–345, Apr. 2006.

[43] R. J. Kozick and B. M. Sadler, "Source localization with distributed sensor arrays and partial spatial coherence," *IEEE Transactions on Signal Processing*, vol. 52, no. 3, pp. 601–616, Mar. 2004.

[44] V. M. Chiriac, A. M. Haimovich, S. C. Schwartz, and J. A. Dabin, "Performance bound for localization of a near field source," in *Proc. 44ed Asilomar Conference on Signals, Systems and Computers*, Pacific Grove, CA, Nov. 2009, pp. 130 – 135.

[45] V. M. Chiriac and A. M. Haimovich, "Ziv - Zakai lower bound on target localization estimation in MIMO radar systems," in *Proc. IEEE Radar Conference*, Washington, DC, May 2010, pp. 678 – 683.

[46] P. M. Woodward, *Probability and information theory, with applications to radar.* New York, NY: McGraw-Hill, 1957.

[47] E. Weinstein and A. J. Weiss, "A general class of lower bounds in parameter estimation," *IEEE Transactions on Information Theory*, vol. 34, no. 2, pp. 338–342, Mar. 1988.

[48] B. Z. Bobrovsky and M. Zakai, "A lower bound on the estimation error for certain diffusion processes," *IEEE Transactions on Information Theory*, vol. 22, no. 1, pp. 45–52, Jan. 1976.

[49] A. J. Weiss, "Fundamental bounds in parameter estimation," Ph.D. dissertation, Tel-Aviv University, Tel-Aviv, Israel, 1985.

[50] A. J. Weiss and E. Weinstein, "A lower bound on the mean square error in random parameter estimation," *IEEE Transactions on Information Theory*, vol. 31, no. 5, pp. 680–682, Sep. 1985.

[51] D. Chazan, M. Zakai, and J. Ziv, "Improved lower bounds on signal parameter estimation," *IEEE Transactions on Information Theory*, vol. 21, no. 1, pp. 90–93, Jan. 1975.

[52] S. Bellini and G. Tartara, "Bounds on error in signal parameter estimation," *IEEE Transactions on Communications*, vol. 22, no. 3, pp. 340–342, Mar. 1974.

[53] E. Cinlar, *Introduction to stochastic processes.* Englewood Cliffs, NJ: Prentice Hall PTR, 1975.

[54] M. A. Haleem and A. M. Haimovich, "On the distribution of ambiguity levels in MIMO radar," in *Proc. 43ed Asilomar Conference on Signals, Systems and Computers*, Pacific Grove, CA, Oct. 2008, pp. 198–202.

[55] A. Papoulis, *Probability Random Variables and Stochastic Processes.* New York, NY: McGraw-Hill, 1991.

[56] J. Nocedal and S. J. Wright, *Numerical Optimization.* New York, NY: Springer, 2007.

[57] E. M. T. Hendrix and B. G. Toth, *Introduction to nonlinear and global optimization.* New York, NY: Springer, 2010.

[58] A. Zhigljasky and A. Zilinskas, *Stochastic global optimization.* New York, NY: Springer, 2008.

[59] D. R. Jones, C. D. Perttunen, and B. E. Stuckman, "Lipschitzian optimization without the Lipschitz constant," *Journal of Optimization Theory and Applications*, vol. 79, no. 1, pp. 157–181, Oct. 1993.

[60] B. Shubert, "A sequential method seeking the global maximum of a function," *SIAM Journal on Numerical Analysis*, vol. 9, no. 1, pp. 379–388, 1972.

[61] H. Godrich, A. M. Haimovich, and R. S. Blum, "Target localization accuracy gain in MIMO radar-based systems," *IEEE Transactions on Information Theory*, vol. 56, no. 6, pp. 2783–2803, Jun. 2010.

[62] L. D. Collins, "Asymptotic approximation to the error probability for detecting Gaussian signals," Ph.D. dissertation, Massachusetts Institute of Technology, Cambridge, MA, 1968.

[63] D. F. DeLong, "Use of the Weiss-Weinstein bound to compare the direction-finding performance of sparse arrays," MIT Lincoln Lab., Lexington, MA, Tech. Rep. Tech. Rep. 982, Aug. 1993.

[64] B. D. Steinberg, "The peak sidelobe of the phased array having randomly located elements," *IEEE Transactions on Antennas and Propagation*, vol. 20, no. 2, pp. 129–136, Mar. 1972.

[65] M. A. Haleem and A. M. Haimovich, "Sidelobe mitigation in MIMO radar with multiple subcarriers," in *Proc. IEEE Radar Conference 2009*, Pasadena, CA, May 2009, pp. 1–6.

[66] J. Li and P. Stoica, "MIMO Radar with Colocated Antennas," *IEEE Signal Processing Magazine*, vol. 24, no. 5, pp. 106–114, Sep. 2007.

[67] A. M. Haimovich, R. S. Blum, and L. J. Cimini, "MIMO radar with widely separated antennas," *IEEE Signal Processing Magazine*, vol. 25, no. 1, pp. 116–129, 2008.

[68] E. Fishler, A. M. Haimovich, R. S. Blum, L. J. Cimini, D. Chizhik, and R. A. Valenzuela, "Spatial Diversity in Radars - Models and Detection Performance," *IEEE Transactions on Signal Processing*, vol. 54, no. 3, pp. 823–838, Mar. 2006.

[69] J. Li and P. Stoica, *MIMO radar signal processing*. Hoboken, NJ: John Wiley and Sons, 2009.

[70] A. W. Rihaczek, *Principles of high-resolution radar*. Norwood, MA: Artech House, 1996.

[71] R. Sivaswamy, "Multiphase complementary codes," *IEEE Transactions on Information Theory*, vol. 24, no. 5, pp. 546–552, Sep. 1978.

[72] J. P. Costas, "A study of a class of detection waveforms having nearly ideal range-Doppler ambiguity properties," *Proceedings of the IEEE*, vol. 72, no. 8, pp. 996–1009, Aug. 1984.

[73] J. C. Guey and M. R. Bell, "Diversity waveform sets for delay-Doppler imaging," *IEEE Transactions on Information Theory*, vol. 44, no. 4, pp. 1504–1522, Jul. 1998.

[74] I. Gladkova and D. Chebanov, "On the synthesis problem for a waveform having a nearly ideal ambiguity surface," in *Proc. The International Conference RADAR 2004*, Toulouse, France, Oct. 2004.

[75] A. Pezeshki, A. R. Calderbank, W. Moran, and S. D. Howard, "Doppler resilient Golay complementary waveforms," *IEEE Transactions on Information Theory*, vol. 54, no. 9, pp. 4254–4266, Sep. 2008.

[76] H. He, P. Stoica, and J. Li, "On synthesizing cross ambiguity functions," in *Proc. IEEE International Conference on Acoustics, Speech, and Signal Processing,(ICASSP'11)*, Prague, Czech, May 2011, pp. 3536–3539.

[77] J. J. Zhang, G. Maalouli, A. Papandreou-Suppappola, and D. Morrell, "Cramer-Rao lower bounds for the joint estimation of target attributes using MIMO radar," in *International Conference on Waveform Diversity and Design*, Feb. 2009, pp. 103–107.

[78] Q. He, R. S. Blum, and A. M. Haimovich, "Noncoherent MIMO radar for location and velocity estimation: More antennas means better performance," *IEEE Transactions on Signal Processing*, vol. 58, no. 7, pp. 3661–3680, Mar. 2010.

[79] N. Levanon and E. Mozeson, *Radar Signals*. Hoboken, NJ: John Wiley and Sons, 2004.

[80] R. A. Horn and C. R. Johnson, *Matrix analysis*. New York, NY: Cambridge Univ Pr, 1990.

[81] H. L. V. Trees, *Optimum array processing, Part IV*. New York, NY: John Wiley and Sons, 2002.

[82] P. M. DeRusso, R. J. Roy, and C. M. Close, *State Variables for Engineers*. New York,NY: John Wiley and Sons, 1965.

[83] T. Tsao, M. Slamani, P. Varshney, D. Weiner, H. Schwarzlander, and S. Borek, "Ambiguity function for a bistatic radar," *IEEE Transactions on Aerospace and Electronic Systems*, vol. 33, no. 3, pp. 1041–1051, Jul. 1997.

[84] M. K. Simon and M. S. Alouini, *Digital communication over fading channels: a unified approach to performance analysis*. New York, NY: John Wiley and Sons, 2000.

[85] I. S. Gradshteyn and I. M. Ryzhik, *Table of Integrals, Series, and Products*. San Diego, CA: New York: Academic, 2000.

[86] G. San Antonio, D. Fuhrmann, and F. Robey, "MIMO radar ambiguity functions," *IEEE Journal of Selected Topics in Signal Processing*, vol. 1, no. 1, pp. 167–177, Jun. 2007.

[87] S. Kay, *Fundamentals of Statistical Processing, Volume I: Estimation Theory*. Englewood Cliffs, NJ: Prentice Hall PTR, 1993.

[88] S. S. Mischa Schwartz William R. Bennett, *Communication systems and techniques*. New York, NY: McGraw-Hill, 1966.

[89] M. J. D. Rendas and J. M. F. Moura, "Ambiguity in radar and sonar," *IEEE Transactions on Signal Processing*, vol. 46, no. 2, pp. 294–305, Feb. 1998.

[90] L. Hanzo, M. Münster, B. Choi, and T. Keller, *OFDM and MC-CDMA for broadband multi-user communications, WLANs, and broadcasting*. Chichester, West Sussex, UK: John Wiley and Sons Ltd., 2003.

[91] N. Levanon, "Multifrequency complementary phase-coded radar signal," in *IEE Proc., Radar, Sonar and Navigation*, vol. 147, no. 6, 2000, pp. 276–284.

[92] C. C. Tseng and C. L. Liu, "Complementary sets of sequences," *IEEE Transactions on Information Theory*, vol. 18, no. 5, pp. 644–652, Sep. 1972.

[93] C. Zhang, X. Lin, and M. Hatori, "Two dimensional combined complementary sequence and its application in multi-carrier CDMA," *IEICE transactions on communications*, vol. 88, no. 2, pp. 478–486, 2005.